UNIVERSITAT POLITÈCNICA DE VALÈNCIA

INSTITUTO INTERUNIVERSITARIO DE INVESTIGACIÓN DE RECONOCIMIENTO MOLECULAR Y DESARROLLO TECNOLÓGICO

UNIVERSITAT
POLITÈCNICA
DE VALÈNCIA

Pharmacological senolysis as a new therapeutic approach for the prevention of doxorubicin-induced cardiotoxicity

PhD. THESIS

Submitted by

Araceli Lérida Viso

PhD. Supervisors:

Prof. Ramón Martínez Máñez

Dra. Alba García Fernández

València, Marzo 2023

RAMÓN MARTÍNEZ MÁÑEZ, PhD in Chemistry and Professor at the *Universitat Politècnica de València*, and ALBA GARCÍA FERNÁNDEZ, PhD in Biotechnology at the *Universitat Politècnica de València*.

CERTIFY:

That the work "**Pharmacological senolysis as a new therapeutic approach for the prevention of doxorubicin-induced cardiotoxicity**" has been developed by Araceli Lérida Viso under their supervision in the Instituto Interuniversitario de Investigación de Reconocimiento Molecular y Desarrollo Tecnológico (IDM) of the *Universitat Politècnica de València*, forming part of the *Unidad Mixta UPV-IIS La Fe*, as a Thesis Project in order to obtain the degree PhD in Biotechnology at the *Universitat Politècnica de València.*

Valencia, Marzo 2023

Prof. Ramón Martínez Máñez — Director

Dra. Alba García Fernández — Directora

A mi madre,

siempre.

"Defiende tu derecho a pensar,
porque incluso pensar de manera errónea
es mejor que no pensar."

Hipatia

"...hay que mejorar las condiciones sociales,
compartir más las cargas familiares.
Si se hace, en un futuro no muy lejano
la mujer ocupará el lugar que le corresponde."

Margarita Salas

Agradecimientos

Acknowledgments

Los agradecimientos, sin duda la parte que más ganas tenía de escribir, porque esta tesis, por supuesto, no la he escrito yo sola. Aunque me va a costar resumir estos últimos cinco años y daros a todos el espacio que merecéis.

En primer lugar, me gustaría agradecer a mi director, Ramón, por darme la oportunidad de realizar esta tesis doctoral. Gracias por todas las oportunidades que me has dado para crecer profesional y, aún más importante, personalmente. A mi directora, Alba, por haberme acompañado de manera incansable en los últimos años de tesis. Empezamos como compañeras de bancada y realmente no sé qué habría hecho sin ti al final. Gracias por llegar en el momento más indicado, por tu disponibilidad a cualquier hora (gracias por no bloquearme en whatsapp), y por acompañarme en el (inserte su adjetivo) proceso de publicar. Gracias por haber hecho este camino más fácil. Eres una de las personas más resolutivas e inteligentes que he conocido, espero que no se te olvide este poder.

Gracias a todos mis compañeros del IDM. A todas las personas de administración, gracias por hacer más fácil el camino. A todos mis compañeros repartidos por los numerosos laboratorios (2.6, CPI, La Fe…) y a los investigadores seniors del grupo. Hemos sido tantos en el laboratorio que no os podría mencionar de manera individual, así que os incluyo en un agradecimiento común, ha sido un placer aprender a vuestro lado y haber compartido momentos con vosotros. Aunque sí tengo que hacer especial mención a aquellos con los que he tenido la suerte de trabajar a su lado. A María, por tu paciencia infinita para explicarme las cosas más simples,

mientras yo te seguía a todas partes en aquel frustrado intento de ser química. A Angy, que heredó la carga de educarme en un laboratorio de química. Gracias por ser mi *partner*, por tu esfuerzo para que esta tesis siguiera adelante, gracias por tener siempre las mejores nanopartículas preparadas para mí y gracias por tu ayuda cuando he necesitado una mano química amiga, tu trabajo está en esta tesis. Y por las buenas risas también, por qué no decirlo, durante el intento frustrado de hacer unas "nanos barrocas". A todos los que formáis la CPI, gracias por acogerme, recuerdo con mucho cariño mi tiempo allí.

Me paso ya a agradecer a mis compañeros y amigos del CIPF, mi mayor suerte en este camino. Primero a mi gente del I-12, que estuvo ahí cuando llegué tan perdida y que han seguido ahí a lo largo del camino. A Mar, gracias por tener siempre las puertas abiertas para mí. Gracias por tus palabras de ánimo, por tus consejos, por tu ayuda desinteresada y principalmente, por ser un ejemplo de investigadora. A Mónica, gracias por toda la ayuda, por tu eficacia y por tener siempre la solución a cualquier problema en el lab, he aprendido mucho de ti. A Ally, (¡Ay, Dios mío por dónde empiezo…!), yo ya sabía qué eras una persona importante antes de conocerte (estaba tu nombre escrito en todas partes). Aunque en tu inicio necesitaras subtítulos para entenderme (ejem…), se ve que has conseguido adaptar el oído al andaluz para acabar compartiendo brunchs y gintonics. Gracias por tu risa, por ser la persona a la que siempre he podido acudir, por estar siempre dispuesta a ayudar y, en resumen, por hacer la vida en el laboratorio (y fuera) mucho más fácil y divertida. Eres una grande y te quiero muchísimo.

A todas mis chicas compis de bancada, del I-12 y UPV (mis principesas), a fin de cuentas, no puedo diferenciar. Desde las que estaban al principio, y se han ido doctorando por el camino, a los que han ido llegando para compartir alegrías (y algunas penas) día tras día. Gracias por crear un gran entorno de trabajo, una de las mejores cosas que me llevo de estos años. A Paula Soriano (Paula Rubia), gracias por tu energía y por transmitir tu alegría y positividad allá por donde pasas. A Paula Carrascosa (Paula Morena) por toda tu ayuda y todas las risas, que fueron muchas, el tiempo que estuviste con nosotras. A Irene, por introducirme en el maravilloso mundo de la senescencia y por acompañarme en los primeros pasos en el laboratorio. A mis principesos que fueron llegando después: Elena, Blanca, Javi, Juanjo, David. Gracias por todos los momentos compartidos, las comidas en endogamia postpandemia y por las risas que hacen que el trabajo sea más fácil. Gracias por ser compañeros y estar siempre para echarme una mano cuando lo he necesitado. Sois muy grandes. Ya os queda nada para estar escribiendo vuestros propios agradecimientos.

Especial mención a mis chicas, Estefi, Gema y Alejandra, que han sido fundamentales no solo en mi tesis, si no en mi vida, todos estos años. Me falta páginas para vosotras. A Estefi, no sé por dónde empezar a agradecerte. He aprendido tanto contigo que ahí sí que me da para escribir un libro (aunque tú te empeñes en que escriba otro). Gracias por confiar en que yo podía ser tu amiga. Gracias por todas las infinitas conversaciones, por tu apoyo incondicional, por tu capacidad crítica, por hacerme despertar muchas veces. Por escuchar todas mis ideas, unas más locas que otras, analizarlas conmigo y darles alas. También por estar para recogerme después del naufragio (jaja).

Lo simplifico, porque si no, no acabo. Gracias por ser una AMIGA, en mayúsculas. Sé que te llevo para toda la vida, igual que tú me llevas a mí. A Gema, mi agapornis, gracias por haber sido parte indispensable para mí durante esta etapa. Gracias por todo tu apoyo dentro y fuera del laboratorio. Por el tiempo compartido, los millones de momentos, viajes, risas y entrenamientos diarios durante la pandemia. Gracias por escuchar y por preocuparte con tanto cariño y por compartir y dar valor a las cosas importantes de la vida. Aunque tus comentarios inapropiados me hayan traído algún problema (jaja), estoy dispuesta a ver que más momentos nos trae la vida. A Alejandra, mi siamesa en la tesis. No puedo estar más agradecida de haberte encontrado como compañera de batalla durante este camino. Gracias por todo lo que hemos aprendido juntas (dentro y fuera del lab), por todo el trabajo que hemos sacado mano a mano, gracias por ir siempre un paso por delante para hacerme el camino más fácil. Ha sido una etapa llena de aprendizaje y de crecimiento y no podía haber encontrado alguien mejor para formar equipo. Ya estabas en mi vida antes de la tesis (TFM, jeje), así que imagina el camino que aún nos queda. A las 3, os quiero con todo mi corazón. Gracias, una vez más.

A todas las personas que formáis el CIPF, gracias por hacerme sentir una más de esta gran casa. Recuerdo con mucho cariño aquellas mesas prepandemia infinitas a la hora de comer, cada día con una historia diferente. A Pilar, el CIPF no podría tener una mejor cara representativa, gracias por toda tu ayuda, al personal de mantenimiento, personal de informática, limpieza, administración,… gracias por tener siempre una solución para mí, por vuestra amabilidad y por vuestro trabajo, muchas veces invisible, que

hace que el CIPF funcione. A mis chicos de cafetería, Javi, Mónica (mi lagarta) y Emilio, gracias por alimentarme cada día, literalmente. Gracias por tener siempre una sonrisa y una broma para mí, tan necesarias en las laaargas jornadas. Sois increíbles. Gracias a todas las personas que formáis los servicios científicos del CIPF, Alberto (confocal), Mario (histología), Alicia (citometría), Laura (genómica), y Viviana, Nerea y Amparo (animalario), vuestra ayuda ha sido fundamental durante todos estos años. Gracias por toda vuestra sabiduría, gracias por estar siempre dispuestos a orientarme y a formarme. Gracias por haber trabajado, mano a mano, conmigo, en muchas ocasiones. Agradezco especialmente a Viviana, mi compañera ecógrafa. Solo tú y yo sabemos las horas que hemos pasado en esos sótanos ecografiando corazones enanos. Gracias por estar siempre dispuesta, por no abandonarme nunca en este arduo aprendizaje. Si puedo presentar estos datos, es gracias a ti. Y gracias, por supuesto, por hacer de esos meses, contra todo pronóstico, una experiencia divertida. Nos hemos contado la vida en verso en esa sala, medio intoxicadas de sevofluorano y si eso no une… que me diga alguien qué. Especial mención también al responsable de microscopía (jaja), mi Xiti. Alberto, primero te agradezco toda tu ayuda profesional, ¡cuántas horas a oscuras buscando lo que no había! Cuanta paciencia infinita hora tras hora optimizando condiciones y aclarándome, con esa sabiduría que te caracteriza, una y otra vez todas mis dudas. Eres un gran profesional, pero eres aún mejor persona. Gracias por ser un pilar básico también fuera de la ciencia, por todas las risas, por tener siempre una cena lista, una palabra de apoyo y un hombro donde llorar. Gracias por aguantar con talante todas mis ocurrencias y por aconsejarme cuando se me iba de las manos. Gracias por aguantar todos los

temas en bucle a los que te hemos arrastrado Estefi y yo, paseando por el Leroy. Gracias, por estar. Te quiero mucho, ya lo sabes.

También tengo palabras para todas las personas que he conocido en el CIPF: Mari Paz, Magda, Carmen, Angie, Ana, Carlos, Rubén… Gracias por esas comidas cargadas de debate y risas. A Mari Paz, gracias por estar siempre dispuesta a ayudar y por todos los momentos compartidos. A Carlos, no solo por las conversaciones que tanto han dado para debatir, gracias por ayudarme experimentalmente en todos mis inicios con el RNA, gracias por ser mi referente en ese campo. En este punto, no puedo olvidar a Juan Ureña. Muchas gracias por toda tu ayuda, las qPCR que presento en esta tesis tienen mucho de ti. Gracias por ayudarme a planificar, diseñar, analizar, por contestar a todas mis dudas, también las más básicas, siempre con una sonrisa. No sé qué habría hecho sin ti en ese camino. Y qué injusto que ya no estés para verlo, yo conservo todo ese aprendizaje con todo mi cariño.

Gracias a mi familia de Valencia, las personas con las que he convivido durante estos años, a las que les tengo que agradecer en gran parte el cuidado de mi salud mental. A Vanessa, por ser una hermana mayor y una amiga. Fuiste mi primer contacto en Valencia, y qué suerte tuve. Gracias por acogerme entre tus amigos y tu familia, gracias por los años de convivencia que son inolvidables, por las risas, por los viajes, por las mil historias vividas, por escucharme, por apoyarme y por tener siempre palabras de cariño. Gracias por ser un ejemplo de empatía y por ser un lugar seguro. Y, por supuesto, gracias por darme un sobri tan guapo, Elián, que ha llegado, como bien predije, justo en el momento que tenía que llegar. A Anabel y Albert, tan indispensables en aquellas primeras etapas de mi vida en Valencia, por formar

mi primer equipo valenciano y por hacerme la vida más divertida, e intensita. A Leire, gracias por llegar en el momento que más necesitaba. Gracias por salvar esa postpandemia con millones de horas de conversación, por darle vueltas y vueltas al río junto a mí, por las tardes en Yu y por las pizzas de los viernes. Gracias por dejarme conocerte con tanta honestidad y por querer conocerme a mí, de la misma forma. Gracias por salvar el mundo juntas tantas veces y todos los días. Gracias por aguantar esta última etapa de crisis existencial y por compartir tantos momentos juntas, que solo son el principio. Gracias, por supuesto, por tus memes, que deberían ser patrimonio cultural. A Sara, que también llegó en el momento más oportuno, después de los años. Fue una suerte tenerte de vuelta a mi vida cada día. Gracias por haber estado en esta última parte de la aventura, gracias por ser un ejemplo de fortaleza, de inconformismo. Gracias por siempre tener un detalle para alegrarme y gracias por tus aventuras que tantas risas nos traen. A las 3, os quiero siempre cerca.

Gracias a mis amigos de toda la vida, mis amigos de Lucena, por seguir alegrando cada momento de vacaciones, por vuestra amistad a lo largo de los años, gracias por recordarme siempre de dónde vengo. A los amigos que llegaron con la carrera y forman parte de mi vida. Azahara y Ana, gracias por ser las personas que más me han visitado en la terreta, para nosotras quedan todas las risas (y la última fiesta que vivimos en dos años). A Azahara, por demostrarme una y otra vez que siempre eres casa. A Jose, mi eterno compañero de aventuras, no quiero otro. A mis chicas del máster, Cris, Inés, Clara y Sara, porque veros siempre es una recarga de energía.

A mi familia, que son parte de mi identidad. A mi padre, por trabajar de manera inagotable para darnos las oportunidades que tú no has podido

tener. Gracias por mantenerte, a pesar de todo, cuando el camino no es fácil. A mis hermanos, Paco y Jesús, porque juntos hemos demostrado, muchas veces, poder con todo. A Paco, gracias por tu sensibilidad, es tu mayor fortaleza. A Jesús, gracias por tu lealtad, por ser un apoyo incondicional. A mi Arya, ojalá te tuviera más cerca. A mi abuela, que nunca tuvo la oportunidad de leer y escribir y es la que mejor sabe definir mi trabajo. Aunque ella no lo sabe, es una gran feminista. A mi tío, siempre fuerte. A Laura, mi hermana de no sangre, pero familia igualmente. A ti, te lo agradezco todo y te lo agradeceré siempre. Gracias por acompañarme, cada uno a vuestra manera, en un camino que no llegáis a comprender.

A mi madre, que te fuiste demasiado pronto. A ti te agradezco gran parte de lo que soy. Estás conmigo siempre y por eso este nuevo logro, al igual que todos, tiene mucho de ti.

A todos los que me habéis acompañado en esta etapa, los que han venido para quedarse y los que me han acompañado de manera temporal, los que me habéis ofrecido vuestra ayuda, vuestro cariño, vuestras palabras de ánimo, vuestros abrazos, a los que habéis estado en los planes de sol, de tardes de cerveza y de noches que se alargan, a los que habéis estado lejos, pero habéis estado, y a todos los que me hacéis sentir segura y confiáis en mí, más de lo que yo misma hago. En conclusión, gracias a todos los que habéis hecho que este camino pueda parecer si no fácil, mucho menos difícil. A todos vosotros, muchas gracias, esta tesis lleva mucho de vuestro amor.

Os quiero mucho y os quiero siempre.

Ara.

Resumen

Muchos agentes anticancerígenos utilizados en la clínica inducen senescencia prematura en los tejidos sanos que genera procesos de envejecimiento acelerado y efectos secundarios adversos en los pacientes. En particular, la administración de doxorrubicina, una antraciclina muy eficaz y ampliamente utilizada como terapia antitumoral en la práctica clínica, induce la aparición de cardiotoxicidad irreversible. La exposición a doxorrubicina afecta gravemente a la población de células cardíacas tanto en ratones como en corazones humanos al inducir senescencia prematura, lo que puede representar la base molecular de la cardiomiopatía inducida por este tratamiento.

La presente tesis doctoral titulada "La terapia senolítica como nuevo enfoque terapéutico para la prevención de la cardiotoxicidad inducida por la doxorrubicina" se centra en explorar la eliminación de células senescentes (senolisis) *in vitro* e *in vivo* mediante la administración del fármaco senolítico, navitoclax, como opción terapéutica para prevenir la cardiotoxicidad asociada al tratamiento antitumoral con doxorrubicina. Navitoclax es uno de los senolíticos más potentes y ampliamente conocido en el campo de la senescencia celular pero su administración está asociada a la aparición de efectos adversos, principalmente trombocitopenia. Con el objetivo de mejorar el perfil terapéutico del fármaco, se han desarrollado dos estrategias específicamente dirigidas a células senescentes que incluyen la encapsulación y el desarrollo de un profármaco basado en navitoclax.

En la introducción se incluye una descripción general de la senescencia celular, incluyendo su mecanismo y características específicas,

así como su papel a nivel fisiológico y patológico. También se abordan las diferentes terapias senolíticas, su implicación en clínica y especialmente se introduce el fármaco navitoclax. Con el objetivo de mejorar la terapia dirigida, se exponen los conceptos básicos de nanotecnología y nanomedicina, poniendo especial atención en las nanopartículas de sílice mesoporosas (MSNs) y su potencial traslacionalidad a la práctica clínica. Finalmente, se detalla el papel de la senescencia en diferentes problemas cardíacos y el potencial terapéutico de las terapias senolíticas para su prevención.

A continuación, se presentan los objetivos específicos que se abordan en este proyecto de tesis y los diferentes métodos experimentales.

En la primera sección experimental, abordamos la inducción de senescencia en un modelo *in vitro* de cardiomiocitos y evaluamos la terapia senolítica como estrategia terapéutica. Desarrollamos y caracterizamos, así mismo, las nanopartículas y la prodroga basada en navitoclax. Este nanodispositivo senolítico se basa en MSNs cargadas con navitoclax y funcionalizadas con un hexa-galacto-oligosacárido (galactán). Por su parte, la prodroga se obtiene tras la conjugación del navitoclax a una molécula de galactosa acetilada. En ambos casos, el mecanismo de la terapia dirigida radica en la presencia de la enzima lisosomal β-galactosidasa, la cual presenta mayor expresión en las células senescentes. Al entrar en el lisosoma de células senescentes, los enlaces glicosídicos se hidrolizan por acción de la enzima, liberando el fármaco para su función. Los resultados muestran un aumento del efecto terapéutico del fármaco libre.

Tras la validación de los sistemas *in vitro*, ponemos a punto un modelo murino de cardiotoxicidad donde demostramos que la administración sistémica de doxorrubicina induce la expresión de marcadores de cardiotoxicidad y senescencia en el corazón de ratones tratados y contribuye al deterioro de la función cardíaca de los animales seguido por ecografía. En este modelo preclínico, el tratamiento combinado de doxorrubicina con el senolítico navitoclax, en las diferentes formulaciones descritas, conduce a la disminución significativa de los marcadores de senescencia y cardiotoxicidad junto con el restablecimiento de la función cardíaca y, se observa, de manera similar con las tres estrategias mencionadas: fármaco libre, fármaco encapsulado y fármaco en formulación de prodroga. Estos resultados evidencian el potencial uso clínico de las terapias senolíticas para aliviar la cardiotoxicidad inducida en pacientes tratados con quimioterapia.

Finalmente, se presenta una discusión de nuestros resultados con el resto de los trabajos publicados en este campo, así como unas conclusiones generales derivadas de esta tesis doctoral. Los resultados científicos presentados en esta tesis resaltan el papel de la senescencia en la progresión de cardiotoxicidad por la administración de doxorrubicina. Se concluye que los sistemas senolíticos aquí evaluados podrían ser una herramienta importante para el desarrollo de nuevas estrategias terapéuticas en el campo de la prevención de efectos secundarios asociados a terapia y supone una alternativa para las limitaciones presentadas de los tratamientos actuales. Esperamos que estos resultados abran nuevas oportunidades de investigación e inspiren el desarrollo de nuevas estrategias para solventar un problema sin solución clínica actual.

Resum

Molts agents anticancerígens utilitzats en la clínica indueixen senescència prematura en els teixits sans que genera processos d'envelliment accelerat i efectes secundaris adversos en els pacients. En particular, l'administració de doxorrubicina, una antraciclina molt eficaç i àmpliament utilitzada com a teràpia antitumoral en la pràctica clínica, indueix l'aparició de cardiotoxicitat irreversible. L'exposició a doxorrubicina afecta greument a la població de cèl·lules cardíaques tant en ratolins com en cors humans en induir senescència prematura, la qual cosa pot representar la base molecular de la cardiomiopatia induïda per aquest tractament.

La present tesi doctoral titulada "La teràpia senolítica com a nou enfocament terapèutic per a la prevenció de la cardiotoxicitat induïda per la doxorrubicina" se centra en explorar l'eliminació de cèl·lules senescents (senolisis) *in vitro* i *in vivo* mitjançant l'administració del fàrmac senolític, navitoclax, com a opció terapèutica per a previndre la cardiotoxicitat associada al tractament antitumoral amb doxorrubicina. Navitoclax és un dels senolítics més potents i àmpliament conegut en el camp de la senescència cel·lular però la seua administració està associada a l'aparició d'efectes adversos, principalment trombocitopenia. Amb l'objectiu de millorar el perfil terapèutic del fàrmac, s'han desenvolupat dues estratègies específicament dirigides a cèl·lules senescents que inclouen l'encapsulació i el desenvolupament d'un profàrmac basat en navitoclax.

En la introducció s'inclou una descripció general de la senescència cel·lular, incloent-hi el seu mecanisme i característiques específiques, així com el seu paper a nivell fisiològic i patològic. També s'aborden les diferents

teràpies senolítiques, la seua implicació en clínica i especialment s'introdueix el fàrmac navitoclax. Amb l'objectiu de millorar la teràpia dirigida, s'exposen els conceptes bàsics de nanotecnologia i nanomedicina, posant especial atenció en les nanopartícules mesoporoses de sílice (MSNs) i la seua potencial traslacionalitat a la pràctica clínica. Finalment, es detalla el paper de la senescència en diferents problemes cardíacs i el potencial terapèutic de les teràpies senolítiques per a la seua prevenció.

A continuació, es presenten els objectius específics que s'aborden en aquest projecte de tesi i els diferents mètodes experimentals.

En la primera secció experimental, abordem la inducció de senescència en un model *in vitro* de cardiomiòcits i avaluem la teràpia senolítica com a estratègia terapèutica. Desenvolupem i caracteritzem, així mateix, les nanopartícules i la prodroga basada en navitoclax. Aquest nanodispositiu senolític es basa en MSNs carregades amb navitoclax i modificades amb un hexa-galacto-oligosacàrid (galactán). Per part seua, la prodroga s'obté després de la conjugació del navitoclax a una molècula de galactosa acetilada. En tots dos casos, el mecanisme de la teràpia dirigida radica en la presència de l'enzim lisosòmic β-galactosidasa, la qual presenta major expressió en les cèl·lules senescents. En entrar en el lisosoma de cèl·lules senescents, els enllaços glicosídics s'hidrolitzen per acció de l'enzim, alliberant el fàrmac per a la seua funció. Els resultats mostren un augment de l'efecte terapèutic del fàrmac lliure.

Després de la validació dels sistemes *in vitro*, posem a punt un model de ratolí on vam demostrar que l'administració sistèmica de doxorrubicina indueix l'expressió de marcadors de cardiotoxicitat i senescència en el cor de

ratolins tractats i contribueix a la deterioració de la funció cardíaca dels animals seguit per ecografia. En aquest model preclínic, el tractament combinat de doxorrubicina amb el senolític navitoclax, en les diferents formulacions descrites, condueix a la disminució significativa dels marcadors de senescència i cardiotoxicitat juntament amb el restabliment de la funció cardíaca i, s'observa, de manera similar amb les tres estratègies esmentades: fàrmac lliure, fàrmac encapsulat i fàrmac en formulació de prodroga. Aquests resultats evidencien el potencial ús clínic de les teràpies senolítiques per a alleujar la cardiotoxicitat induïda en pacients tractats amb quimioteràpia.

Finalment, es presenta una discussió dels nostres resultats amb la resta dels treballs publicats en aquest camp, així com unes conclusions generals derivades d'aquesta tesi doctoral.

Els resultats científics presentats en aquesta tesi ressalten el paper de la senescència en la progressió de cardiotoxicitat per l'administració de doxorrubicina. Es conclou que els sistemes senolítics ací avaluats podrien ser una eina important per al desenvolupament de noves estratègies terapèutiques en el camp de la prevenció d'efectes secundaris associats a teràpia i suposa una alternativa per a les limitacions presentades dels tractaments actuals. Esperem que aquests resultats inspiren noves oportunitats d'investigació així com el desenvolupament de noves estratègies per a solventar un problema sense solució clínica actual.

Abstract

Many anticancer agents used in the clinic induce premature senescence in healthy tissues leading to accelerated aging processes and adverse side effects in patients. In particular, the administration of doxorubicin, a highly effective anthracycline widely used as antitumor therapy in clinical practice, induces the development of irreversible cardiotoxicity. Doxorubicin exposure severely affects the cardiac cell population in both mouse and human hearts by inducing premature senescence, which may represent the molecular basis of cardiomyopathy induced by this treatment.

The present PhD thesis entitled " Pharmacological senolysis as a new therapeutic approach for the prevention of doxorubicin-induced cardiotoxicity" focuses on exploring the elimination of senescent cells (senolysis) *in vitro* and *in vivo* by administration of the senolytic drug, navitoclax, as a therapeutic option to prevent cardiotoxicity associated with antitumor treatment with doxorubicin. Navitoclax is one of the most potent and widely known senolytics in the field of cellular senescence, but its administration is associated with the occurrence of adverse effects, mainly thrombocytopenia. In order to improve the therapeutic profile of the drug, two strategies specifically targeting senescent cells have been developed, including encapsulation and the development of a navitoclax-based prodrug.

The introduction comprises a general description of cellular senescence, including its mechanism and specific characteristics, as well as its role at physiological and pathological levels. The different senolytic therapies, their clinical implication and especially the drug navitoclax are also

discussed. With the aim of improving targeted therapy, the basic concepts of nanotechnology and nanomedicine are presented, paying special attention to mesoporous silica nanoparticles (MSNs) and their potential translatability to clinical practice. Finally, the role of senescence in different cardiac problems and the therapeutic potential of senolytic therapies for its prevention are detailed.

The specific objectives addressed in this thesis project and the different experimental methods are presented below.

In the first experimental section, we addressed the induction of senescence in an *in vitro* cardiomyocyte model and evaluated senolytic therapy as a therapeutic strategy. We also developed and characterized the nanoparticles targeting senescent cells and the navitoclax-based prodrug. The senolytic nanodevice is based on MSNs loaded with navitoclax and functionalized with a hexa-galacto-oligosaccharide (galactan). The prodrug is obtained after conjugation of navitoclax to an acetylated galactose molecule. In both cases, the mechanism of targeted therapy lies in the presence of the lysosomal enzyme β-galactosidase, which is highly expressed in senescent cells. Upon entering the lysosome of senescent cells, the glycosidic bonds are hydrolyzed by the action of the enzyme, releasing the drug. The results show an increase in the therapeutic effect of the free drug.

After validation of the *in vitro* systems, we developed a murine model of cardiotoxicity in which we demonstrated that systemic administration of doxorubicin induces the expression of markers of cardiotoxicity and senescence in the heart of treated mice and contributes to the deterioration of the cardiac function of the animals followed by echocardiography. In this

preclinical model, the combined treatment of doxorubicin with the senolytic navitoclax, in the different formulations described above, leads to significant decrease in senescence and cardiotoxicity markers along with restoration of cardiac function. Similar results were observed with the three strategies mentioned: free drug, encapsulated drug, and prodrug formulation. These results demonstrate the potential clinical use of senolytic therapies to alleviate cardiotoxicity induced in patients treated with chemotherapy.

Finally, a discussion of our results taking into account other published work in this field is presented, as well as some general conclusions derived from this doctoral thesis. The scientific results presented in this thesis highlight the role of senescence in the progression of cardiotoxicity by doxorubicin administration. It is concluded that the senolytic systems evaluated here could be an important tool for the development of new therapeutic strategies in the field of prevention of therapy-associated side effects and represent an alternative to the limitations of current treatments. We hope that these results will open new research opportunities and inspire the development of new strategies to solve a problem with no current clinical solution.

Publications

Results of this PhD thesis and other contributions have resulted in the following scientific publications:

- **Lérida-Viso, A.**, Estepa-Fernández, A., Morellá-Aucejo, Á., Lozano-Torres, B., Alfonso, M., Blandez, J. F., Bisbal, V., Sepúlveda, P., García-Fernández, A., Orzáez, M., Martínez-Máñez, R. Pharmacological senolysis reduces doxorubicin-induced cardiotoxicity and improves cardiac function in mice. *Pharmacoligal Research.* **2022**, Sep;183:106356. doi: 10.1016/j.phrs.2022.106356.
- Prieto-Castañeda, A., **Lérida-Viso, A**., Avellanal-Zaballa, E., Sola-Llano, R., Bañuelos, J., Agarrabeitia, A. R., Martínez-Máñez, R., Ortiz, M. J. Phosphorogenic dipyrrinato-iridium(III) complexes as photosensitizers for photodynamic therapy. *Dyes and Pigments*, **2022**, 197, 109886. doi: 10.1016/J.DYEPIG.2021.109886
- González-Gualda, E., Pàez-Ribes, M., Lozano-Torres, B., Macias, D., Wilson III, J. R., González-López, C., Ou, H.-L., Mirón-Barroso, S., Zhang, Z., **Lérida-Viso, A**., Blandez, J. F., Bernardos, A., Sancenón, F., Rovira, M., Fruk, L., Martins, C. P., Serrano, M., Doherty, G. J., Martínez-Máñez, R., Muñoz-Espín, D. Galacto-conjugation of navitoclax as an efficient strategy to increase senolytic specificity and reduce platelet toxicity. *Aging Cell*, **2020** Apr;19(4):e13142. doi: 10.1111/acel.13142
- Estepa-Fernández, A., Alfonso, M., Morellá-Aucejo, Á., García-Fernández, A., **Lérida-Viso, A**., Lozano-Torres, B., Galiana, I.,

Soriano-Teruel, P. M., Sancenón, F., Orzáez, M., Martínez-Máñez, R. Senolysis Reduces Senescence in Veins and Cancer Cell Migration. *Advanced Therapeutics*, **2021**. 4: 2100149. doi:10.1002/adtp.202100149

- Estepa-Fernández, A., García-Fernández, A., **Lérida-Viso, A**., Blandez, J. F., Galiana, I., Sancenón, F., Orzáez, M., & Martínez-Máñez, R. Combination of palbociclib with Navitoclax based-therapies shows antitumoral activity *in vivo* in triple-negative breast cancer. *Pharmacological Research*. **2022**, Dec 21;187:106628. doi: 10.1016/j.phrs.2022.106628.
- Estepa-Fernández, A., García-Fernández, A., **Lérida-Viso, A**., Morellá-Aucejo, Á., Esteve-Moreno, J. J., Blandez, J. F., Alfonso, M., Candela-Noguera, V., Vivo-Llorca, G., Sancenón, F., Orzáez, M., & Martínez-Máñez, R. Engineering nanoparticle communication in living systems by stigmergy: an application to enhance antitumor therapy in triple-negative breast cancer. *Nano Today*, **2023**, 48:101692. doi.org/10.1016/j.nantod.2022.101692
- **Lérida-Viso, A.**, Estepa-Fernández, A., García-Fernández, A., Martí-Centelles V., Martínez-Máñez, R. Biosafety features of mesoporous silica nanoparticles towards clinical translation. *Submitted,* **2022.**
- Estepa-Fernández, A., Galiana, I**., Lérida-Viso, A**., García-Jareño, A. B., García-Fernández, A., Sancenón, F., Martínez-Máñez, R., & Orzáez, M. Identification of a novel senolytic hexapeptide for malignant melanoma. *Submitted.*

Abbreviations and Acronyms

α-Fuc	α-L-fucosidase
ABT-263	Navitoclax
ACE	Angiotensin-converting enzyme
Actb	Actin beta
Akt	Protein kinase B
ALB	Albumin
ALP	Alkaline phosphatase
ALT	Alanine transaminase
ANF	Atrial natriuretic factor
ANOVA	Analysis of variance
APTES	(3-Aminopropyl)triethoxysilane
ATP	Adenosine triphosphate
ATR	Attenuated total reflectance
β-gal	β-galactosidase
B2M	Beta-2 microglobulin
Bak	Bcl-2 associated killer protein
Bax	Bcl-2 associated X protein
BCA	Bicinchoninic acid
Bcls	B-cell lymphoma proteins
Bcl-2	B-cell lymphoma 2
Bcl-w	Bcl-2-like protein 2
Bcl-xL	B-cell lymphoma-extra large
BET	Brunauer−Emmett−Teller
Bim	Bcl-2-interacting mediator of cell death
BJH	Barret-Joyner-Halenda
Bok	Bcl-2-related ovarian killer

BrdU	Bromodeoxy uridine or 5-bromo-2'-deoxyuridine
BSA	Bovine serum albumin
BUN	Blood urea nitrogen
C57BL/6J	Mice strain
CCL	Chemokine C-C motif ligand
cDNA	Complementary DNA
C_{12}FDG	5-dodecanoylaminofluorescein di-β-D-galactopyranoside
CD9	Cluster of differentiation 9
CDK	Cyclin-dependent kinase
CDKi	Cyclin-dependent kinase inhibitor
CMs	Cardiomyocytes cells
CRBN	Cereblon
COSY NMR	Two-dimensional nuclear magnetic resonance spectroscopy
CPCs	Cardiac progenitor cells
CREA	Creatinin
CSNRs	Core–shell spiky nanorods
CTAB	Cetyltrimethylammonium bromide
Cu_xCo_yS	Chiral nanoparticles
CXCL	Chemokine C-X-C motif ligand
DAPI	4′,6-diamidino-2-phenylindole
DDR	DNA-damage checkpoint responses
DLS	Dynamic light scattering
DMEM	Dulbecco’s Modified Eagle’s Medium
DMSO	Dimethylsulfoxide
DNA	Deoxyribonucleic acid
DNase I	Deoxyribonuclease I
DOX	Doxorubicin
D+Q	Dasatinib and Quercetin

DSBs	Double-strand breaks
E2F	E2 promoter binding factor
EA	Elemental analysis
Echo	Echocardiography
ED	End diastole
Edn3	Endothelin 3
EDTA	Ethylenediaminetetraacetic acid
EF	Ejection fraction
EGTA	Ethylene glycol-bis(β-aminoethyl ether)-N,N,N',N'-tetraacetic acid
EMA	European Medicines Agency
eNOS	Endothelial nitric oxide synthase
ES	End systole
EVs	Extracellular vesicles
FBS	Fetal bovine serum
FDA	Food and Drug Administration
FOXO	Forkhead box protein O
FS	Fractional shortening
Gal	Hexa-galacto-oligosaccharide (galactan)
GalNP	Galactan nanoparticles
GAPDH	Glyceraldehyde-3-Phosphate Dehydrogenase
GDF15	Growth and differentiation factor 15
γH2AX	Phosphorylated H2A histone family member X
GMD	Galactose-modified duocarmycin
Gos	Galacto-oligosaccharides
HF	Heart failure
HIF-1α	Hypoxia-inducible factor 1-alpha
^{1}H-NMR	Proton nuclear magnetic resonance

HL-1	Cardiac muscle cell line
HRMS	High-resolution mass spectrometry
HSP90	Heat shock protein 90
hTNBC	Human triple-negative breast cancer
IP	Intraperitoneal injection
IV	Intravenous injection
IC50	Half maximal inhibitory concentration
ICG	Indocyanine green
IGFBP7	Insulin-Like Growth Factor-Binding Protein-7
IL-1α	Interleukin 1 alpha
IL-6	Interleukin 6
IL-8	Interleukin 8
IP	Intraperitoneal administration
IPF	Idiopathic pulmonary fibrosis
IRI	Ischaemia-Reperfusion Injury
IV	Intravenous administration
Ki67	Marker of proliferation Ki-67
LV	Left ventricle
LVEDD	Left ventricular end-diastolic dimension
LVESD	Left ventricular end-systolic dimension
MAPK	Mitogen-activated protein kinase
Mcl-1	Myeloid cell leukemia 1
MCM-41	Mobile Composition of Matter No. 4
MI	Myocardial infarction
MMP	Matrix metalloproteinase
mRNA	Messenger ribonucleic acid
MSNs	Mesoporous Silica Nanoparticles
mTOR	Mammalian target of rapamycin

NADH	Nicotinamide adenine dinucleotide
nanoMIPs	Molecularly imprinted polymer nanoparticles
Nav	Navitoclax
Nav-Gal	Galacto-conjugated navitoclax
NIR	Near-infrared
nm	Nanometers
NMR	Nuclear magnetic resonance
NP	Nanoparticle
OCT	Optimal cutting temperature
OG	Oral gavage
PAI1	Plasminogen activator inhibitor 1
p15	Cyclin-dependent kinase inhibitor 4B
p16	Cyclin-dependent kinase inhibitor 2A
p21	Cyclin-dependent kinase inhibitor 1
p27	Cyclin-dependent kinase inhibitor 1B
p53	Tumor protein p53
PAGE	Polyacrylamide gel electrophoresis
PBS	Phosphate buffer saline
PFA	Paraformaldehyde
PI	Propidium iodide
PI3K	Phosphatidylinositol-3-kinase
pRb	Phosphorylated retinoblastoma protein
PROTAC	Proteolysis-targeting chimera
PXRD	Powder X-ray diffraction
PZ	PZ15227
qRT-PCR	Quantitative real time-polymerase chain reaction
Rb	Retinoblastoma
RNA	Ribonucleic acid

ROS	Reactive oxygen species
RT	Room temperature
SA-β-Gal	Senescence-associated β- galactosidase
SAMP8	Senescence-accelerated mouse model
SAHF	Senescence-associated heterochromatic foci
SASP	Senescence-Associated Secretory Phenotype
SCs	Senescent cells
SCAPs	Senescent Cell Anti-Apoptotic Pathways
SD	Standard Deviation
SDS	Sodium dodecyl sulfate
SEM	Standard Error of Mean
SIPS	Stress-induced premature senescence
SMAD	SMA (small body size) MAD (mother against decapentaplegic)
SSK1	Senolytic prodrug of gemcitabine
TAF	Telomere-associated DNA damage foci
TBS	Tris-hydroxymethyl-aminomethane
TEM	Transmission electron microscopy
TEOS	Tetraethyl orthosilicate
TERT	Telomerase reverse transcriptase
TfR1	Transferrin receptor 1
TGA	Thermogravimetric analysis
TGFβ	Transforming growth factor β
TIS	Therapy-induced senescence
TMS	Trimethoxysilane
TNFα	Tumor necrosis factor α
Top2	Topoisomerase II
TPP	Triphenylphosphonium

Tris	Tris-buffered saline
UV	Ultraviolet
VEGF	Vascular endothelial growth factor
WGA	Wheat Germ Agglutinin
X-Gal	5-bromo-4-chloro-3-indolyl-β-D-galactopyranoside
ZP	Zeta potential
53BP1	p53-binding protein-1
5FURGa	Senolytic prodrug of 5-fluorouracil

List of Figures

List of Tables

Table of Contents

Introduction

1. Cellular senescence

Cellular senescence is a phenomenon defined as a stable cell cycle arrest in response to damaging or stressing stimuli, in which cells lose the proliferative capacity while remaining metabolically active (Hernandez-Segura et al., 2018; López-Otín et al., 2013). The phenotype associated with cellular senescence is heterogeneous and depends on cell type and context (Kirschner et al., 2020). Senescence differs from quiescence, a state of reversible growth arrest in response to nutrient signaling, in that senescence cell-cycle arrest is generally irreversible and is accompanied with macromolecular damage, specific signaling and an altered secretory phenotype affecting the nearby tissue (Gorgoulis et al., 2019).

The first evidence of senescence occurred in the 1960s when Leonard Hayflick and Paul Moorhead discovered that human diploid fibroblasts cultured *in vitro* have a limited proliferative capacity (Hayflick, 1965; Hayflick et al., 1961). Today, we know that the senescence observed by Hayflick is triggered by telomere shortening after successive replications, and thus is now defined as replicative senescence (Shay et al., 2000). Subsequent studies demonstrated that many different stimuli such as DNA damaging agents, oncogenic activation or loss of tumor suppressor genes, epigenetic changes, metabolic dysfunction, or the presence of reactive oxygen species (ROS), among others, contribute to another type of senescence known as stress-induced premature senescence (SIPS) or "premature senescence" (Herranz et al., 2018; Muñoz-Espín et al., 2014). Besides, many chemotherapeutic drugs can promote therapy-induced senescence (TIS)

either as the therapeutic mechanism of action or as a side effect (Campisi et al., 2007; Herranz et al., 2018; Muñoz-Espín et al., 2014) (**Figure 1**).

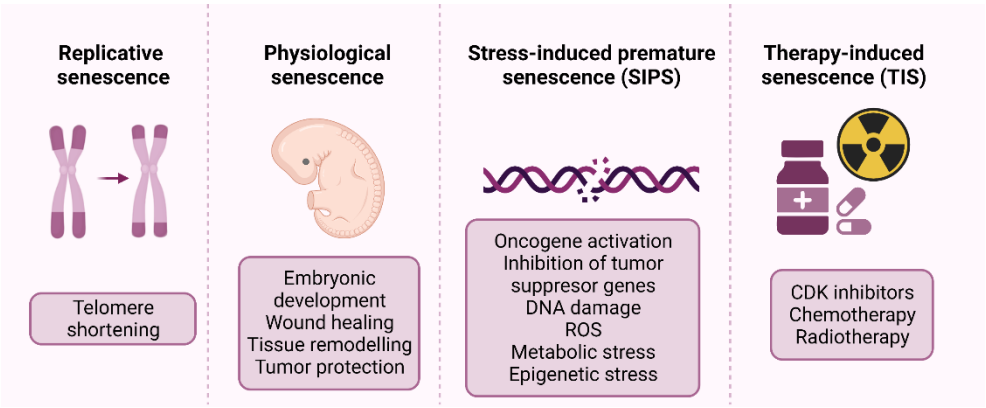

Figure 1. Types of cellular senescence.
Senescence can be triggered and classified in response to various intrinsic and extrinsic stimuli, including progressive telomere shortening (replicative senescence); developmental signal or wound healing (physiological senescence); oncogenic activation, DNA damage, oxidative and genotoxic stress, epigenetic changes, mitochondrial dysfunction (stress-induced premature senescence (SIPS)); and irradiation, or chemotherapeutic agents (therapy-induced senescence (TIS)), among others. ROS, reactive oxygen species; CDK, cyclin-dependent kinases. Adapted from Lozano-Torres et al., 2019.

1.1 Mechanism of cellular arrest

The senescence program is conserved across vertebrates and is controlled by diverse signaling pathways that block cell proliferation upon different stimuli triggers (Collado et al., 2010). The cell cycle exit is controlled by the activation of the p53/$p21^{CIP1}$ and/or $p16^{Ink4a}$/Rb axis, which converge in the activation of the cyclin-dependent kinase (CDK) inhibitors (CDKi) such as $p16^{INK4A}$, $p21^{CIP1}$, $p15^{INK4B}$ or $p27^{KIP1}$ (Campisi et al., 2007; Herranz et al., 2018; Muñoz-Espín et al., 2014). As a result of CDKs

inhibition, cell proliferation is arrested due to the hypophosphorylation of retinoblastoma protein (Rb), which sequesters the transcription factor E2F, preventing the expression of cell cycle progression genes (Chicas et al., 2010) (**Figure 2**).

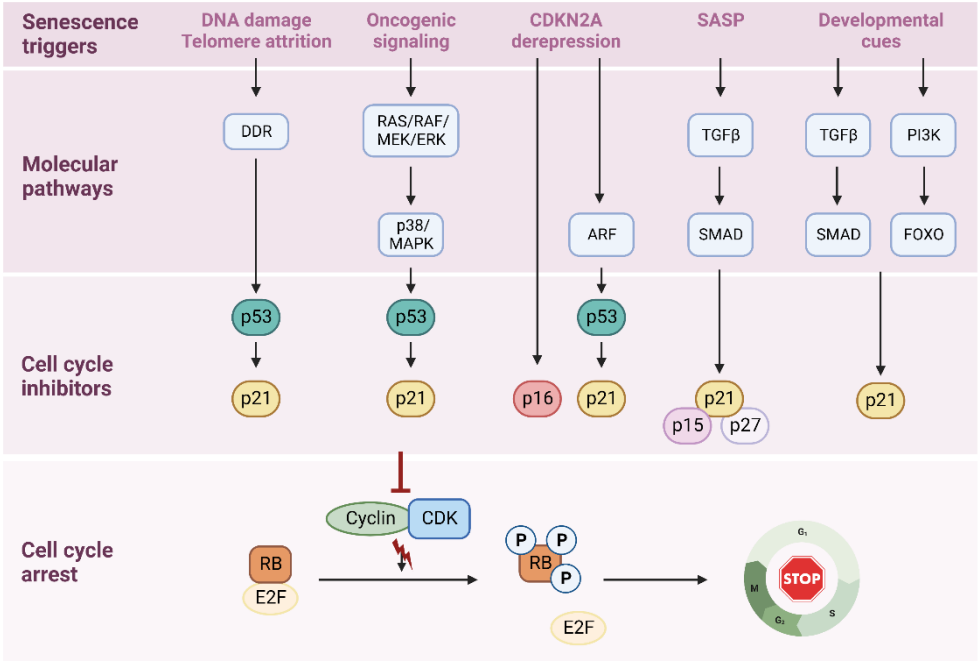

Figure 2. Molecular pathways of senescence cell cycle arrest.
Various senescence triggers can affect signaling pathways converging in the overexpression of cell cycle inhibitors, such as $p21^{CIP1}$ and $p16^{Ink4a}$. These proteins stop cyclin-dependent kinases (CDK)–cyclin complexes from phosphorylating the retinoblastoma protein (Rb). Consequently, the transcription factor E2F, which is usually responsible for the expression of the genes needed for cell cycle progression, is sequestered by Rb. The subsequent cell cycle arrest can be transient if cell damage is repaired and can lead to cell death by apoptosis or to permanent arrest known as senescence. DDR, DNA-damage response; SASP, senescence-associated secretory phenotype; TGFβ, transforming growth factor β; SMAD, SMA (small body size), MAD (mother against decapentaplegic); PI3K, phosphatidylinositol-3-kinase; FOXO, forkhead box protein O. Adapted from Lozano-Torres et al., 2019.

P53 is a transcription factor that regulates genes associated with cellular stress responses, DNA repair, apoptosis, and cell-cycle control (Rufini et al., 2013). The activation of p53 via phosphorylation (p-p53) upregulates the expression of the CDKi $p21^{CIP1}$, which inhibits CDK2-cyclin E and mediates cell cycle arrest at G1/S or G2/M, preventing cellular apoptosis through binding of caspases, and promotes the senescence state (Yosef et al., 2017). The activation of the p53/p21 pathway has been described in senescence induced by DNA-damage checkpoint responses (DDR), telomere shortening, ROS, and oncogene induction (Beauséjour et al., 2003; Fumagalli et al., 2012; Herbig et al., 2004). The p16/Rb pathway, upon activation of the INK4a/ARF genetic locus, is regulated by the action of the CDKi $p16^{INK4a}$ which binds to CDK4/6-cyclin D to arrest the cell cycle (Rayess et al., 2012). The p16/Rb pathway is also involved in ROS Induction through the mitogenic signaling cascade, which cooperates in maintaining the senescence state (Beauséjour et al., 2003; Takahashi et al., 2006).

1.2 Hallmarks of senescent cells

Due to the heterogenous senescent phenotype and the lack of universal or specific markers of senescence, the identification of senescent cells can be challenging, and it is a major limitation for their identification *in vitro* and *in vivo* (Kirschner et al., 2020; Sharpless et al., 2015). Thus, senescent cells are defined by a set of hallmarks that indirectly indicate senescence, including the implementation of cell cycle arrest, epigenetic changes, upregulation of pro-survival pathways, and a high metabolic active state which includes a context-dependent secretome (González-Gualda et al., 2021; Gorgoulis et al., 2019; Hernandez-Segura et al., 2018) (**Figure 3**).

The main hallmark of cellular senescence is the inability to progress through the cell cycle, therefore, the expression of markers responsible for cell proliferation such as p53, p21, or p16, and the decrease in phosphorylated Retinoblastoma protein (pRb) are suitable markers to identify senescent cells (Hernandez-Segura et al., 2018). Other markers associated with activation of the DNA damage response (DDR) as p38 mitogen-activated protein kinase (MAPK) or the CDKi $p15^{INK4b}$ and $p27^{KIP1}$ can also be indicative of senescence (González-Gualda et al., 2021). As a consequence of cell cycle arrest, cells lose the capacity to replicate, therefore the assessment of DNA synthesis, through 5-bromodeoxyuridine (BrdU) incorporation or the absence of proliferation markers as the nuclear protein Ki67 are also considered makers of senescence (Galvis et al., 2019; Muñoz-Espín et al., 2014). Other genetic and epigenetic alterations present in senescent cells are phosphorylated histone H2AX (γH2AX), p53-binding protein-1 (53BP1), the loss of lamin B1, shortening of telomere length and telomere-associated DNA damage foci (TAFs) (González-Gualda et al., 2021; Hewitt et al., 2012). Some cells also display senescence-associated heterochromatin foci (SAHF), where heterochromatin alterations silence the proliferation-related genes (Narita et al., 2003).

Because of changes in these signaling pathways, senescent cells show a series of morphological and structural changes *in vitro* (Hernandez-Segura et al., 2018). Senescent cells exhibit an enlarged and flattened shape, and enlarged nuclei and multinucleation can also occur *in vitro* (Campisi et al., 2007). Typically, senescent cells also present an altered composition of the plasma membrane and increases in granularity, presenting enlarged lysosomes and increased Golgi apparatus (Frescas et al., 2017; Hernandez-

Segura et al., 2018; Kuilman et al., 2010). Senescent cells are also characterized by the presence of lipofuscin granules and non-degradable aggregates of oxidized proteins, lipids, and oligosaccharides that accumulate progressively in the lysosomes (Evangelou et al., 2017; Georgakopoulou et al., 2012; Katz et al., 1984). It is important to note that *in vivo* senescent cells tend to maintain the morphology established by tissue architecture (Muñoz-Espín et al., 2014).

One of the most widely accepted markers of senescence is the activity of the lysosomal β-galactosidase enzyme, known as senescence-associated β-galactosidase (SA-β-Gal), an enzyme that catalyzes the hydrolysis of lysosomal β-galactosides into monosaccharides (Dimri et al., 1995). This activity is detectable due to the increased lysosomal content of senescent cells, which allows for the detection of lysosomal β-Gal even at suboptimal pH (pH 6.0) (Debacq-Chainiaux et al., 2009; Kurz et al., 2000; Lee et al., 2006). Nevertheless, SA-β-Gal activity is also induced by stresses such as prolonged confluence in culture or under serum starvation (Yang et al., 2005). Other lysosomal hydrolases, such as α-L-fucosidase (α-Fuc), have also been used to detect senescent cells (Hildebrand et al., 2013; Knaś et al., 2012).

Remarkably, senescent cells generally exert a complex secretion of factors, known as Senescence-Associated Secretory Phenotype, or SASP, which are also used as senescence markers (Coppé et al., 2010). The SASP is highly dynamic, its expression varies widely over time and depends on the inducer of senescence, the cell type, and the cellular context. The SASP has been extensively profiled by proteomics resulting in the SASP Atlas database (Basisty et al., 2020; Coppé et al., 2008).

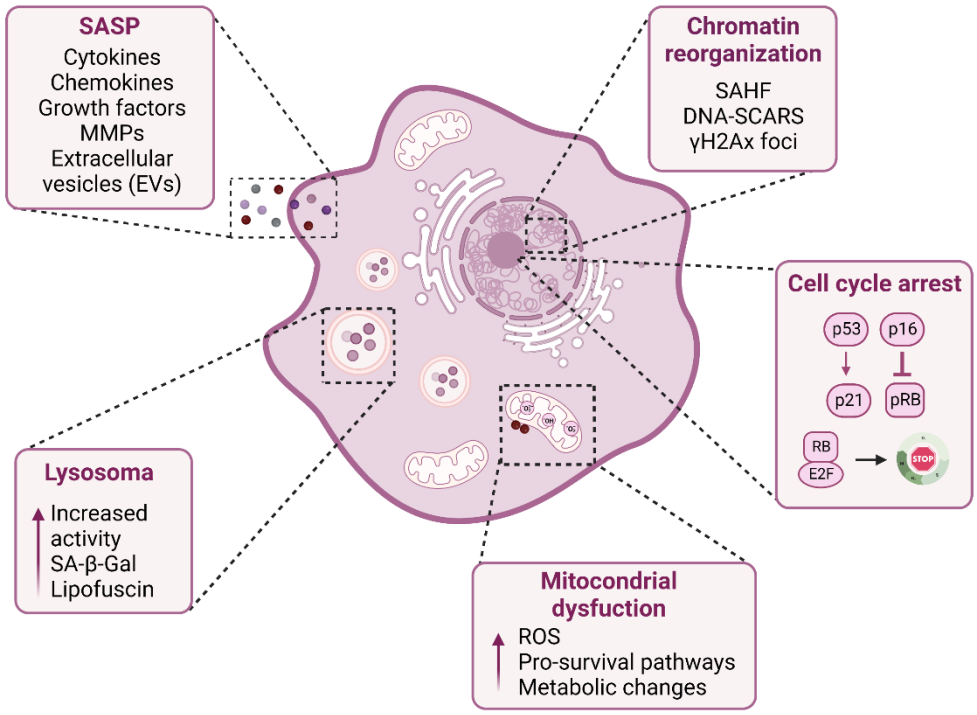

Figure 3. Hallmarks of senescence.
Several cellular mechanisms and alterations constitute the general features of cellular senescence: stable cell cycle arrest, driven by the action and cooperation of several proteins implicated in the $p16^{INK4a}$/Rb and $p53/p21^{CIP1}$ axes; dysfunctional mitochondrial including increased ROS levels, metabolic changes, and resistance to apoptosis; increased lysosomal compartment, which is characterized by the well-known overexpression of SA-β-Gal, and the implementation of a strong paracrine secretion termed SASP; chromatin alteration and reorganization, which includes SAHFs and DNA-SCARS marks and also results in the disruption of the nuclear envelope. Senescent cells *in vitro* also generally present a characteristic enlarged and flattened morphology. SAHF, senescence-associated heterochromatic foci; γH2AX, phosphorylated H2A histone family member X. Adapted from González-Gualda et al., 2021.

SASP components include pro-inflammatory cytokines (e.g., IL-1α, IL-6, and IL-8), chemokines (e.g., CXCL/CCL family, as CCL2), growth factors (e.g., TGFβ and VEGF), proteases and extracellular matrix-remodeling factors as metalloproteinases (e.g., MMP-1 and MMP-3), and extracellular vesicles (EVs) containing multiple cargoes (Acosta et al., 2013; Basisty et al., 2020; Coppé et al., 2010; Demaria et al., 2014; Ritschka et al., 2017; Saleh et al., 2018). The SASP can signal in both autocrine and paracrine manners to reinforce the cell cycle arrest and induce bystander senescence in nearby cells (Birch et al., 2020; Coppé et al., 2010; Nelson et al., 2012).

The accumulation of dysfunctional mitochondria is also a well-established characteristic of senescent cells (Correia-Melo et al., 2016). Upon senescence, the number of mitochondria increases significantly, and they enlarge, as a result of a decrease in mitophagy (Korolchuk et al., 2017). Mitochondria from senescent cells have an impaired electron transport chain, resulting in altered membrane potential (Passos et al., 2007, 2010; Wiley et al., 2016). As consequence, these changes lead to elevated levels of mitochondrial-derived ROS, which can trigger senescence both in an autocrine and paracrine manner after they release by senescent cells (Nelson et al., 2012; Victorelli et al., 2019). An important hallmark related to mitochondria is their resistance to apoptosis, resulting from the upregulation of pro-survival pathways (Childs et al., 2014; Hampel et al., 2004; Ryu et al., 2007; E. Wang, 1995; Y. Zhu et al., 2015). The survival of senescent cells depends on the expression of anti-apoptotic B-cell lymphoma proteins (Bcls), such as Bcl-2, Bcl-xL, Bcl-w, and Mcl-1, located on the membranes of mitochondria as well as the endoplasmic reticulum (Yosef et al., 2016). The overexpression of antiapoptotic Bcls prevents the release of cytochrome c to

assemble the apoptosome, which triggers intrinsic apoptosis via caspase signaling (Childs et al., 2014; Marcotte et al., 2004).

Although the senescent program becomes better defined, its high heterogeneity hampers the identification of cellular senescence confidently, particularly within complex tissues and living organisms (Kirschner et al., 2020). Significant efforts are currently underway to find new and more specific biomarkers, optimize combinatorial strategies and develop new detection techniques to solve these challenges.

1.3 Senescence in physiology and disease

Senescence induction plays complex biological roles in the organism which can be related either to normal physiological or pathological conditions (**Figure 4**) (López-Otín et al., 2013). On one hand, programmed activation of cellular senescence is required for tissue remodeling during normal embryonic development, and it contributes to the control of normal morphogenesis (Davaapil et al., 2017; Storer et al., 2013). Also, senescence has a beneficial role in wound healing and tissue regeneration, primarily due to the secretion of SASP factors which stimulate the immune response to clear the senescent cells and promote the healing of the damaged tissue (Demaria et al., 2014; Watanabe et al., 2017). Furthermore, its antiproliferative effect due to the arrested cell cycle is considered a key protective role in cancer prevention (Campisi, 2001; Collado et al., 2010). Oncogenic stimuli can up-regulate p53 or p16 to induce senescence and prevent the proliferation of damaged cells to a tumorigenic state (Serrano et al., 1997). On the other hand, the accumulation of senescent cells due to continuous damage increases with

aging as a result of a deficiency in senescent cell clearance (López-Otín et al., 2013). This excessive accumulation of senescent cells has several deleterious effects on tissue homeostasis and led to chronic inflammation and the progression of various age-related pathologies, including cancer, cardiovascular pathologies, fibrosis, diabetes, osteoarthritis, hepatic steatosis, chronic kidney diseases, among many others (Aguayo-Mazzucato et al., 2019; Childs et al., 2016; Dookun et al., 2020; Jeon et al., 2017; Ogrodnik et al., 2017; Paez-Ribes et al., 2019; Roos et al., 2016; Schafer et al., 2017; J. Wang et al., 2015).

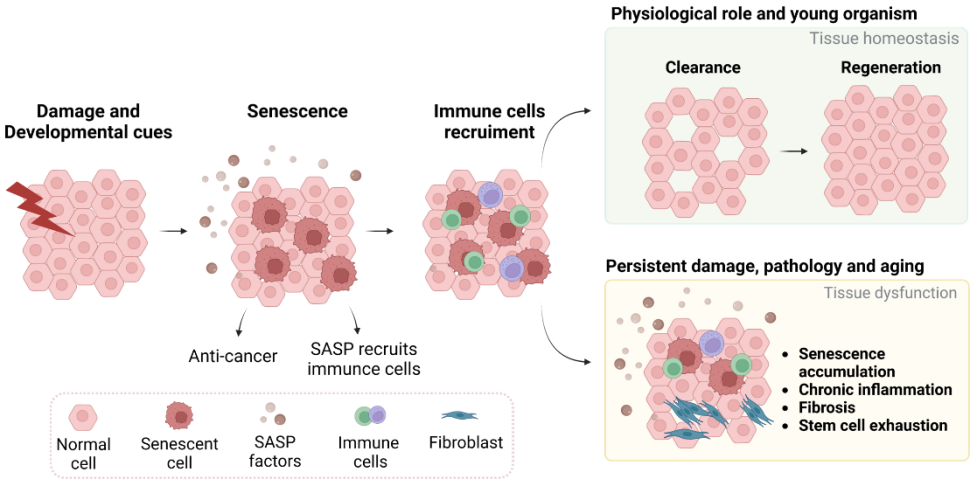

Figure 4. Physiological and pathological role of senescence.
In young organisms, cellular senescence prevents the proliferation of damaged cells, thus protecting from cancer, and initiates the recruitment of immune cells through the SASP, contributing to tissue homeostasis. In old organisms, the persistent damage and the deficient clearance of senescent cells result in their accumulation, SASP leads to chronic inflammation and initiates fibrosis and stem cell exhaustion that contribute to tissue dysfunction. Adapted from Muñoz-Espín et al., 2014.

In the maintenance of the senescence state, the SASP appears to be a mechanism of great importance, however, its behavior can be deleterious or

beneficial depending on the biological context (Faget et al., 2019; Watanabe et al., 2017). The SASP has been associated with negative effects such as inflammation and tumorigenesis (Canino et al., 2012; Coppé et al., 2010). The SASP leads to the recruitment of inflammatory cells to the damaged area, activates immune surveillance, and paradoxically also has pro-tumorigenic properties (Acosta et al., 2013). Nevertheless, the SASP also promotes the activation of cell plasticity and stemness in non-damaged surrounding cells (Ritschka et al., 2017).

Therefore, cellular senescence is described as a protective response to cell damage that turns harmful and accelerates aging when tissues lose their ability to regenerate. This duality is known as antagonistic pleiotropy whereby cellular senescence is considered a double-edged sword in health and disease (Muñoz-Espín et al., 2014).

2. Senolytic therapy

Senotherapy is an early-stage research field aiming the development of therapeutic agents and strategies to specifically target cellular senescence. Due to their distinct phenotype, senescent cells provide potential targets for pharmacological drugs. Current senotherapies are focused on limiting the deleterious effects of senescent cells by intervening in four main ways: i) the selective elimination of senescent cells by senolytics (senolysis); ii) inhibition of SASP production and activity by senomorphics; iii) improving the clearance of senescent cells by the immune system (immunosurveillance); and iv) blocking or preventing the senescence induction by senoblockers (Demirci et al., 2021; Ekpenyong-Akiba et al., 2020; Ovadya et al., 2018;

Serrano et al., 2019; von Kobbe, 2019). In this thesis, we will focus on senolytic therapy.

The specific clearance of senescent cells using drug therapy is known as senolysis and the pharmacological compounds that preferentially kill senescent cells are known as senolytics (Kirkland et al., 2017; Serrano et al., 2019; Y. Zhu et al., 2015). These senolytic therapies, including small molecules and peptides, aim to eliminate senescent cells that accumulate in tissues during aging and age-associated pathologies without impacting healthy cells (Kirkland et al., 2017; Myrianthopoulos et al., 2019). This novel approach has been demonstrated to enhance health- and lifespan in old mice while improving the symptoms of aging-related disorders (Baar et al., 2017; Baker et al., 2016; Y. Wang et al., 2016; Xu et al., 2018; Yousefzadeh et al., 2018)

Senescent cells can evade apoptosis through the activation of anti-apoptotic and pro-survival mechanisms, known as Senescent Cell Anti-Apoptotic Pathways (SCAPs)(Kirkland et al., 2017). Nevertheless, these pathways are druggable vulnerabilities and the senolytic drugs act to target components of SCAPs to inhibit cellular survival (Kirkland et al., 2017; Y. Zhu et al., 2015). To date, the SCAPs identified include the Bcl-2 family (e.g., Bcl-2, Bcl-xL, Bcl-w, Mcl-1), p53-p21 axis, hypoxia-inducible factor 1-alpha (HIF-1α), heat shock protein 90 (HSP90), several receptor tyrosine kinases, and the PI3K/Akt/mTOR pathway (**Figure 5**) (Fuhrmann-Stroissnigg et al., 2017; Y. Zhu et al., 2015).

Two of the first senolytic agents identified were dasatinib and quercetin (Y. Zhu et al., 2015). Dasatinib is a tyrosine kinase inhibitor and

quercetin is a flavonoid with multiple mechanisms of action, including the PI3K/Akt/mTOR signaling inhibition (Soto-gamez et al., 2017; Y. Zhu et al., 2015). The combination of dasatinib and quercetin (D+Q) effectively reduces the burden of senescent cells with beneficial results in mouse models of aging (Y. Zhu et al., 2015), alleviates vasomotor dysfunction in aged and hypercholesterolemic mice (Roos et al., 2016), improves pulmonary function and physical health in a model of bleomycin-induced lung fibrosis (Schafer et al., 2017), decreases high fat diet-induced liver steatosis (Ogrodnik et al., 2017), and reduces osteoporosis in aged mice (Farr et al., 2017). Fisetin is another flavonoid with senolytic activity through the targeting of the PI3K/Akt/mTOR pathway (Yousefzadeh et al., 2018).

Over the years, new drugs have been identified to exert senolytic behaviors including a D-retro Inverso (DRI)-isoform of FOX4 (Baar et al., 2017), HSP90 inhibitors (Fuhrmann-Stroissnigg et al., 2017), or the caspase-3 inhibitor Piperlongumine (Y. Wang et al., 2016). Another example includes the cardiac glycosides (digoxin, ouabain, and proscillaridin A) derived from the foxglove plant that acts by inhibiting the activity of the Na^+/K^+ ATPase pump (Fozzard et al., 1985). Because senescent cells have a more depolarized plasma membrane than non-senescent cells, they are more vulnerable to the effects of these compounds (Triana-Martínez et al., 2019). Other examples of potent Bcl-2 family inhibitors with senolytic activity are venetoclax (ABT-737) and navitoclax (ABT-263), which is extensively described in the next section (Yosef et al., 2016; Y. Zhu et al., 2016).

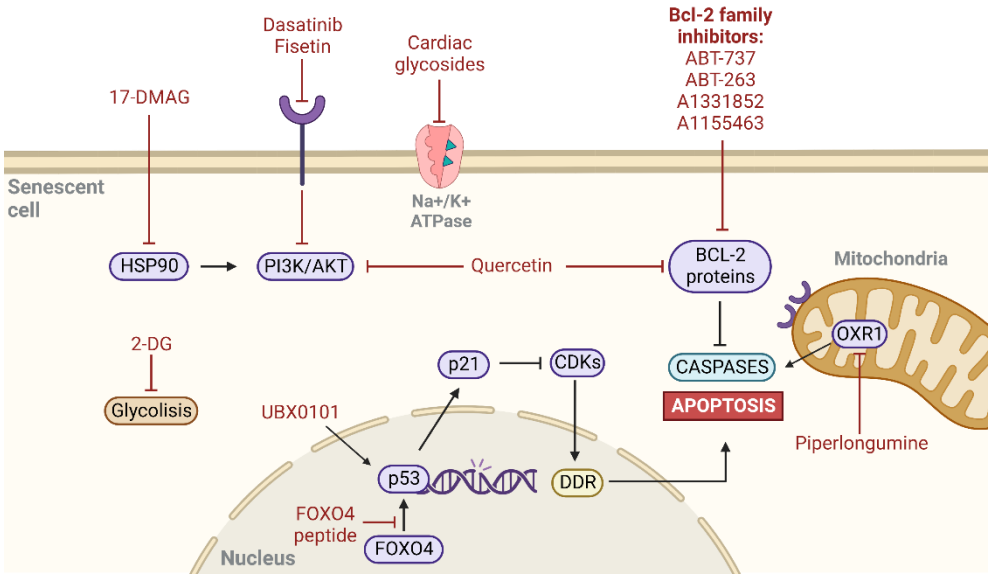

Figure 5. Senolytic therapies inducing apoptosis.
Senolytics mainly target the Senescent Cell Anti-apoptotic Pathways (SCAPs). The most common SCAPs are HSP90, Bcl-2 family proteins, p53, and the PI3K/Akt/mTOR pathway. Several senolytic agents identified to date are depicted. Adapted from Paez-Ribes et al., 2019.

2.1 Navitoclax

Among all the senolytic drugs, we focus this thesis on the use of navitoclax (ABT-263; Nav). Navitoclax is a BH3 mimetic drug that binds to the BH3 binding domain of the anti-apoptotic members Bcl-2, Bcl-w, and Bcl-xL, acting as an inhibitor (Y. Zhu et al., 2016). This union causes the displacement of the pro-apoptotic protein Bak and Bax, which oligomerize in the outer mitochondria membrane resulting in its permeabilization and release

of cytochrome c into the cytosol, thereby committing the cell to apoptosis (**Figure 6**)(Kalkavan et al., 2018; Y. Zhu et al., 2016).

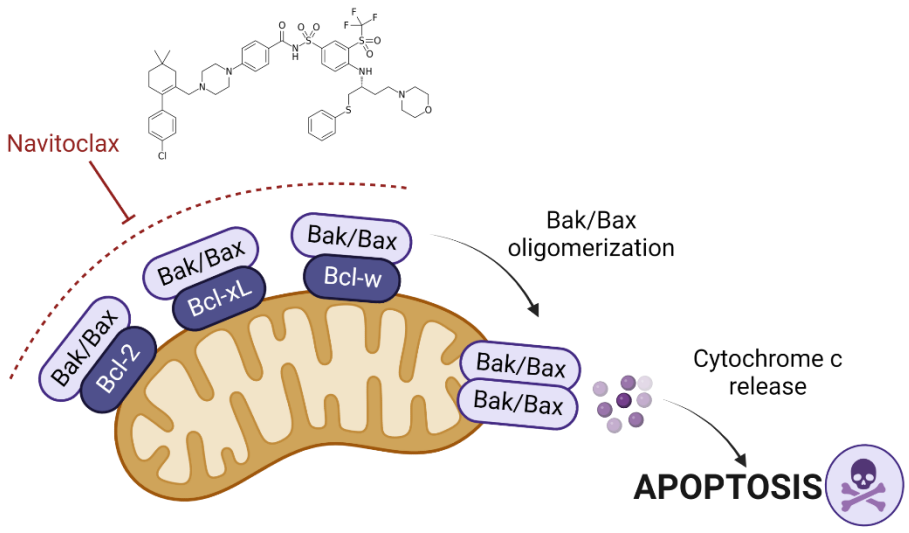

Figure 6. Navitoclax induces apoptosis.
Navitoclax, a BH3 mimetic, binds to the BH3 biding domain of the antiapoptotic members Bcl-2, Bcl-xL, and Bcl-w, which recruit and inactivate the proapoptotic proteins Bak and Bax. Consequently, the Bak and Bax oligomerize in the outer mitochondria membrane. This results in the permeabilization of the outer membrane, and cytochrome c release to the cytosol, ultimately leading to cell death.

Navitoclax is a broad-spectrum senolytic, with high potency and efficiency, which reduced senescence-associated dysfunction in several experimental *in vivo* models (J. Chang et al., 2016; Y. Zhu et al., 2016). Navitoclax has been shown to combat the premature aging of the hematopoietic stem cell populations caused by whole-body radiation (J. Chang et al., 2016), eliminate senescent foam cell macrophages from atherosclerotic lesions with beneficial effects (Childs et al., 2016), and target senescent type II pneumocytes in radiation-induced lung fibrosis to reverse

the disease (Pan et al., 2017). Navitoclax has also been demonstrated to rejuvenate bone marrow stromal cells (H. N. Kim et al., 2017). Besides, the use of navitoclax in cardiovascular diseases has resulted in a significant improvement in their outcome, which will be broadly described below.

Despite their robust senolytic activity, navitoclax administration, like other Bcl-2-targeting inhibitors, is unfortunately associated with severe hematological toxicity, which has limited its translation to clinical practice (Kile, 2014; Q. Li et al., 2019; Rudin et al., 2012; Tse et al., 2008; H. Zhang et al., 2007). In particular, the most relevant adverse effect is thrombocytopenia due to the dependence of platelets on Bcl-xL for survival. After initial navitoclax administration, it is observed a fast drop of platelets and a long-term decline after continuous administration (Cang et al., 2015; Kaefer et al., 2014). New strategies have been developed to overcome these challenges, including proteolysis-targeting chimera (PROTAC) technology, and prodrugs modified with a galactose (**Figure 7**)(Ge et al., 2021).

PROTACs are bivalent small molecules consisting of a ligand that recognizes a target protein connected via a linker to a recruitment moiety for an E3 ubiquitin ligase. A Bcl-xL specific PROTAC was designed by converting navitoclax into PZ15227 (PZ), which targets Bcl-xL to the E3 ligase cereblon (CRBN) that is poorly expressed in platelets and therefore PZ remains predominantly inactive in these cells (**Figure 7A**). PZ effectively cleared senescent cells and rejuvenates tissue stem and progenitor cells in naturally aged mice without causing severe thrombocytopenia, thereby limiting the off-target effect of free Nav (He et al., 2020).

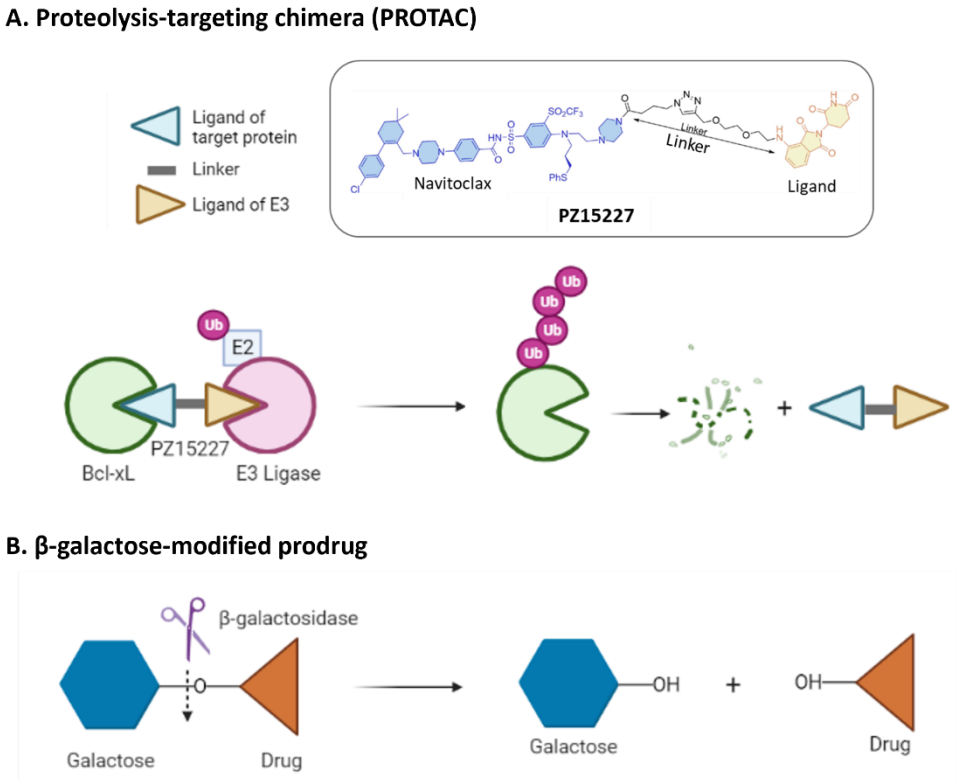

Figure 7. New strategies targeting senescent cells.
(A) BCL-xL proteolysis-targeting chimera (PROTAC) induces BCL-xL degradation. PROTAC recruits an E3 ligase to BCL-xL followed by polyubiquitination of the BCL-xL by an E2 conjugating enzyme. The polyubiquitinated BCL-xL is recognized and degraded by the proteasome. The PROTAC molecule can be recycled to induce the next round of BCL-xL degradation. **(B)** Upon cellular uptake, β-galactose-modified prodrugs are specifically cleaved by lysosomal β-galactosidase into cytotoxic drug that selectively induces apoptosis in senescent cells.

2.2 Galactose-modified senolytic pro-drugs

Although senolytic drugs are supposed to be specific for senescent cells, they have significant off-target effects. Thus, normal cells could be

affected by either the lack of specificity from the senolytic drugs or chronic treatment, leading to tissue dysfunction (von Kobbe, 2019). Thus, a second generation of targeted senolytic agents, such as prodrugs, is emerging as a promising alternative (**Figure 7B**).

For instance, the anti-neoplastic agent duocarmycin has been modified with a glycosidic derivative, producing galactose-modified duocarmycin (GMD) (Guerrero et al., 2020). GMD showed broad-spectrum senolytic activity *in vitro* and reduced the senescent burden in the lung of whole-body irradiated mice (Guerrero et al., 2020). A similar strategy was performed to develop the prodrug of the cytotoxic drug gemcitabine (known as SSK1), with a broader and stronger senolytic activity compared to standard senolytic drugs (D+Q, navitoclax or fisetin) (Y. Cai et al., 2020). SSK1 has been demonstrated to remove senescent cells and reverse lung fibrotic pathology and improve muscle strength in a bleomycin-induced mouse model of senescence, remove senescent cells in the liver and kidney of aged mice reducing age-associated inflammation and improve the physical function of mice (Y. Cai et al., 2020). Also, the anti-cancer drug, 5- fluorouracil, was modified with a β-D-galactosyl moiety to obtain the senolytic prodrug 5FURGa, with superior potency before the prodrug derivation without evident toxicity (Doan et al., 2020).

To improve the safety of navitoclax, our group also designed a prodrug with a cleavable acetylated-galactose molecule attached to navitoclax (known as **Nav-Gal**) (González-Gualda et al., 2020). **Nav-Gal** has been demonstrated to induce apoptosis specifically in senescent cells in a broad spectrum, independent of the senescent inducers, cell types, and mice models,

while enhancing the senolytic index of free navitoclax. Particularly, **Nav-Gal** has proved to reduce tumor size in mice models of lung adenocarcinoma and non-small-cell lung cancer when administered in combination with senescence-inducing therapies. Importantly, **Nav-Gal** did not reduce platelet counts in treated mice or *ex vivo* in human blood samples, suggesting protection against hematological toxicity when compared to its counterpart, free navitoclax (González-Gualda et al., 2020)**.** Recently, our group have also demonstrated its efficacy in a mouse xenograft model of aggressive human triple-negative breast cancer (hTNBC). Concomitant treatment with palbociclib and Nav-Gal *in vivo* results in the eradication of senescent hTNBC cells with consequent reduction of tumor growth, while reducing the cytotoxicity of navitoclax (Estepa-Fernández et al., 2022).

To date, galactose modification has been the most widely used method for improving senolytic specificity, showing improvements in safety profiles. Clinically relevant *in vivo* models have been developed, but further testing and monitoring of the context-dependent senescent burden *in vivo* is needed in order to move them into trials and clinics.

2.3 Senolytics in clinics

Due to the promising result shown in multiple preclinical disease models, some senolytics such as D+Q, fisetin, and navitoclax, are already in the early phase of clinical trials for the treatment of senescence-associated disorders. The first report was a brief course of D+Q that provides initial evidence that senolytics may alleviate physical dysfunction in patients with idiopathic pulmonary fibrosis (IPF), a fatal senescence-associated disease

(NCT02874989) (J. N. Justice et al., 2019). More recently, D+Q and fisetin are being evaluated for the treatment of patients with advanced chronic kidney disease (NCT02848131, NCT03325322) and osteoporosis in elderly women (NCT04313634). Initial findings showed that people with advanced chronic kidney disease receiving D+Q experienced a significant reduction in the burden of senescent cells (Hickson et al., 2019). An open-label pilot study of intermittent administration D+Q is also ongoing for subjects with Alzheimer´s disease (NCT04785300). Fisetin is also in Phase I/II for treating osteoarthritis (NCT04210986). On their part, navitoclax efficacy was evaluated for the treatment of small cell lung cancer (NCT00445198), and recurrent ovarian cancer (NCT02591095) and is now being evaluated for the treatment of solid tumors in combination with senescence-inducing chemotherapy (NCT02520778; NCT02079740).

Although the therapeutic benefit of senolytics has accelerated their progress from discovery to clinical studies, they are not yet perfect. The lack of bioavailability in the target site, and both off-target and side effects associated with their administration hamper their clinical translation. Therefore, novel and more effective senolytics are expected in the coming years with the help of new technologies for treating and preventing senescence associated disorders.

3. Nanotechnology and nanomedicine

Nanotechnology is a very recent field of study in which nanoscale structures of one to a few hundred nanometers (nm, 10^{-9} m) are used (**Figure 8**) (Feynman, 1960). As a result of improved features of materials at the

nanoscale dimensions, the development of nanomaterials, in many industries and research fields, such as chemistry, biology, and medicine has been extended (Khan et al., 2016; Pelaz et al., 2017; Szefler, 2018).

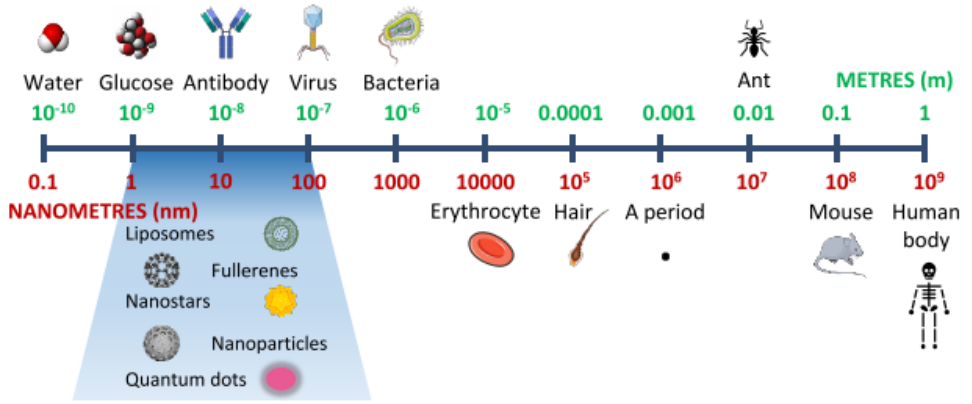

Figure 8. Scheme of nanomaterials scale.
Comparison to biomolecules, cells, and other items are described.

One appealing field in nanotechnology is nanomedicine. Nanomedicine is the result of combining nanotechnology with the interaction of biomolecules at the extracellular and intracellular levels in human cells. The main areas in nanomedicine include applications in diagnostics/imaging, for the recognition of specific biomolecules; regenerative medicine, including nanodevices that allow cell growth and tissue repair; and drug delivery, for targeted drug release at a specific site (Chaudhury et al., 2014; Navya et al., 2018). Among them, the development of new drug delivery nanosystems is likely the most advanced of these three areas. Designed nanodevices can target specific cells or tissues and release drugs in those regions, enhancing drug biodistribution and treatment effectiveness while decreasing unwanted side effects (Farokhzad et al., 2009). In this context, interesting examples of

smart nanodevices have been developed for different biomedical applications based on both organic supports (e.g., liposomes and polymers) and inorganic supports (including quantum dots, gold, metal oxides, and silica-based materials, among others) (Y. H. Choi et al., 2018; Lombardo et al., 2019).

Nanomedicine is advancing rapidly, with more than 50 nanomedicines approved by the Food and Drug Administration (FDA) in the last decades and over 100 which are currently in clinical trials (Bobo et al., 2016; Saha et al., 2020). Remarkably, due to their properties, nanoparticles have been used for developing vaccines either as antigen delivery, adjuvants, or mimics of viral structures. Thus, it is not surprising that the first developed COVID-19 vaccines were made by mRNA delivered via lipid nanoparticles (Anselmo et al., 2021; Chung et al., 2020; Kulkarni et al., 2020; Shin et al., 2020). Despite there being still many clinical concerns to be answered in the close future, nanomedicines seem to play a key role in the coming clinical settings (Genchi et al., 2017).

3.1 Nanodevices targeting senescent cells

Taking this into account, it is not surprising that several functional nanoparticles targeting senescent cells have been described recently. These nanodevices are based on different materials such as mesoporous silica nanoparticles (MSNs), calcium carbonate nanoparticles ($CaCO_3$), magnetite nanoparticles, molecularly imprinted polymer nanoparticles (nanoMIPs), gold nanoparticles, and core-shell spiky nanorods (CSNRs) chiral nanoparticles (**Figure 9**) (Morsli et al., 2022).

The first nanoparticle targeting senescent cells was designed by our group in 2012 and consisted of the encapsulation of a fluorophore in MSNs, coated by galacto-oligosaccharides (Gos) of mixed lengths, referred to as GosNPs (Agostini et al., 2012). The β-galactosidase, overexpressed in senescent cells, can digest the sugar coating of the GosNP, thus allowing the diffusion of the cargo out of the silica scaffold and showing a preferential release within senescent cells. A few years later, we improved the system using a homogeneous coating consisting of a hexa-galacto-oligosaccharide (galactan) (GalNPs) to successfully transport and deliver cytotoxic drugs, preferentially in senescent cells. In this thesis, we focus on the use of these mesoporous silica-based nanoparticles (GalNPs) to target senescent cells, which will be described in more detail below (**Figure 9A**).

Other strategies are based on the conjugation of senescence-associated antibodies to the nanoparticles. For instance, the CD9 receptor is a glycoprotein overexpressed in the cell surface of senescent cells (T. W. Kim et al., 2008). Therefore, antibodies to CD9 were conjugated to lactose-coated porous calcium carbonate ($CaCO_3$) nanoparticles to deliver the senomorphic drug rapamycin (CD9-Lac/$CaCO_2$/Rapa) to senescent cells (**Figure 9B**) (Thapa et al., 2017). When the nanoparticles target the senescent cells, the SA-β-Gal breaks down the lactose, thus favoring the drug release exhibiting anti-senescent effects *in vitro* (Thapa et al., 2017). More recently, CD9 antibodies have been conjugated to hyaluronic acid-coated MSNs to target senescent cells and deliver rosuvastatin in response to the hyaluronidase present in atherosclerotic plaques (termed CD9-HMSN@RSV). This strategy showed senolytic efficacy *in vivo* by mitigating atherosclerosis through senescent cell clearance (Pham et al., 2021).

Because senescent cells have an altered iron metabolism and have increased levels of transferrin receptor 1 (TfR1), promoting the uptake and intracellular accumulation of iron was considered a suitable strategy. The use of magnetite (Fe_3O_4) nanoparticles, coated with the senolytic quercetin, has been shown to induce apoptosis and reduce proliferation in oxidative-stress (H_2O_2)- induced senescent fibroblasts *in vitro* (Lewinska et al., 2020; Masaldan et al., 2018).

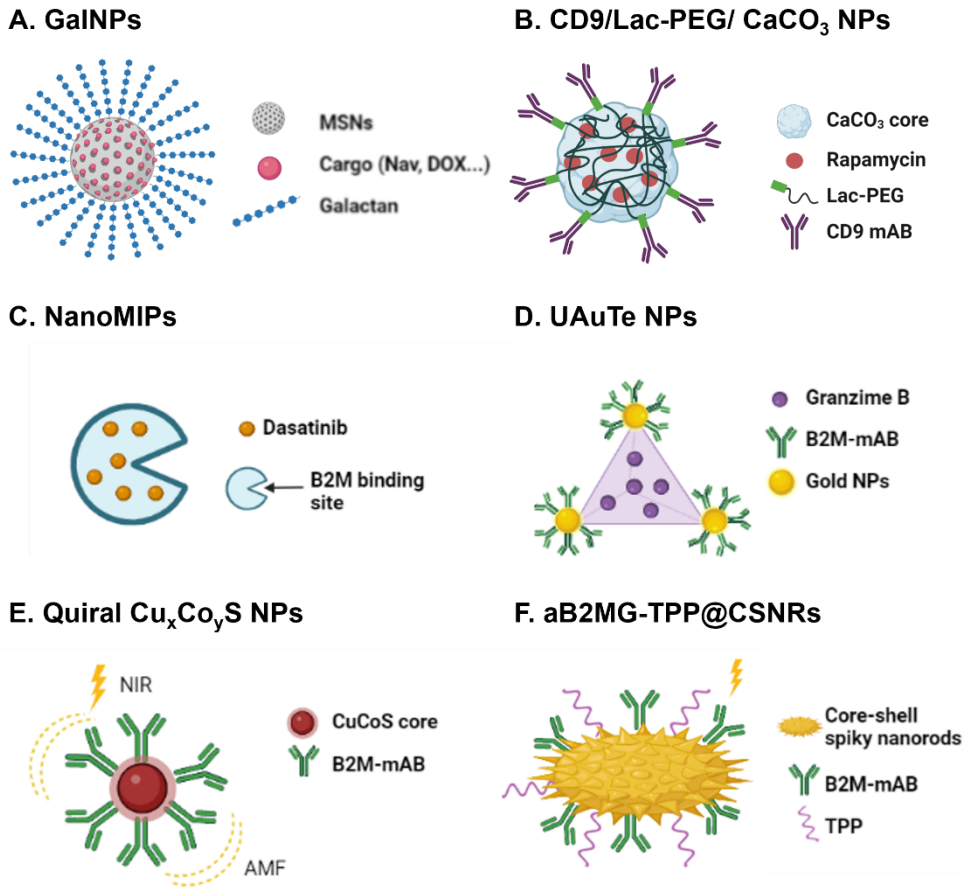

Figure 9. Scheme of nanodevices targeting senescent cells.

(A) Porous calcium carbonate nanoparticles ($CaCO_3$) with a lactose-PEG derivative and an anti-CD-9 antibody to target a cell membrane glycoprotein in senescent cells (SCs). The lactose-coating breaks down with SA-β-gal activity to release rapamycin cargo. **(B)** Galactan-coated nanoparticles can be loaded with either dye or cytotoxic drug (e.g., DOX or Nav). After being endocytosed, the lysosomal SA-β-Gal enzyme cleaves galactose-conjugated residues, and the cargo is released. **(C)** Molecularly imprinted nanoparticles (nanoMIPs) target senescent cells taking advantage of the overexpression of the membrane protein β2 microglobulin (B2MG) in SCs. nanoMIPs can be loaded with dasatinib or a fluorescent dye. **(D)** Gold tetrahedron nanoparticles (UauTe) functionalized with the anti-B2M antibody to release granzyme-B in response to near-infrared (NIR) light have also been used to target senescent cells. **(E)** Chiral Cu_xCo_yS nanoparticles functionalized with a B2M antibody have shown to be senolytic using both an alternating magnetic field (AMF) and near-infrared (NIR) light. **(F)** Plasmonic core-shell spiky nanorods (CSNRs) functionalized with anti-B2MG antibody, and triphenylphosphonium (TPP) moieties (aB2MG-TPP@CSNRs) were able to target mitochondria in senescent cells. Adapted from Morsli et al., 2022.

Following mass spectrometry studies, the protein β2 microglobulin (B2M) was found to be highly expressed in the plasma membranes of senescent cells (Althubiti et al., 2014). Taking advance of this biomarker, molecularly imprinted nanoparticles (nanoMIPs) have been developed by forming polymerization complexes around an epitope template against B2M. NanoMIPs were then loaded with dasatinib and demonstrated a much greater senolytic effect compared to other senolytic drugs (**Figure 9C**) (Ekpenyong-Akiba et al., 2019). The use of anti-B2M has also been proposed using gold tetrahedron nanoparticle to release granzyme-B in response to near-infrared (NIR) light. This application restored the renal function and mobility of the mice in a senescence-accelerated mouse model (SAMP8) (**Figure 9D**) (Qu et al., 2020). Similarly, the anti-B2M was also functionalized in chiral Cu_xCo_yS nanoparticles with senolytic properties upon alternating magnetic field

(AMF) and NIR irradiation, inducing apoptosis through photo-redox damage and mechanical forces (**Figure 9E**). Doxorubicin-treated mice showed reduced signs of senescence in the liver and kidneys along with improving fur coverage, mobility, and weight (S. Li et al., 2020). Similar results were observed when anti-B2M was attached to plasmonic core-shell spiky nanorods (CSNRs) functionalized together with triphenylphosphonium (TPP) moieties (Ab2MG-TPP@CSNRs) to specifically target mitochondria in senescent cells (**Figure 9F**). These nanorods were irradiated with NIR light to induce apoptosis in senescent cells by increasing mitochondrial ROS while acting as an immune adjuvant and showing a synergistic effect accelerating the clearance of senescent cells in mice (Lu et al., 2020).

3.2 Mesoporous silica nanoparticles (MSNs)

Mesoporous silica nanoparticles (MSNs) have gained attention since their first synthesis in the early 1990s (Yanagisawa et al., 1990) and their first use in drug delivery in 2001 (Vallet-Regi et al., 2001) due to their unique chemical properties, stability, inertness, and biocompatibility. These nanoparticles usually present a spherical shape (ca. 80-100 nm of diameter), with cylindrical unidirectional channels of approximately 2.5 nm in diameter and arranged in a hexagonal pattern. The unique mesoporous structure of silica facilitates the effective loading of drugs and their subsequent controlled release to the target site. MSNs can be functionalized on their surface with organic groups, yielding hybrid organic-inorganic materials. Incorporating these organic molecules modifies specific surface properties such as reactivity, hydrophilicity, hydrophobicity, and stabilization of final materials against hydrolysis or chemical attack, which introduces additional versatility

to the nanoparticles (Hoffmann et al., 2006). These advanced functionalities promote the development of smart nanodevices with advanced applications in several scientific fields such as the controlled release and the design of (bio)chemical sensors (Castillo et al., 2019; Y. Zhang et al., 2016).

In many examples, these materials are composed of two subunits: (i) the inorganic porous scaffold loaded with a cargo (e.g. drugs, dyes, fluorophores, etc.) and (ii) (bio)molecules or supramolecular ensembles attached to the external surface acting as gatekeepers (also known as molecular gates or nanovalves) (Aznar et al., 2016; García-fernández et al., 2020). These gatekeepers are responsible for keeping the cargo enclosed in the porous support, which in response to external stimuli, change dimensions, shapes, or configurations to allow cargo release in a controlled manner. A large variety of supramolecular structures, organic molecules, polymers, peptides, aptamers, or enzymes have been used as gatekeepers (Aznar et al., 2009; Coll et al., 2011; Llopis-Lorente et al., 2017; Wen et al., 2017). Several stimuli have been used to trigger the release of guest molecules from gated materials (Aznar et al., 2016; García-fernández et al., 2020), including pH (Bernardos et al., 2008; Cauda et al., 2010), redox potential (Giménez et al., 2015; Liu et al., 2008), target molecules (Y. L. Choi et al., 2011; Y. Zhao et al., 2009), light (Lin et al., 2010), temperature (C. Chen et al., 2011) and magnetic fields (Bringas et al., 2012) (**Figure 10**).

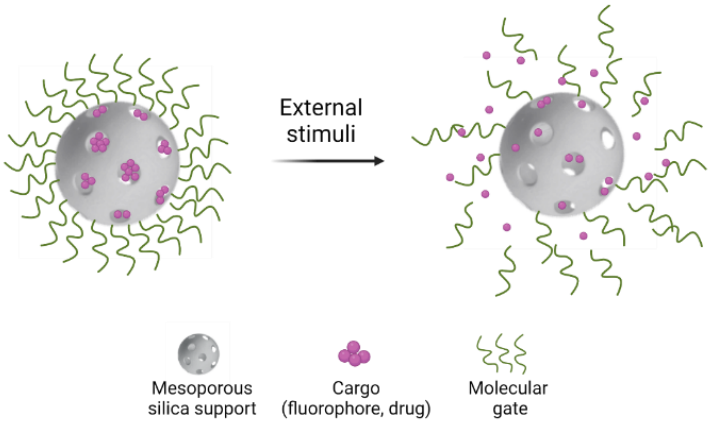

Figure 10. Scheme of gated MSNs.
Mesoporous silica nanoparticle functionalized with a molecular gate that opens in response to an external stimulus releasing its cargo.

Remarkably, due to their compatibility and low toxicity, silica nanoparticles are also beginning to be studied in clinical trials for biomedical applications (drug delivery, diagnosis, and therapy) (**Figure 11**) (Janjua et al., 2021). Nevertheless, to date, only one study has been conducted using MSN as a proof of concept in humans (Bukara et al., 2016). In this study, 12 healthy men volunteers were given fenofibrate acid orally to compare the bioavailability of the drug loaded onto MSNs to Lipanthyl, a commercially available formulation. Compared with the marketed product, the results showed improved tolerance and bioavailability of fenofibrate in MSNs. With these promising results, clinical translation of silica nanoparticles is expected to increase in the next years and MSNs may open new avenues for nanomedicine.

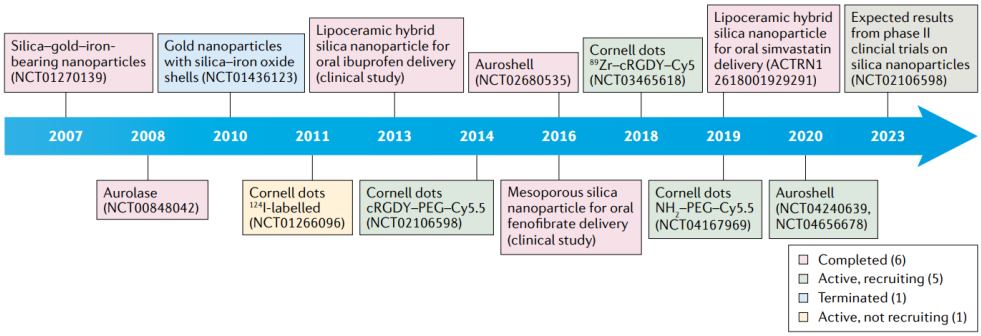

Figure 11. Clinical trials of silica nanoparticles.
Reprinted with permission of *Nat Rev Mater* 6, 1072–1074 (2021). Copyright © 2021, Springer Nature Limited.

3.2.1 Galacto-coated mesoporous silica nanoparticles (GalNPs)

In the context of this thesis, the used MSN-based nanodevices, GalNPs, can be classified as stimuli-responsive gated nanomaterials. These GalNPs can successfully transport and deliver small molecules such as doxorubicin (**GalNP(Dox)**) or navitoclax (**GalNP(Nav)**) to target senescent cells *in vivo* (Muñoz-Espín et al., 2018). The mechanism of action is mediated by endocytosis and fusion with lysosomal vesicles. Then, the galactan cap is hydrolyzed mediated by the lysosomal β-Gal and the cargo is delivered to the required site of action, the senescent cells, while minimizing systemic side effects.

The administration of **GalNP(Dox)** resulted in a drastic reduction of melanoma xenograft tumors in mice in combination with palbociclib, a senescence-inducing drug while reducing the cardiotoxicity associated with doxorubicin. Furthermore, in a bleomycin-induced model of lung fibrosis,

GalNP(Dox) reduced collagen deposits and resulted in the recovery of pulmonary function in mice. **GalNP(Nav)** was also effective at inhibiting tumor development and promoting regression when used in combination with palbociclib while minimizing the off-target effects of free navitoclax (Muñoz-Espín et al., 2018). Subsequent studies have also demonstrated the increased antitumoral therapeutic efficacy of **GalNP(Nav)** in models of triple-negative breast cancer while limiting lung metastases and improving the survival of mice upon palbociclib administration (Estepa-Fernández et al., 2021, 2023; Galiana et al., 2020).

Overall, these findings open a new clinical opportunity for the treatment of diverse age-associated disorders. Although many of the currently available senolytic drugs have certain drawbacks, those with strong preclinical data and limited off-target toxicities are likely to translate into clinical research in the near future. Therefore, in this thesis, we evaluate the therapeutic outcome of the nanosystem **GalNP(Nav)** and the prodrug **Nav-Gal** for the targeted elimination of senescent cells in cardiac disorders.

4. Senescence and the heart

In the last decade, growing clinical evidence and experimental studies have linked cellular senescence, the accumulation of senescent cells, and the release of SASP factors with age-related cardiac pathologies, including heart failure (HF), myocardial infarction, cancer chemotherapy-related cardiotoxicity among other cardiomyopathies (Shimizu et al., 2019). The initiation and maintenance of cellular senescence in the heart result in worse cardiac outcomes predisposing the patient to HF (M. S. Chen et al., 2022).

Nevertheless, the role of senescence in these conditions is unclear as both detrimental and beneficial effects have been reported (Mehdizadeh et al., 2021). Therefore, a better understanding of the role of cellular senescence in cardiac complications has great translational value.

Traditionally, telomere shortening during cell proliferation was recognized as the main mechanism of senescence accumulation, but this explanation seemed unlikely as the main driver of senescence in the heart, which is a relatively quiescent organ (Childs et al., 2015). Some studies have demonstrated that telomere dysfunction is associated with changes in the heart that resemble myocardial aging. For instance, the heart of mice lacking telomerase reverse transcriptase ($TERT^{-/-}$), the enzymatic component of telomerase, exhibited an increased expression of p53 in the cardiomyocyte population as well as functional changes including left ventricular dysfunction, decreased number of cardiomyocytes (CMs) and increased hypertrophy (Blasco et al., 1997; Leri et al., 2003). However, cardiac senescence during a normal physiological state may not be caused by replicative senescence (Anderson et al., 2019). As we described previously, the senescence state can be also induced by different stressors such as oxidative stress, metabolic dysfunction, or DNA damage (Herranz et al., 2018). Indeed, a previous study demonstrated that cardiomyocyte senescence can be triggered as a result of the accumulation of telomere-associated DNA damage foci (TAF) caused by mitochondrial dysfunction and increased oxidative stress, independent of cellular replication (Anderson et al., 2019). Nevertheless, the role of cellular senescence in other cardiac cell types should be also considered.

4.1 Senescence in specific cardiac cell types

The heart is a multicellular organ that includes cardiomyocytes (CMs), endothelial cells, fibroblasts, cardiac progenitor cells (CPCs), immune cells, and epithelial cells. It has been demonstrated that all these cells contribute to cardiac homeostasis and can become senescent with age or cardiac disease (Anderson et al., 2019; Baker et al., 2016; J. Li et al., 2019). Nevertheless, it is still unknown which cardiac cell type is most susceptible to drive cardiac disorders during senescence-related diseases.

Among the different cardiac cell types, CMs, mostly post-mitotic cells, comprise over 30-40% of the total cellular population in the heart, and over 80% of the cellular volume (Anderson et al., 2019; Pinto et al., 2016). Nowadays it is known that post-mitotic cells, such as CMs or neurons also develop a senescent-like phenotype (Anderson et al., 2019; Jurk et al., 2012; Von Zglinicki et al., 2021). This refutes the traditional view that terminally differentiated cells cannot become senescent (Vicencio et al., 2008). Recent data suggest that cardiomyocyte senescence accumulates with age by persistent DNA damage, and promotes myocardial remodeling dysfunction both directly because the senescent phenotype is associated with cardiomyocyte hypertrophy and indirectly via the production of SASP factors which mediates chronic sterile inflammation and induces senescence in surrounding cell types (Anderson et al., 2018; Tang et al., 2020). Senescent CMs show upregulation of classic senescence markers such as p16, p21, and p53 together with different SASP components. The secretome of senescent CMs includes the inflammatory cytokines IL-1 and IL-6, and tumor necrosis factor-α (TNFα), which induce local inflammation in the surrounding cardiac

microenvironment (Cui et al., 2018). Also, transcriptomic studies have identified that aged CMs express an atypical SAPS including endothelin 3 (Edn3), the growth and differentiation factor 15 (GDF15), and TGFβ2 (Anderson et al., 2019).

Other senescent cardiac cells, such as endothelial cells, fibroblast, immune cells, and epithelial cells, are characterized by cell cycle arrest, DNA damage, upregulation of p16, p21, and p53, and SASP production including IL-6, CXC- chemokine ligand 1 (CXCL1) and CXCL2, tumor necrosis factor (TNF), vascular endothelial growth factor (VEGF), matrix metalloproteinase 1 (MMP1), MMP3 and plasminogen activator inhibitor 1 (PAI1) (Shimizu et al., 2019). The SASP products from different cardiac cells have been demonstrated to exert paracrine effects in neighboring cells leading to fibroblast activation and differentiation, diminished angiogenic potential, promotion of prothrombotic phenotype in endothelial cells, cardiomyocyte death and hypertrophy (**Figure 12**) (Anderson et al., 2019; Mehdizadeh et al., 2021).

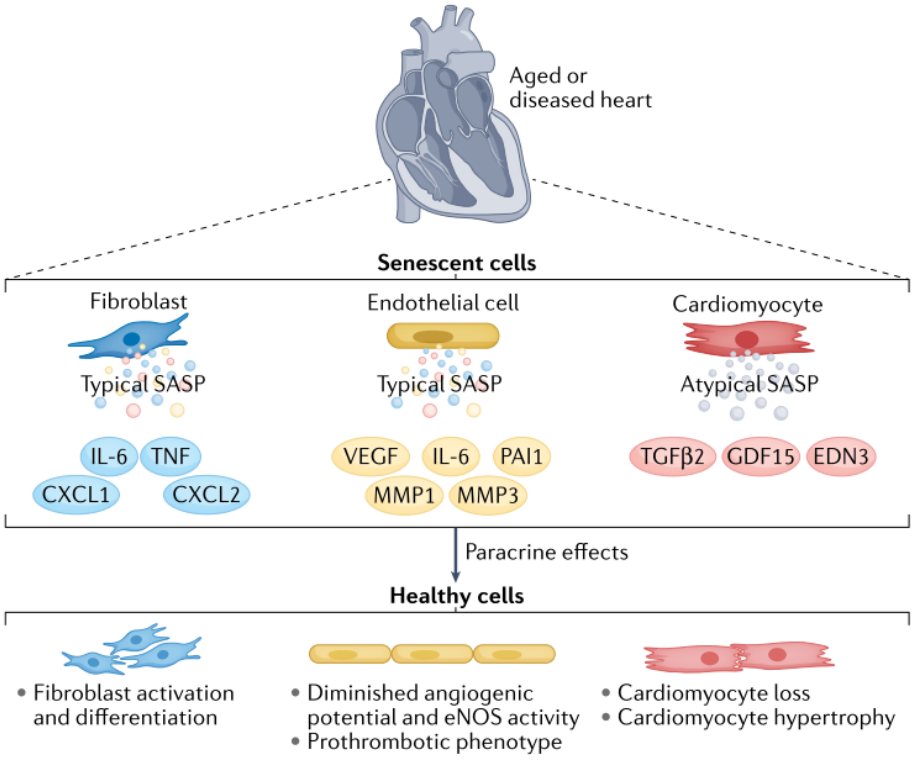

Figure 12. Paracrine communication between cardiac cells via SASP.
The intercellular communication in the heart can affect healthy neighboring cells via SASP factors release. The consequences include fibroblast activation and differentiation; diminished angiogenic potential, decreased endothelial nitric oxide synthase (eNOS) activity and a prothrombotic phenotype in endothelial cells; and cardiomyocyte death and hypertrophy. Reprinted with permission of *Nat Rev Cardiol* 19, 250–264 (2022). Copyright © 2021, Springer Nature Limited.

4.2 Senescence and heart regeneration

The progression of degenerative diseases in other self-renewing tissues is associated with senescence and impaired regenerative potential during aging, however, the capacity of the heart for self-renewal has been actively debated (Sahin et al., 2010). The adult mammalian heart lacks an effective regenerative response and cardiomyocyte loss is generally an irreversible process that leads to adverse remodeling, fibrosis, and HF (Yutzey, 2017). Nevertheless, studies investigating cardiomyocyte turnover in both mice and humans point out that the heart does have a limited potential to regenerate CMs during normal myocardial homeostasis throughout life (Bergmann et al., 2015). Nonetheless, this ability is reduced with age and it is at a much lower rate than other cardiac cell types such as endothelial and mesenchymal cells, leading to turnover rates of <1% in adulthood (Bergmann et al., 2015; Laflamme et al., 2011; Walsh et al., 2010).

In young hearts, the source of new CMs has been attributed both to the division of existing myocytes and to progenitors residing within the heart (CPCs) or in exogenous niches such as bone marrow (Oldershaw et al., 2019; Orlic et al., 2001) The formation of new CMs correlates with a low rate of cardiomyocyte apoptosis (Beltrami et al., 2003; Kikuchi et al., 2010). However, according to additional research, senescence within stem/progenitor cells could prevent efficient differentiation of CMs during repair (Cesselli et al., 2011; Chimenti et al., 2003; Lewis-McDougall et al., 2019). Expression of p16, SA-β-Gal, and DNA damage markers in these stem progenitor cells increased proportionally with age (Lewis-McDougall et al., 2019). Therefore, a progressive decline to replace apoptotic CMs driven by

progenitor senescence leads to compensatory hypertrophy. This adaptive change partially preserves heart function but upon further stress (such as diabetes or hypertension) the aged myocardium exceeds its functional reserve, hypertrophy no longer preserves function, and excessive fibrosis leads to defects, such as arrhythmia and HF (**Figure 13**) (Childs et al., 2018).

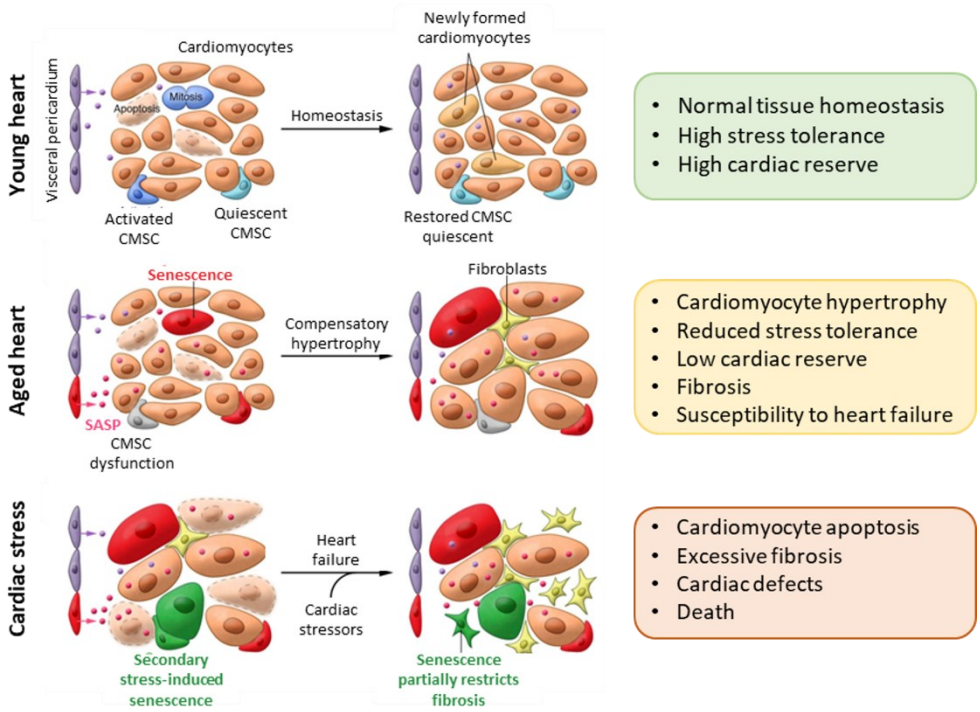

Figure 13. Senescent cardiac cells drive heart failure.
In young hearts, the myocardium homeostasis and normal tissue function are maintained through the de novo formation of cardiomyocytes (CMs) from resident cardiomyocyte stem cells (CMSCs) or division of incompletely differentiated, small CMs. In aging hearts, a declining ability to replace apoptotic CMs due to progenitor dysfunction/senescence, and SASP factors, conspires with an increasing rate of cardiomyocyte death to produce compensatory hypertrophy, which preserves heart function. Upon cardiovascular stressor, the aged myocardium exceeds its functional reserve and decompensates, and excessive fibrosis leads to arrhythmia and heart failure. Adapted from Childs et al., 2018.

Additional research demonstrated that SASP factors generated from both senescent stem progenitor cells and CMs induced senescence in healthy cells through the bystander effect, preventing proliferation that contributes to cardiac dysfunction with age or after injury (Anderson et al., 2019; Lewis-McDougall et al., 2019). This adverse environment may explain in part why cardiac regeneration based on autologous therapy has failed to efficiently translate from the lab to the clinic, hindering the success of regeneration transplant strategies (Gude et al., 2018; Lewis-McDougall et al., 2019; Oldershaw et al., 2019).

4.3 Senescence in cardiac pathology

Aging is the leading risk factor for several cardiac diseases. Therefore, cellular senescence is involved in the pathogenesis of different cardiac diseases such as cardiac fibrosis, cardiac hypertrophy, heart failure, myocardial infarction, and cardiotoxicity (**Figure 14**) (Mehdizadeh et al., 2021). Although cardiac senescence is widely investigated in models of aging, it has also been shown that induced senescence in young animals, through overproduction of oxidative stress, was associated with increased cardiomyocyte senescence showing cardiomyocyte hypertrophy, adverse myocardial remodeling, and cardiac dysfunction (Anderson et al., 2019).

Cardiac fibrosis is caused by the overproduction of extracellular matrix proteins within the myocardium by the activation of cardiac fibroblasts. The accumulation of senescent fibroblast has been described in fibrotic areas of animals and human hearts during aging but the role of senescence in cardiac fibrosis is complex (Meyer et al., 2016; F. Zhu et al.,

2013). On one hand, the global elimination of senescent cells in aged mice have reduced fibrosis suggesting the causal role of senescence in this pathology (Anderson et al., 2019). Controversy, several studies indicate that senescence induction and regulation within the fibroblast population are essential for the formation of a scar, which is needed to prevent cardiac rupture and retain as much cardiac function as possible, and to restrict excessive fibrosis, by limiting fibroblast proliferation and antifibrotic SASP factor release (Meyer et al., 2016; Xie et al., 2017; F. Zhu et al., 2013). Also, decreased fibroblast senescence in mice leads to greater cardiac fibrosis and impaired left ventricular ejection fraction (EF) (L. Jia et al., 2017).

Cardiac hypertrophy refers to the physiological response to biomechanical stress resulting in increased left ventricular mass and reduced cardiac function, which can lead to HF (L. Jia et al., 2017). Senescence has been extensively associated with the development of cardiac hypertrophy and, at the cellular level, with cardiomyocyte hypertrophy, while ROS and mitochondrial dysfunction were considered the main players of this pathology through the SASP signaling (Anderson et al., 2019; Dai et al., 2010; Morin et al., 2019).

HF results from a variety of stressors, but several studies have indicated the correlation between cellular senescence and HF, which suggest a new therapeutical target for HF prevention or treatment (Anderson et al., 2019; Din et al., 2014; Kosugi et al., 2006). A common hallmark in HF is mitochondrial dysfunction, which is also frequently associated with cellular senescence. For example, mice with a global deficiency of PIM1, a kinase with protective effects on mitochondria and telomere length, develop HF at 6

months of age and have increased levels of p16, p53, and SA-β-gal accompanied by a deterioration of mitochondrial structure and function in cardiac tissue (Din et al., 2014). Also, in a mouse model of diabetes mellitus, treatment with an angiotensin II- receptor blocker (Candesartan) improved cardiac function and reduced the levels of senescence markers in cardiac tissue (Kosugi et al., 2006). Moreover, clinical studies have found that increased levels of SASP components, such as IL-6 and IGFBP7, in the serum correlate with HF disease severity. These molecules are being actively investigated as biomarkers for diagnosis and prognostication in patients with HF (Januzzi et al., 2018; Youn et al., 2019).

In MI, cardiac cell death occurs because of a crucial imbalance between blood flow needs and supply in the myocardium. Cardiac cell death activates inflammatory cascades, leading to fibrosis and scar formation, which can also contribute to HF (Mauro et al., 2019). Current evidence from human studies and animal models suggests an important role of cellular senescence in the infarcted heart although the pathogenesis of MI is controversial as both positive and negative effects have been reported. On one hand, reduces the scar size by limiting fibrosis and, on the other hand, contributes to myocardial remodeling by exacerbating the inflammatory response through SASP (Cui et al., 2018; Walaszczyk et al., 2019; F. Zhu et al., 2013).

Other evidence that senescence may be detrimental to myocardial health is the link between cardiomyopathy and chemotherapeutic drugs and radiation therapy (Altieri et al., 2016; Ewer et al., 2015; Mitry et al., 2020).

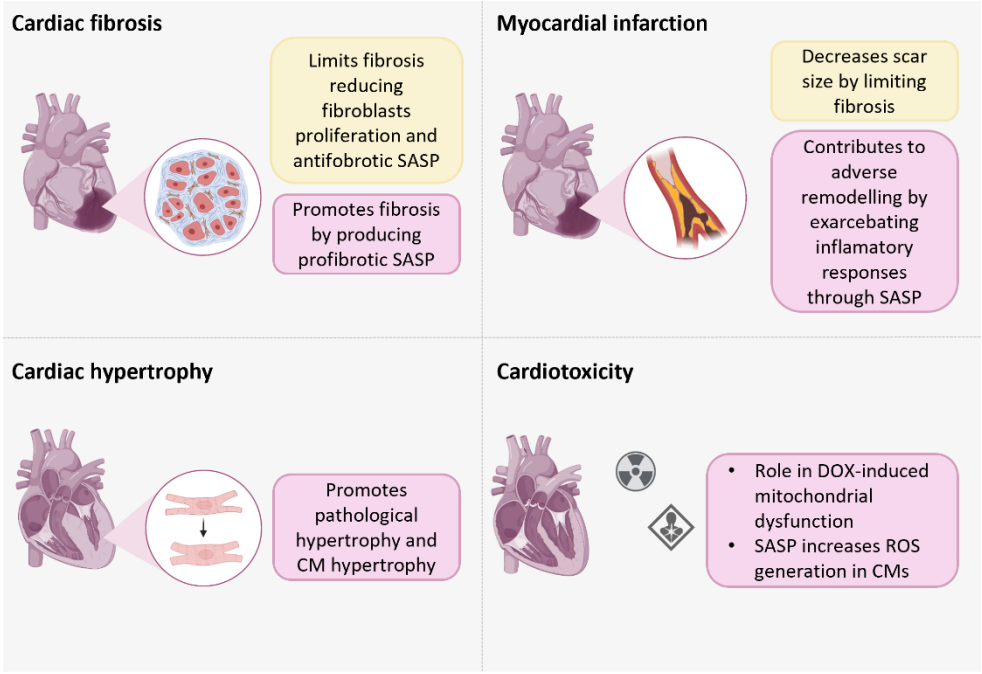

Figure 14. Cellular senescence in cardiac pathology.
The presence of cellular senescence in cardiac disease is associated with different effects. Yellow boxes indicate the beneficial effects and purple boxes the detrimental effects reported. Adapted from Mehdizadeh et al., 2021.

Cardiotoxicity related to chemotherapy is a major healthcare problem and chemotherapy-induced HF has a three-fold higher mortality rate than idiopathic dilated cardiomyopathy (Nair et al., 2016). Therefore, a main leading cause of death in cancer survivors seems to be cardiac (Ewer et al., 2015). In this context, many chemotherapy drugs promote therapy-induced senescence (TIS) either as a therapeutic mechanism of action or as a side effect (Demaria et al., 2017). For instance, drugs with cardiotoxic effects, such as doxorubicin, upregulates senescent makers in the heart which indicates the potential mechanism of senescence in the development of

cardiac disease (Spallarossa et al., 2009). This question will be extensively discussed below.

4.4 Targeting cardiac senescence therapeutically

The contribution of senescent cells to cardiac-related pathologies was further demonstrated with the use of a genetically engineered INK-ATTAC mouse model, in which p16-positive cells are selectively cleared after drug (AP20187) treatment (Baker et al., 2016). The pharmacogenetic depletion of accumulated p16-positive senescent cells delayed the acquisition of aged phenotypes in the heart of old mice preventing or reversing the onset of different cardiac pathologies (Anderson et al., 2019; Baker et al., 2011, 2016; Hernandez-Segura et al., 2017; Lewis-McDougall et al., 2019). Besides, AP20187 therapy restored cardiomyocyte hypertrophy in irradiated-mice expressing p16-positive cells (Anderson et al., 2019). However, the INK-ATTAC mouse is bred onto a mouse line that is associated with augmented cardiovascular dysfunction (BubR1), unrelated to cellular senescence and p16 expression, which may be too severe to allow senescence cell clearance to improve life expectancy (Baker et al., 2011; Naylor et al., 2013).

Therefore, the use of senolytics has also been envaulted in preclinical models of natural aging to modulate cardiac pathologies. Zhu et al. demonstrated that treatment of 24-month-old mice with a single dose of a combination (D+Q) (D: 5 mg/kg body weight and Q: 50 mg/kg) significantly ameliorated age-related heart dysfunction improving left ventricular ejection fraction (LVEF or EF) and fractional shortening (FS) (Y. Zhu et al., 2015). The treatment also improved the vascular relaxation of carotid arteries,

suggesting that the clearance of senescent endothelial cells underlies the benefits (Y. Zhu et al., 2015). Otherwise, the administration of navitoclax to 24-month-old mice (two 1-week cyclic doses over a month), has been shown to reduce cardiomyocyte senescence, attenuate SASP components, reduced cardiomyocyte hypertrophy and cardiac fibrosis, all characteristics of aged-associated myocardial remodeling (Anderson et al., 2019). Additionally, both senolytics stimulated cardiomyocyte renewal, through the activation of senescent CPCs, restoring the regenerative capacity of the heart following clearance of senescence in old mice, based on the increased number of CMs positive for Ki67 proliferative marker (Anderson et al., 2019; Lewis-McDougall et al., 2019).

The used of navitoclax therapy also demonstrated improved cardiac function and electrophysiological abnormalities in a mouse model of angiotensin II-induced HF (K. Jia et al., 2020). Also, navitoclax administration in aging mice before MI induction ameliorated diastolic function, and significantly improved survival rate (Walaszczyk et al., 2019). These navitoclax-treated mice also showed reduced functional deterioration after MI, suggesting that senescent cells promote adverse remodeling. A different study showed that the global clearance of senescent cells with navitoclax treatment after myocardial ischemia-reperfusion injury (IRI) improves cardiac function, reduces the inflammatory response, and increases angiogenesis (Dookun et al., 2020).

The association between senescence and cardiac pathologies, together with promising preclinical data, suggest that senotherapy may serve as a preventative or reversible method for several senescence-associated cardiac

diseases. Based on this, senolytics may have further applications in the prevention or treatment of chemotherapy-induced cardiac dysfunction, such as the administration of doxorubicin. Despite the good results obtained with the administration of navitoclax, it must be taken into account that the clinical use of this drug is hampered due to its associated hematological toxicity, and targeted senolytics with fewer systemic side effects are highly expected.

5. Cardiotoxicity of doxorubicin

Anthracyclines such as doxorubicin (DOX), epirubicin, and idarubicin are potent cytotoxic antibiotics with broad clinical use as antitumoral therapy (Podyacheva et al., 2021). In particular, DOX is the most potent member of the family. Although several new-generation targeted therapies have been developed for the treatment of cancer, DOX remains the first-line treatment against a broad spectrum of adult and pediatric cancers, including leukemias, lymphomas, and several solid tumors (Carvalho et al., 2009). However, its clinical use is hampered by severe cardiac side effects culminating in HF (Zamorano et al., 2016). The incidence of developing HF is dose-dependent, ranging from 4.7-48 % at 400-700 mg/m^2, respectively (Swain et al., 2003). Cardiotoxicity can appear in an acute manner at the time of chemotherapeutic treatment, or it may not be detected for many years and remains a life-long threat (X. Li et al., 2017). Remarkably, 1-5% of cancer survivors treated with anthracyclines develops late HF (Oliveira et al., 2014). Nevertheless, early-onset chronic cardiotoxicity within the first year is the most prevalent and clinically relevant form (Cardinale et al., 2015). Therefore, the clinical use of DOX is hindered due to the development of irreversible cardiotoxicity, which represents an important public health concern, related to late morbidity and

mortality (Octavia et al., 2012; Oliveira et al., 2014). For this reason, early detection and targeted treatment of patients at risk from cardiotoxicity are paramount to reducing the incidence of life-limiting DOX-HF in cancer survivors (Timm et al., 2020).

The current understanding of the underlying pathophysiology of DOX is highly complex and multifactorial as it acts on a range of cellular targets simultaneously (Sawicki et al., 2021). Over time, the leading theory has been that oxidative stress is the primary cause of DOX-induced cardiomyopathy (Octavia et al., 2012; Rawat et al., 2021). Nevertheless, much evidence supports the role not only of oxidative stress but also of genotoxic stress, systemic inflammation, autophagy, mitochondrial dysfunction, or iron and calcium metabolism disorders with impaired apoptosis (**Figure 15**) (Timm et al., 2020; Varela-López et al., 2019; Wallace et al., 2020).

DOX is easily captured by cells and localized in the nucleus. DOX can intercalate in the DNA forming the ternary DOX-DNA-topoisomerase II (Top2) complexes. This ternary complex causes DNA double-strand breaks (DSBs) and activates DNA damage responses (DDR), leading to cell death (S. Zhang et al., 2012). Top2 is expressed as isoenzymes Top2α and Top2β. Top2α is highly expressed in rapidly proliferating malignant cells, being the key mechanism of antitumor treatment with DOX. Conversely, Top2β is more common in quiescent cells, such as mammalian CMs. The union DOX-Top2β leads to the activation of the altered p53 tumor suppressor pathway, mitochondrial dysfunction, and increased apoptosis, leading to the development of cardiomyopathy (Rawat et al., 2021). Animal studies with Top2β knockout (KO) mice have shown that the absence of Top2β protects

against DOX-induced cardiotoxicity (McGowan et al., 2017; S. Zhang et al., 2012).

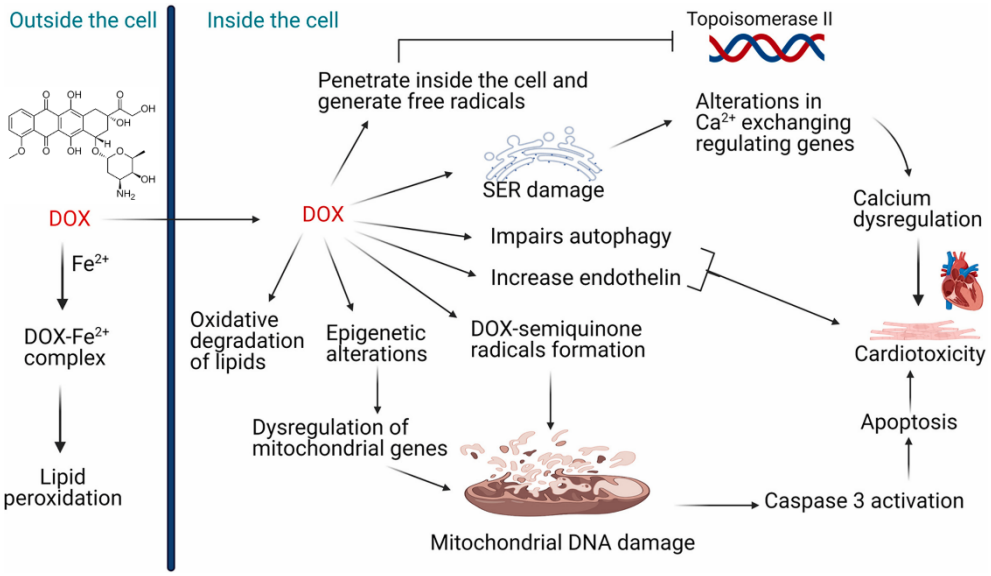

Figure 15. Mechanisms of action of DOX-induced cardiotoxicity.
DOX acts on a range of cellular targets simultaneously driving to oxidative stress, genotoxic stress, systemic inflammation, autophagy, mitochondrial dysfunction, or iron and calcium metabolism disorders with impaired apoptosis. Adapted from Rawat et al., 2021.

Also, the quinone fragment of anthracyclines can undergo redox reactions with the formation of excess reactive oxygen species (ROS) in the presence of oxidoreductive enzymes such as NADH dehydrogenase, and xanthine oxidase (Podyacheva et al., 2021). Besides, DOX influence the release of calcium ions from the sarcoplasmic reticulum of CMs inducing ROS formation. In its turn, oxidative stress provokes the activation of the apoptosis regulators, such as Bcl-2 associated X protein (Bax), which activates the release of cytochrome c through the pores in the mitochondrial

membrane, activating the caspase cascade of the external and internal pathways of apoptosis, which ultimately leads to the death of CMs and the impairment of the contractile function of the heart (Varela-López et al., 2019). Additionally, DOX has a strong affinity for iron and the DOX-iron complex can induce lipid peroxidation by interacting with negatively charged membranes. The reduction of DOX in the presence of free iron starts the cycle of free radical formation (Šimůnek et al., 2009).

Since several mechanisms are involved in the development of cardiac toxicity, the primary target of DOX has not yet been identified and different strategies are being evaluated to prevent the associated cardiomyopathies. Among them, the use of protective antioxidant approaches has been widely investigated, however, only limited cardioprotection has been demonstrated in clinically relevant trials (van Dalen et al., 2011). One of these strategies is the use of dexrazoxane, an iron-chelating agent, acting as a free radical scavenger. Although the beneficial effects of dexrazoxane have been demonstrated in murine models, it has not shown the expected efficacy in humans and its safety has been questioned for years (Dewilde et al., 2020; Lipshultz et al., 2010; Tebbi et al., 2007). Currently, it is the only approved treatment for anthracycline cardiotoxicity but, unfortunately, according to the FDA approval statement and European Medicines Agency (EMA), the use of this drug as a cardioprotective is limited to women with metastatic breast cancer who have received cumulative doses of 300 mg/m^2 (Santos et al., 2018). Different strategies also included angiotensin-converting enzyme (ACE), beta-blockers, angiotensin antagonists, and other cardioprotective approximations without demonstrating a reliable and protective effect (van

Dalen et al., 2011). For instance, the use of ACE showed short benefits, which were lost 6 to 10 years after (Silber et al., 2004). At present, the most effective tool to prevent DOX-induced cardiotoxicity is modulating the dosage, and cardiac transplantation remains a vital option for survivors who developed HF due to the treatment (Oliveira et al., 2014).

Accordingly, different studies in mice have shown protection from DOX by using very different and distinct pathways (DNA damage, mitophagy, nitrosative/oxidative stress) by knocking out Top2β, BNIP3, or iNOS (inducible nitric oxide synthase), respectively (Timm et al., 2020). These different model systems and treatment regimens introduce phenotypes with underlying pathology that do not necessarily mimic DOX-HF in patients. Therefore, the exact mechanism behind DOX cardiotoxicity remains unclear so it is difficult to exploit therapeutically and it remains the most significant challenge to the development of new methods of prevention and treatment (Rawat et al., 2021).

5.1 Doxorubicin-induced senescence

Despite the mechanism underlying DOX-induced cardiotoxicity remaining controversial, previous studies demonstrated that DOX promote senescence in different cardiac cell types, resulting in heart failure years after the cancer treatment (De Angelis et al., 2016). Thus, DOX is postulated to induce significant damage to cardiomyocyte cells that eventually leads to premature senescence being the first cause of cardiomyopathies (Maejima et al., 2008; Piegari et al., 2013; Spallarossa et al., 2009).

Several animal models have been proposed to study the mechanism underlying cardiac senescence *in vitro* and *in vivo* (Ghosh et al., 2016; Sahin et al., 2011). DOX has been proved to cause mitochondrial DNA (mtDNA) damage, and increase oxidative stress in CMs and CPCs resulting in cellular senescence (Maejima et al., 2008). Also, DOX-treated mice had increased cardiac levels of p53 and increased binding to the promoter PGC1α, a master regulator of mitochondrial function, suggesting the role of cellular senescence in mitochondrial dysfunction (Sahin et al., 2011). Thus, the senescence phenotype seems to be activated by ROS generation due to the accumulation of dysfunctional mitochondria after DOX exposure. DOX has also been proposed to induce senescence by targeting and downregulating telomeric binding factors that under normal physiological conditions aid in telomere and chromosomal stability. However, if the level of downregulation exceeded a certain threshold, then the cell may undergo the apoptosis pathway (Spallarossa et al., 2009).

Cardiomyocytes from DOX-treated rats showed increased senescent markers, p16, and SA-β-gal activity in the left ventricle six months after drug exposure (Mitry et al., 2020). Furthermore, DOX treatment caused senescent CPCs accumulation in both human and murine models, which contributes to long-term toxicity (Mitry et al., 2020; Piegari et al., 2013). Indeed, heart samples from patients treated with DOX, showed increased CPCs expressing p16 in association with DNA damage, ROS production, and CPC migration impairment (Piegari et al., 2013).

The implication of DOX administration in cardiac tissue was evaluated by Demaria et al., in a genetically engineered mouse model (p16-

3MR), in which p16-positive cells are selectively cleared after ganciclovir administration (Demaria et al., 2017). In this work, it was demonstrated that in DOX-treated mice, the depletion of senescent cells was associated with a reduction in SASP-induced systemic inflammation, diminished organ toxicity, and preserved cardiac function (Demaria et al., 2017). Moreover, endothelial cells and fibroblast-like cells in the heart also achieve a senescence phenotype in DOX-treated mice (Demaria et al., 2017).

Due to the senescence-promoting effects of DOX treatment on multiple cardiac cell populations, cellular senescence may therefore represent a novel therapeutic target in related cardiac disease (Abdelgawad et al., 2021). As with aging, the use of pharmacological senolytics, such as navitoclax, post-chemotherapy could therefore improve cardiac function via clearance of senescence and attenuation of myocardial SASP. However, to the best of our knowledge, such an appealing concept has never been studied in a model of cardiotoxicity-induced senescence.

Objectives

The use of chemotherapy is unfortunately associated with adverse complications. Considering the evidence in the literature supporting the treatment with doxorubicin induces premature senescence in cardiac cells which correlates with heart dysfunction, the present PhD thesis has attempted to explore the clearance of senescence as a therapeutical option in DOX-associated cardiomyopathy through the design, synthesis, characterization, and preclinical evaluation of different senolytic strategies. In particular, our therapeutical approach explores different targeted strategies based on navitoclax therapy, to limit its associated hematological toxicity, which could improve treatment effectiveness while diminishing undesired side effects (**Figure 16**).

The specific objectives of this doctoral thesis are as follows:

- To establish a senescence-induced model in the HL-1 cardiac myocyte cell line upon doxorubicin treatment for the validation of the senolytic therapy.
- Synthesize and characterize the different systems targeting senescent cells: (i) navitoclax encapsulated in mesoporous silica nanoparticles and capped with a hexa-galacto-oligosaccharide (galactan) (**GalNP(Nav)**) and (ii) a prodrug obtained by galacto-conjugation with navitoclax (**Nav-Gal**).
- To establish an *in vivo* model of doxorubicin-induced cardiotoxicity which correlates with a senescent phenotype in the heart tissue, leading to cardiac dysfunction.

- Investigate the potential of senolytic therapy for clearing senescent cells in the heart and the prevention of cardiac dysfunction in a mouse model of doxorubicin-induced cardiotoxicity.

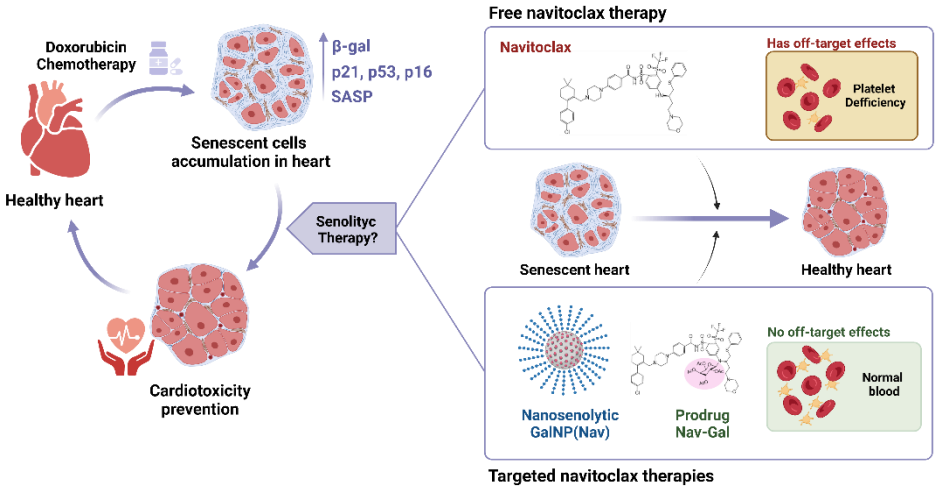

Figure 16. Graphical summary.
The use of doxorubicin (DOX) chemotherapy induces premature senescence in cardiac cells which correlates with heart dysfunction. The clearance of senescent cells (SCs) through senolytic therapy might be a therapeutical option to prevent DOX-associated cardiomyopathy. Our therapeutical approach explores different targeted strategies based on navitoclax therapy, to limit its associated hematological toxicity, which could improve treatment effectiveness while diminishing undesired side effects.

Materials and methods

1. Cell culture

HL-1 Cardiac Muscle Cell Line was obtained from Sigma (SCC065). HL-1 is an immortalized mouse cardiomyocyte cell line that proceeds from AT-1 subcutaneous tumor excised from an adult female C57BL/6J mouse. The parental AT-1 line was originally derived from an atrial tumor growing in a transgenic mouse in which expression of the SV40 large T-antigen was targeted to atrial CMs via the atrial natriuretic factor (ANF) promoter. HL-1 cells continuously divide without losing their differentiated cardiac myocyte phenotype and spontaneously contract while maintaining a differentiated cardiac phenotype. HL-1 cells have been utilized to investigate pathological situations such hypoxia, hyperglycemia-hyperinsulinemia, apoptosis, and ischemia-reperfusion as well as normal cardiomyocyte function.

Cells were grown, as protocol detailed, in fibronectin (Sigma, F1141) or gelatin-coated cell plates containing Claycomb medium (Sigma, 51800C) and supplemented with 10% fetal bovine serum (FBS) (Sigma, F7524), 2 mM L-glutamine (Sigma, G7513) and 0.1 mM norepinephrine (Sigma, A0937), made up in 30 mM ascorbic acid. Cells were incubated at 37 °C in an atmosphere of 5% CO_2 and 95% air. Cells were passaged every three days after reaching full confluency.

1.1 Senescence induction

For senescence induction, cells were supplemented with the same medium containing doxorubicin (DOX) (Carbosynth, AD15377) at 100 nM for 3 days. After senescence induction, cells were washed with PBS and centrifuged to eliminate the DOX from the medium and were ready to use for

further experiments. The experiments were carried out with low cell passages to ensure quality and reproducibility. Cells were routinely tested for mycoplasma contamination.

2. Senescence characterization

2.1 β-galactosidase activity assay

β-galactosidase staining was performed in cells using the Senescence β-galactosidase Staining Kit (Cell Signaling, 9860) following the manufacturer's instructions. After senescence induction, control and DOX-treated cells were seeded at a slow density in 6-well plates. The day after, the supernatant was removed, and cells were washed three times with PBS. Cells were fixed at RT 10 min with a solution containing 2% formaldehyde and 0.2% glutaraldehyde in PBS. After being washed with fixative solution, cells were stained with 1 mL of the X-Gal Staining Solution (pH 6.0) and incubated overnight at 37 °C without CO_2. The staining solution was then removed and rinsed in PBS and then detected for blue staining under a bright-field microscope.

2.2 β-galactosidase determination by flow cytometry

To quantify β-galactosidase activity by flow cytometry, the fluorogenic substrate 5-dodecanoylaminofluorescein di-β-D-galactopyranoside (C_{12}FDG) (Santa Cruz Biotechnology, Inc., sc-284621A) was used (J. Zhao et al., 2017). Control and senescent HL-1 cells were seeded in a 6-well culture plate. The following day, cells were pretreated with 0.1 mM bafilomycin A1 (Sigma, B1793) for 1 h to induce lysosomal

alkalinization in a fresh culture medium. Cells were washed with PBS and treated with C_{12}FDG in an optimal concentration for HL-1 cells of 33 µM for 3 h at 37 °C under 5% CO_2. Next, cells were washed with PBS and harvested by adding 0.5% Trypsin-EDTA (Gibco). Cells were collected, centrifuged (1200 rpm, 5 min, 4 °C), and resuspended in 200 µL of cold PBS. Flow cytometry assay was carried out on a CytoFlex S instrument (Beckman Coulter) followed by data analysis using CytoExpert software. For analysis, we used a negative control as a reference to determine the percentage of positive cells. We divided the C_{12}FDG fluorescence histogram into two compartments by setting up a boundary between the negative (dim fluorescence) and positive cells (bright fluorescence). The percentage of positive cells is obtained by dividing the number of events within the bright fluorescence compartment by the total number of cells in the histogram (J. Zhao et al., 2017).

2.3 Cell cycle assay

For the cell cycle evaluation assays, control and DOX-treated HL-1 cells (3 days at 100 nM) were fixed and permeabilized with ethanol for 1 h at -20 °C. Then, cells were centrifuged and 0.5 mL of PI/RNAse buffer solution from Immunostep was added to each control or DOX-treated cell (1 x 10^6 cells) and incubated overnight at 4 °C before analysis. Samples were acquired by flow cytometry using the CytoFLEX S Beckman Coulter and analyzed by FlowJo software.

2.4 Cell proliferation

Time-lapse images were acquired for control and DOX-treated HL-1 cells (3 days at 100 nM) seeded in p96-multiwell plates at a density of 15,000 cell/well using Cytation 5 Cell Imaging Multi-Mode Reader while maintained in BioSpa8 (BioTek, USA). Images were taken every 3 h up to 48 h and were analyzed for confluence increment using BioTek Gen5 Data Analysis Software.

2.5 Clonogenic assay

For the clonogenic assay, control and senescent cells were seeded at increasing cell densities in a 24-well plate and incubated at 37 °C in an atmosphere of 5% CO_2 and 95% air for 1 week. Then, cells were washed with PBS and fixed with 4% paraformaldehyde (PFA) for 10 min. After eliminating the fixative solution, cells were stained with 0.05% crystal violet for 45 min. The staining was removed, and the excess was washed with deionized water. Images were taken under a bright-field microscope.

2.6 Western blot

The analysis of the protein content of the different samples in the study was performed using the Western Blot technique. Firstly, both control and DOX-treated cells were scraped-harvested in lysis buffer (25mM Tris-HCl pH 7.4, 1mM EDTA, 1mM EGTA, SDS 1%, and protease and phosphatase inhibitors), passed through a 25G needle, and boiled for 10 min to prepare whole-cell extracts. Protein quantification was performed using a BCA

protein assay (Pierce BCA Protein Assay kit, Thermofisher Scientific) in order to resolve an identical amount of whole-cell extracts (at least, 70 µg).

SDS-PAGE (sodium dodecyl sulfate–polyacrylamide gel electrophoresis) gels with different percentages of acrylamide (8-12%) were used according to the molecular weight of the proteins studied. The obtained samples were mixed with 6X loading buffer (350mM Tris pH 6.8, 30% glycerol, 100 g/L SDS, 200 mg/L bromophenol blue, 30% β-mercaptoethanol) and boiled for 5 min. For electrophoresis, a Bio-Rad Mini Protean system was used in the running buffer (25 mM Tris, 190 mM glycine at pH 8.3 with 0.1% SDS). Proteins separated by SDS-PAGE were transferred to nitrocellulose membranes (GE Healthcare, #10600002) in transfer buffer (25 mM Tris, 190 mM glycine, pH 8.3 with 20% methanol (vol/vol)) during 3 h at 400 mA. The membranes were then blocked with 5% skimmed milk prepared in Tris-buffered saline with Tween 20 (TBS-T) buffer (Tris 20 mM y NaCl 50 0mM pH 7.5 with 0.1% Tween 20) solution for 1 h. Then, membranes were incubated at 4 °C overnight, shaking, with primary antibodies (**Table 1**). Membranes were washed 3-4 times with TBS-T 0.1% and incubated with the appropriate secondary antibody conjugated with horseradish peroxidase for 2 h at RT. The secondary antibodies used were anti-Rabbit IgG peroxidase antibody (Sigma, #A6154) and peroxidase conjugate-goat anti-Mouse IgG antibody (Sigma, #A4416). Immunoblot signals were detected using GE Healthcare's ECL chemiluminescence detection reagents using the Amersham Imager 600 equipment.

The quantification of the bands corresponding to the expression of each protein was performed using Image J image analysis software. The

relative intensity of each protein was quantified to the intensity of the GAPDH.

Table 1. Primary antibodies. Dilution (1/1000).

Target Protein	Antibody	Company	Reference
phospo-Rb	Phospho-Rb (Ser780)	Cell Signaling	9307
β-Galactosidase	β-Galactosidase (E2U2I)	Cell Signaling	27198
p21	p21 Waf1/Cip1/CDKN1A (F-5)	Santa Cruz	sc-6246
p53	Anti-p53 antibody [PAb 240]	Abcam	ab26
Bcl-2	Bcl-2 (50E3)	Cell Signaling	2870
Bcl-xL	Bcl-xL (54H6)	Cell Signaling	2764
Bcl-w	Bcl-w (31H4)	Cell Signaling	2724
Bim	Bim Antibody	Cell Signaling	2819
Bok	Recombinant Anti-Bok antibody [EPR15331]	Abcam	ab186745
GAPDH	GAPDH (14C10)	Cell Signaling	2118

2.7 Ki67 immunofluorescence

Control and senescent cells were seeded on coverslips and fixed in 4% PFA for 10 min, permeabilized with 0.3% Triton X-100 and blocked with 5% BSA for 1 h. Cells were incubated with primary antibody solution (1% BSA, 0.3% Triton X-100) containing anti-Ki67 (D3B5) (1:500, Cell Signaling, 9129) overnight at 4ºC. The next day, samples were incubated with Alexa anti-rabbit IgG Fluor Goat 633 (1:100, Fisher, A21071) for 2 h at RT in darkness. For image visualization coverslips were mounted on glass slides

with mounting Hoechst staining solution and visualized in Leica TCS SP8 HyVolution 2 confocal microscope.

3. Synthesis of nanomaterials

3.1 Synthesis of mesoporous silica nanoparticles (MSNs)

The synthesis of mesoporous silica nanoparticles MCM-41 type (MSNs) is based on the Stöber method and the use of four components is required: solvent, surfactant, silica precursor, and catalyzer (Stober et al., 1968). The surfactant molecules self-aggregate to form micelles in a polar solvent. In addition, individual micelles self-assembled into supermicellar structures, which act as a structure-directing agent or template. In the final step, silica precursor molecules are added and hydrolyzed to form silanol groups (Si-OH), which condense over the supermicelles, creating the final network of siloxane linkages (Si-O-Si) and form the final solid mesoporous structure (**Figure 17**) (Raman et al., 1996). The features of MCM-41 materials could be easily adjustable by modifying synthesis parameters such as temperature, stirring, and chemicals utilized (Chan et al., 2001; Corma et al., 1997; Kobler et al., 2008; K. Zhang et al., 2013). In this thesis, a typical synthesis of MCM-41 nanoparticles was carried out using deionized water (dH_20) as a solvent, N-cetyltrimethylammonium bromide (CTAB, Sigma, H6269) as surfactant, tetraethylorthosilicate (TEOS, Sigma, 131903) as a silica precursor, and NaOH (Sigma, 310732) as alkaline catalyst, as previously described (Q. Cai et al., 2001). First, 1 g of CTAB solution (2.74 mmol) was dissolved in 480 mL of deionized water (dH_20). Then, the pH was basified with 3.5 mL of a 2 M NaOH solution, and the surfactant solution was

stirred at 80 °C. Then, 5 mL of TEOS (2.57 x 10^{-2} mol) was added dropwise. The mixture continued stirring for 2 h to give a white precipitate. The solid was isolated by centrifugation (9,500 rpm, 20 min) and washed several times with dH_2O until neutral pH was reached. The material was dried at 80 °C overnight, obtaining de porous scaffold "as made" MCM-41. To obtain the final mesoporous silica nanoparticle MCM-41 (MSNs), the "as made" solid was calcined (Mufla Furnace) at 550 °C in an oxidant atmosphere for 5 h to remove the surfactant CTAB template, obtaining de mesoporous scaffold "calcinated" MSNs. Once the surfactant agent is removed from the structure, the pores are empty for further synthesis steps.

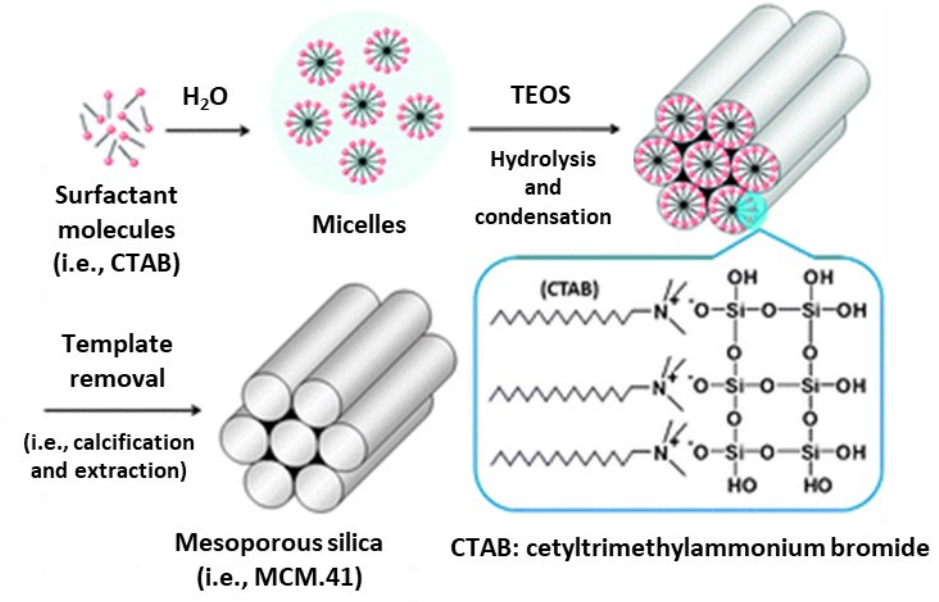

Figure 17. Schematic representation of the synthetic process of mesoporous silica MCM-41 nanoparticles.
Adapted from from Chem. Soc. Rev. 2012, 9, 3679.

3.2 Synthesis of loaded MSNs

Calcined MSNs were loaded with indocyanine green (ICG, Sigma, I2633) or navitoclax (Nav) (Active BioChem, A1001) as described previously (Estepa-Fernández et al., 2021).

- For ICG loading, 9.3 mg of ICG were dissolved in 67.5 mL of water at a pH of 7.5 and 200 mg of calcined MSNs were added. The mixture was stirred for 24 h at RT, and the nanoparticles were filtered and dried under vacuum to obtain ICG-loaded MSNs (**NP(ICG)**).
- For the synthesis of Nav-loaded MSNs (**NP(Nav)**), 156 mg of navitoclax was added to a suspension of 200 mg of calcined MSNs in 6 mL of anhydrous dichloromethane under argon atmosphere and the mixture was stirred for 24 h.

3.3 Functionalization of loaded MSNs

The surface of silica materials can be easily modified, while maintaining the original structure of the mesoporous, due to the presence of high concentrations of silanol groups (Si-OH). These groups act as reactive points to covalently anchor organosilanes containing the desired organic groups. Among organosilanes, the most used are trialkoxysilane derivatives with $(R'O)_3$-Si-R structure (R: organic group). Using this method, the organic groups are preferentially placed on the external surface of the inorganic scaffold (Casula et al., 2017; Stein et al., 2000).

The functionalized nanoparticles loaded with the corresponding fluorophore or drug were finally coated with a hexa-galacto-oligosaccharide (galactan) (Megazyme, P-GALPOT), composed of six repeating galactose

monosaccharides linked through β-1,4 glycosidic bonds, to obtain gated MSNs. In addition, nanoparticles without cargo were also functionalized using only the calcined MCM-41(**GalNP(0)**). The functionalization of the nanoparticles was carried out in two consecutive steps:

- For the solid **GalNP(ICG),** an excess of (3-aminopropyl)triethoxysilane (APTES) (6 mmoles/g solid, 0.28 mL) dissolved in 6 mL of acetonitrile was prepared and the solid **NP(ICG)** previously obtained were added onto the solution. After stirring for 5.5 h at RT the solid **(NP(ICG)-NH_2)** was isolated by filtrations under vacuum.
- For the solid **GalNP(Nav)**, after 24 h of stirring in the reaction mixture previously described, 0.28 mL of APTES were added to the suspension and the stirring was kept for a further 5.5 h under argon atmosphere. Then, the solid was filtered and isolated under vacuum to obtain **NP(Nav)-NH_2**.
- **NP-NH_2** was synthesized by adding 0.28 mL of APTES to a suspension of 200 mg of empty calcined MSNs in 6 mL of anhydrous acetonitrile. After 5.5 h, the functionalized solid was isolated by filtration under vacuum.

For coating MSNs with galactan, the obtained solids functionalized with amino moieties were added to a solution of 383 mg of galactan in 25 mL of water and stirring was continued at RT for 21 h. After this time, the final product, referred to as **GalNP(ICG)**, **GalNP(Nav)**, and **GalNP(0)**, was filtered, washed with plenty of water and ethanol, and dried under vacuum. All the final nanoparticles were stored in a desiccator at RT.

4. Structural characterization of prepared nanoparticles

The characterization of the prepared solids was carried out following the standard techniques. The structural properties and porous characteristics are evaluated by powder X-ray diffraction (PXRD), transmission electron microscopy (TEM), and N_2 adsorption-desorption. Dynamic light scattering (DLS) and zeta potential (ZP) measurements allows to monitor the hydrodynamic size and surface charge of the particles along the synthetic procedure. The organic content is mainly determined by thermogravimetric analysis (TGA), elemental analysis (EA), UV-visible and fluorescence spectrophotometry.

4.1 Powder X-ray diffraction (PXRD)

PXRD was performed on a Seifert 3000TT diffractometer using CuKα radiation. Approximately 200 mg (or the maximum possible amount) of each of the solids was ground to prepare the sample. PXRD measurements were performed at low angles of radiation ($1.3 < 2\theta < 8.3$, with steps of 0.04 degrees and 3 s for step).

4.2 Transmission electron microscopy (TEM)

The TEM images, which allow observing the nanoscopic structure of the synthesized materials, were acquired with a Philips CM10 microscope with 100 KV. Samples were prepared in a solution containing a small amount of each solid in dichloroethane and a drop of the suspension was deposited on copper grids covered with carbon film provided by Electron Microscopy

Sciences to obtain high-resolution images. Micrographs were captured with 200 KV in a JEOL JEM-2100F microscope equipped with an X-ray detector.

4.3 Nitrogen adsorption-desorption (porosimetry)

N_2 adsorption-desorption isotherms were recorded on a Micromeritics TriStar II Plus automated analyzer. Samples were previously degassed at 40 °C in vacuum overnight and measurements were performed at 77 K. The specific surface areas were calculated from the adsorption data in the low pressure range using the Brunauer-Emmett-Teller (BET) model (Brunauer et al., 1938). Pore size was determined using the Barret-Joyner-Halenda (BJH) method (Barrett et al., 1951).

4.4 Thermogravimetric analysis (TGA)

TGA analysis for the determination of the amount of organic matter present in the solids was carried out on a TGA/SDTA 851e Mettler Toledo equipment, using an oxidant atmosphere (air, 80 mL/min) with a heating program consisting of a heating rate of 10 °C/min from 393 K to 1273 K and an isothermal heating step at this temperature for 30 min.

4.5 Dynamic light scattering (DLS) and Zeta Potential (ZP)

DLS and ZP measurements were carried out on a Malvern Zetasizer Nano ZS.

4.6 UV-visible and fluorescence spectrophotometry

In vitro, cargo release experiments were carried out using UV-visible spectroscopy on a Lambda 35 UV/Vis spectrometer (Perkin-Elmer Instruments) and fluorescence spectroscopy was performed with a JASCO FP-8300 spectrofluorometer.

4.7 Cargo release studies *in vitro*

Cargo release studies were carried out to assess the proper working of the molecular gate (galactan) in the presence of the enzymatic stimulus (β- Gal) capable of hydrolyzing the galactan gate. To do this, 4 mg of **GalNP(Nav)** were suspended in 10 mL of water at pH 4.5, stirred, and separated into two suspensions of 5 mL. Then, 7 mg of β-Gal from *Aspergillus oryzae* (Sigma, G5160) was added to one of the aliquots. To follow the release of the encapsulated cargo over the hours, 200 µL of each suspension was taken at different times and 300 µL of ethyl acetate was added to each one, stirred for 1 min and the organic phase was taken. Cargo released in the organic phase was measured by UV-visible spectroscopy (navitoclax absorption band in ethyl acetate at 275 nm). Cargo release studies from **GalNP(ICG)** were obtained following a similar procedure. An aliquot of 300 µL of the suspension was taken at a determined time and 2 µL of NaOH (0.15 M) was added to the aliquot. The suspension was vigorously stirred for 3 min and centrifuged for removing the solid. Then, release was measured by fluorometric spectroscopy (λ_{exc} (ICG) = 775 nm, λ_{em} (ICG) = 805 nm). To acquire a "blank" control, the same approach was carried out without the addition of enzyme.

5. Synthesis of Nav-Gal prodrug

Nav-Gal was synthesized following the literature procedure (González-Gualda et al., 2020). To do this, 40 mg (0.04 mmol) of navitoclax (Eurodiagnostico), 25 mg (0.06 mmol) of 2,3,4,6-tetra-O-acetyl-alfa-D-galactopyranosyl-bromide (Sigma), and 23 mg (0.17 mmol) of K_2CO_3 (Sigma) were mixed, and the solids were purged with argon. Anhydrous acetonitrile 10 mL (Sigma) was added, and the mixture was stirred at 70 °C for 3 h under an argon atmosphere. The solvent was removed under vacuum pressure. The crude product was purified by flash chromatography on silica gel (Sigma), from hexane-ethylacetate (3:7 v/v; Scharlab) to hexane-ethylacetate (7:3 v/v) used as eluent. Purified **Nav-Gal** was obtained as a yellow powder in a 35% yield. For the mice experiment, some batches were mixture before purified by flash chromatography.

6. Characterization of Nav-Gal prodrug

To determine the presence of the acetylated galactose in the structure of **Nav-Gal**, the prodrug was characterized as previously described following conventional techniques: proton nuclear magnetic resonance (^{1}H-NMR), two-dimensional nuclear magnetic resonance spectroscopy (COSY NMR), and high-resolution mass spectrometry HRMS spectrum. To do this, **Nav-Gal** was dissolved in deuterochloroform ($CDCl_3$; Sigma) and transferred to a Wilma NMR tube (Sigma). Samples were evaluated immediately by ^{1}H-NMR and COSY NMR. NMR spectra were acquired with a Bruker FT-NMR Avance 400 (Ettlingen, Germany) at 300 K and analyzed with MestReNova 6.0 software. Chemical shifts are expressed as δH (ppm) relative

tetramethylsilane (TMS). Attenuated total reflectance (ATR) was performed in a Bruker Tensor 27 FT-IR (Ettlingen, Germany) at RT and analyzed with OPUS Data Collection Program (V1.1). HRMS was recorded with an ABSciex TRIPLETOF T5600.

7. Cellular studies

7.1 Cytotoxicity cell studies

Cell viability assays were carried out to determine the doxorubicin response of HL-1 cells and the cytotoxic effect of the different senolytic treatments.

7.2 Doxorubicin dose-response

For doxorubicin dose-response studies, HL-1 cells were seeded in flat-bottom clear white p96-multiwell plates (PerkinElmer, 6005181) at a density of 15,000 cells/well. The next day, cells were treated with different concentrations of DOX (0 – 1 μM) for 72 h. Medium containing DOX was eliminated and replaced with fresh medium. The viability of cells was assessed by measuring luminescence with CellTiter-Glo Luminescent Cell Viability Assay (Promega, G7571) following the manufacturer's instructions. CellTiter-Glo reagent was added to each well and the plate was placed in an orbital shaker for 2 min to induce cell lysis. The plate was then incubated at RT for 10 min to stabilize the luminescent signal. Luminescence was recorded in a Wallac Victor2TM plate reader spectrophotometer (PerkinElmer). The number of viable cells was normalized to the internal control of untreated cells (vehicle only). Control wells containing medium without cells were

included to substrate the value for background luminescence. A dose-response curve was obtained using GraphPad 9.0 software.

7.3 Cytotoxic effect of senolytic treatment

The cytotoxic effect of free navitoclax, **GalNP(Nav)**, and **Nav-Gal** was evaluated for control and senescent HL-1 cells seeded in flat-bottom clear white p96-multiwell plates at a density of 15,000 and 25,000 cells/well, respectively. The following day cells were treated in triplicate as follows:

- Free navitoclax and **Nav-Gal** were both dissolved in DMSO to obtain a 50 mM stock. Small aliquots were prepared to avoid freeze-thaw cycles. Before treatment, fresh solution containing the drug at increasing concentration was prepared up to 50 μM.
- **GalNP(Nav)** was prepared in serial dilution up to 2 mg/mL, which corresponds to a 2.7 μM maximal concentration of free navitoclax. Nanoparticles were prepared in a culture medium, briefly sonicated, and stirred on a magnetic plate for 45 min. Just prior to treatment, the solution was filtrated using a 0.45 μM filter.
- **GalNP(0)** was used as a control to evaluate the possible intrinsic cytotoxicity associated to the nanomaterial. The same concentration of nanoparticles (up to 2 mg/mL, filtrated) was evaluated.

Both control and senescent cells were treated with each of the senolytic drugs and were incubated for 48 h. After this time, cell viability was assessed measuring luminescence with CellTiter-Glo Luminescent Cell Viability Assay following the protocol explained above. The number of viable cells was normalized to the internal control of untreated cells (vehicle

only), either control or DOX-treated cells for each plate. A non-linear fit log(inhibitor) versus response with a variable slope (four parameters) model was used for IC50 estimation in GraphPad 9.0 software.

7.4 Cellular uptake of nanoparticle

To evaluate that the prepared nanomaterials are efficient to target senescent cells, we evaluated the cellular uptake and cargo release of the nanoparticles in control and senescent HL-1 cells by confocal microscopy and flow cytometry.

7.4.1 Cargo release study of GalNP(ICG) by confocal microscopy

For image acquisition by confocal, both control and senescent HL-1 cells were seeded on a coverslip in a 6-well plate at a concentration of 200,000 cells/well. The next day, a suspension of 1 mg/mL **GalNP(IGC)** was added to culture medium, sonicated to avoid nanoparticle aggregates, stirred for 45 min, and filtered using a 0.45 μm filter. The NPs suspension was added to the cells and incubated for 4 h. After this time, medium with NPs was removed, and cells were washed with PBS to eliminate non-internalized NPs. The coverslips were mounted appropriately for confocal imaging, and Hoechst 33342 was added for nuclei staining. Cells were visualized in Leica TCS SP8 HyVolution 2 confocal microscope. ICG signal was detected using an excitation wavelength of 638 nm and with an emission window set between 664-783 nm. The same conditions were applied to non-treated cells to determine the autofluorescence signal. Images were processed using LAS X software and the ICG intensity was analyzed using ImageJ software.

7.4.2 Cargo release study of GalNP(ICG) by flow cytometry

Flow cytometry studies were followed for quantification of the cargo release from nanoparticles in cells. The **GalNP(IGC)** suspension was prepared as above and cells were treated following the same procedure. After the incubation with the nanoparticles, cells were washed with PBS to eliminate non-internalized NPs. Then, cells were collected by adding 0.5% Trypsin-EDTA (Gibco), centrifuged (1200 rpm, 5 min, 4 °C), and resuspended in cold PBS. Flow cytometry assay was carried out on a CytoFlex S instrument (Beckman Coulter) followed by data analysis using CytoExpert software. For data analysis, we also run a non-treated control sample to determine senescence autofluorescence, which was also considered by subtracting it.

8. Mouse model

All mice used for the following experiments were C57BL/6J strain (10 weeks) purchased from Charles River Laboratories and maintained in ventilated racks under pathogen-free conditions at Principe Felipe Research Centre (Valencia, Spain), with food and water *ad-libitum* and alternate dark and light cycles. All animals were treated humanely, and experiments were approved by the Ethical Committee for Research and Animal Welfare Generalitat Valenciana, Conselleria dÀgricultura, Medi ambient, Canvi climàtic i Desenvolupament Rural (2020/VSC/PEA/0217).

8.1 Doxorubicin-induced cardiotoxicity mice model

To establish the mouse model of doxorubicin-induced cardiotoxicity associated with cardiac senescence wild-type male and female C57BL/6J mice (strain code: 632) (10 weeks old) were used. DOX was administered intraperitoneal (IP) once with 10 mg/kg of doxorubicin hydrochloride (Carbosynth, AD15377) in saline (groups DOX10) or eight equal intraperitoneal injections (2.5 mg/kg) for 4 weeks with a total cumulative dosage of 20 mg/kg, (groups DOX20). Control mice were injected with an equal volume of saline following the DOX20 administration regime (eight injections) to discard stress changes due to repeated IP administrations. After 4 weeks, mice were led *ad-libitum* until day 44. Echocardiography analyses were performed every week to follow the cardiac dysfunction of mice. Hearts were collected at the endpoint of the experiment (day 44). C57BL/6J mice in each experimental condition (n=3).

8.2 Senolytic treatment study

After setting the best model of study, wild-type female C57BL/6J mice (10 weeks old) were randomly assigned into the following 6 groups (n = 6/group): Control, DOX, DOX + navitoclax, DOX + **GalNP(Nav)**, DOX + **Nav-Gal**. Doxorubicin was administered as before, in a chronic regime (cumulative dose, 20 mg/kg, IP.), in eight equal intraperitoneal injections (2.5 mg/kg) for 4 weeks (twice a week). Mice received the dose of the senolytic treatment for two consecutive days after DOX administration. An off day was every two cycles. For senolytic treatment, we adopted the dosage regimen based on previous data working with navitoclax in animal models. Free

navitoclax was formulated in 15%DMSO/85%PEG400 and was administered at a dose of 50 mg/kg/day via oral gavage (OG) (Dookun et al., 2020). **GalNP(Nav)** was prepared in free-serum DMEM and administered at the maximum tolerated dose (0.8 mg NP/day) according to (Galiana et al., 2020). A stock of **GalNP(Nav)** was prepared every day before administration at a concentration of 4 mg/mL, slightly sonicated, and stirred on a magnetic plate for 1 h to avoid nanoparticle aggregates. Mice were administered intravenously (via tail) with 200 µL of the prepared suspension. Experimental calculations indicate that approximately 31 mg of the drug is released per gram of **GalNP(Nav).** Therefore, a dose equivalent to 0.025 mg navitoclax/day was administered in the nanoparticle formulation. This dose corresponds with 23x times lower concentration of free navitoclax. Finally, **Nav-Gal** was reconstituted in DMSO and further diluted in saline in a final proportion of 10%DMSO/90%saline. The administered dose was calculated to be equal to the molar equivalents of free navitoclax which corresponds with 67 mg/kg/day, via IP administration as described previously (González-Gualda et al., 2020). Control groups were administered with only vehicle: the same volume of only saline was administered as control of DOX (via IP injection) and for senolytic controls, mice were divided into either 15%DMSO/85%PEG400 (OG) or 10%DMSO/90%saline (IP). Echocardiography analyses were performed every two weeks to follow the cardiac dysfunction of mice. At the end of the experiment, animals were euthanized in a CO_2 atmosphere on day 30.

9. Echocardiography

Parameters of cardiac function were determined using two-dimensional transthoracic echocardiography (Echo) using a Vivid 7 Pro imaging system (GE Medical Systems). Mice were lightly anesthetized using 1.5% sevoflurane mixed with 100% O_2 in an anesthesia induction chamber and then placed on a specially designed stage with integrated electrocardiographic, cutaneous, temperature and respiratory monitors for imaging, while maintain anesthetized by facemask. Echo was performed serially before and during the experimental period as detailed in the mouse experimental section. Once correctly ensured the orientation of the heart for optimal imaging of the left ventricular, we recorded at least 15 frames of the cardiac cycle to accurately detect end-diastole and end-systole. The used parameters to assess left ventricular systolic functions are fractional shortening (FS) and ejection fraction (EF) which were determined from the M-mode of the parasternal short-axis view. The left ventricular end-diastolic dimension (LVEDD) and left ventricular end-systolic dimension (LVESD) were obtained to calculate FS and EF values by using Vivid Analysis software. All parameters were averaged from at least 3 cardiac cycles per animal at each time point.

Since Echo analysis is manual, it can result in incorrect interpretation. Also, Echo studies are challenging because of the mouse's response to stress, as well as the small size, rapid contraction, and orientation of the mouse heart. To minimize errors and to improve the accuracy of the analysis, Echo analysis was performed always by the same operator, the head veterinarian from the

Centro Investigación Príncipe Felipe, Viviana Bisbal, and all analysis was performed in a blinded manner by myself to standardize the process.

10. Tissue collection and processing

Rapidly after being euthanized in a CO_2 atmosphere, animals underwent blood collection with a 25G needle until obtaining 1 mL, for biochemical and hemogram analysis.

The hearts were collected via thoracotomy for *ex vivo* evaluations. Hearts were dissected immediately, washed in PBS, and trimmed to remove any excess fat and connective tissue. Hearts were dissected for histological and gene expression analysis into two halves. For RNA analysis, heart samples were snap-frozen and stored at -80 °C. For histological analysis, heart samples were cryo-embedded and frozen. Firstly, the tissue was fixed in 4% PFA at RT for 4 h and then, the fixative was removed, and samples were washed in PBS and incubated with 30% sucrose with agitation overnight at 4 °C, for cryo-protection. After this time, hearts were washed in PBS and embedded in optimal cutting temperature compound (OCT), in the appropriate orientation, and frozen completely first on dry ice and then stored at -80 °C. The hearts were sectioned to produce 7 μm thick transverse sections on a cryostat and collected as sister sections on Superfrost Plus slides (Thermo Scientific). Additional organs including the liver, lung, spleen, and kidneys were also collected and snap-frozen.

11. Immunofluorescence

Heart sections (7 µm thick) embedded in OCT were first thawed at RT. Samples were permeabilized in 0.025% Triton X-100 in TBS, then incubated in blocking solution consisting of 10% horse serum, 1% BSA, 0.3% Triton X-100, in TBS, for 2 h at RT. Slides were immunostained following incubation with the corresponding primary antibody overnight at 4 °C in a staining solution 1% BSA, 0.3% Triton X-100, in TBS. After more PBS washes the next day, the secondary antibody was applied to the slides and incubated for at least 2 h at RT in the dark. Once stained, slides were washed in PBS, and coverslips were mounted using the Mowiol/DAPI (Sigma). Slices were scanned in a Leica Aperio Versa 200 equipment and fluorescence was quantified with Aperio ImageScope software. Representative images were obtained by using a Leica TCS SP8 HyVolution 2 microscope. Used antibodies can be found in **Table 2.**

Table 2. Antibodies used for immunofluorescence

Antibody	Dilution	Host species/ wavelength	Company	Reference
Primary antibody				
Anti-p53 antibody [PAb 240]	1/100	Mouse	Abcam	ab26
Anti-p21 [HUGO29]	1/75	Rat	Abcam	ab107099
Secondary antibody				
Goat anti-mouse Alexa fluor	1/200	488	Invitrogen	A-11029
Goat anti-rat Alexa fluor	1/200	568	Invitrogen	A-11077
Imaging reagents				
DAPI	1/400	358	Invitrogen	D1306
WGA	1/500	647	Invitrogen	232466

12. WGA staining

Cardiomyocyte hypertrophy was evaluated after staining the cryo-section with the membrane marker Wheat Germ Agglutinin (WGA) (1:500, 647 nm, W32466, Invitrogen) for 1 h at RT. After several PBS washes, slides were mounted in Mowiol/DAPI. Slices were scanned in Leica Aperio Versa 200 equipment and the area of individual CMs in a similar orientation was quantified with ImageJ software (Walaszczyk et al., 2019)

13. Gene expression analysis

To evaluate the levels of gene expression from cells and tissues, samples underwent RNA isolation, followed by cDNA synthesis and analyzed by RT-qPCR.

13.1 RNA isolation

RNA was obtained from the different biological samples by adapting the protocols to obtain, in each case, the best values for the quantity and quality of RNA.

Total RNA from HL-1 cells was isolated from cultured cells centrifuged at 6,000 g for 5 min at 4 °C following the commercial NZY Total RNA Isolation kit (Nzytech, MB13402) instructions. First 350 µL of Buffer NR and 3.5 µL β-mercaptoethanol was used to disrupt the pellet by vortex vigorously. The lysate was homogenized by placing it on an NZYSpin Homogenization column and centrifuged at 11,000 g for 1 minute. 350 µL of 70% EtOH was added to the flow-through lysate mix immediately by

pipetting up and down. The sample was transferred to an NZYSpin Binding column and centrifuged at 11,000 g for 30 s. 350 µL of Buffer NI were added and centrifuged at 11,000 g for 30 s. The flow through was discarded and 95 µL of a DNase I solution (1/10) was added into the column and incubated at RT for 15 min. 200 µL of Buffer NWR1 was applied to the column and centrifuged at 11,000 g for 1 min. Flow through was again discarded and 600 µL of Buffer NWR2 was added to the spin column. The column was spun for 11,000 g for 1 min and repeated the wash with 250 µL of NWR2 buffer and centrifuge for 11,000 g for 1 min to ensure it was dry and RNA was eluted from the column by adding 20-30 µL of RNase-free H_2O and centrifuging at 11,000 g for 1 min to elute the RNA.

RNA from tissue was obtained using frozen heart samples for total RNA extraction. Tissue was disrupted with Trizol (Merck, T9424) with mechanical digestion with a sonicator. Subsequently, the protocol described by Chomczinsky and Sacchi was followed (Chomczynski et al., 1987). To fresh Eppendorf, 1 mL of homogenized tissue in Trizol was added to 200 µL of chloroform, shacked vigorously for 15 s, left to settle for 3 min, and then centrifuged for 15 min at 12,000 g. The aqueous phase was carefully added to a fresh Eppendorf with 500 µL of isopropanol by pipetting, ensuring that the interphase was not disturbed, and mixed gently before 10 min of incubation at RT. The sample was centrifuged for 10 min at 12,000 g. The precipitated RNA was washed twice with 1 mL ethanol 70% and centrifuged for 5 min at 7,500 g. The pellet was left to air-drying for a few min and then resuspended in 20-50 µL of RNase-free H_2O.

13.2 RNA quality control

RNA content was determined using NanoDrop™. The quality of the RNA obtained was measured in two different ways by Nanodrop, using the absorbances 260/230 nm and 260/280 nm, indicators of chemical contamination, and protein contamination, respectively. Concentrations were accepted if there was a 260/280 ratio of 1.8-2.1 and a regular plot on an absorbance spectrum, as this indicated high purity of the RNA, and by using the bioanalyzer 2100 (Agilent) to calculate the RIN (RNA quality value) of each sample. Only samples with acceptable RIN were included in the studies. Samples were stored at -80 °C until further use.

13.3 cDNA synthesis

Samples were treated with DNase I (Nzytech, MB19901) to avoid genomic DNA contamination. The retrotranscription reaction of total RNA was performed using the NZY First-Strand cDNA Synthesis Kit (Nzytech, MB12502) following the manufacturer's protocol. The volume required to contain 1 µg of RNA was added to 10 µL of NZYRT 2× Master Mix containing oligo(dT)$_{18}$, random hexamers, $MgCl_2$ and dNTPs, and 2 µL of NZYRT Enzyme Mix including NZY Reverse Transcriptase and NZY Ribonuclease Inhibitor. The volume was made up of a total volume of 20 µL with ddH_2O. Samples were run on a PCR program with the following stages: 10 min at 25 °C; 30 min at 50 °C, 5 min at 85 °C, to inactivate the reaction, and the chilled on ice; then 1 µL of NZY RNase H was added and incubate at 37 °C for 20 min, to remove RNA residues bound to the cDNA, allowing for greater sensitivity in PCR. Samples were kept at - 20 °C until required.

13.4 Quantitative reverse transcriptase polymerase chain reaction (qRT-PCR)

To obtain a semi-quantitative result of the expression of both genes, we used the RT-qPCR technique, which is based on the relative quantification of mRNA expression levels concerning a reference gene. qRT-PCR reactions were performed using qPCR Green Master Mix (2x) (Nzytech, MB22402) following the protocol: 1 µL of cDNA sample diluted 1:10, 5 µL of the 2x master mix, 0.5 µL of each primer (10 µM), either forward or reverse, and ribonuclease-free water were used, up to 10 µL final reaction mix.

Amplification reactions were performed in 96- or 384-well plates with each sample loaded in triplicate and were run in a LightCycler® 480 System (Roche) the following stages: 1 cycle 5 min at 95 °C for polymerase activation; 45 cycles following 10 s at 95 °C (denaturation), 20 s at 60 °C (annealing/extension) and 10 s at 72 °C (signal acquisition). Data were analyzed using the LightCycler 480 relative quantification software. The melting temperature curve was analyzed to be sure of the efficiency of the primers and the presence of a single amplicon. For gene expression analysis, triplicates with a difference of more than 0.5 cycles between them were discarded. To calculate the relative quantification concerning the reference gene, the delta-delta-method was used (2^-(ΔΔCt)), considering the cycle at which fluorescence is detected (Ct) and the efficiency of the primers used (ideally, 2). The fold gene expression is calculated in comparison to a standard Ct from a reference gene. The housekeeping genes used to normalize data were glyceraldehyde 3-phosphate dehydrogenase (*Gapdh*) and actin beta

(*Actb*). Nucleotide sequences of the primers used for mRNA expression analyses are listed below in **Table 3**.

14. Statistical analysis

Statistical analysis of data was obtained by using GraphPad Prism software 9.0 (San Diego, CA, US). Data were expressed as mean and the error bars represent the standard deviation (SD) or standard error of the mean (SEM), as specified in each experiment. Comparison of results between groups was made by Student's T-test or One-way ANOVA followed by a Tukey post-test at 95% confidence. A p-value below 0.05 was considered statistically significant (*$p<0.05$; **$p<0.01$; ***$p<0.001$; ****$p<0.0001$). Data are expressed in more detail for every figure.

Table 3. Primer sequences used for qPCR experiments.

Gene	Primer	Sequence (5'→ 3')	GeneBank Number	Size (bp)
p21	Forward	GCAGATCCACAGCGATATCCA	NM_007669.5	73
	Reverse	AACAGGTCGGACATCACCAG		
p53	Forward	TGCATGGACGATCTGTTGCT	NM_011640.3	161
	Reverse	AAAGATGACAGGGGCCATGG		
p16*	Forward	CCCAACGCCCCGAACT	NM_001040654.1	79
	Reverse	GCAGAAGAGCTGCTACGTGAA		
Ccl8	Forward	TAAGGCTCCAGTCACCTGCT	NM_021443.3	119
	Reverse	TCTGGAAAACCACAGCTTCC		
IL-1α	Forward	CGTCAGGCAGAAGTTTGTCA	NM_010554.4	102
	Reverse	TGTTGCAGGTCATTTAACCAA		
TNFα	Forward	ACGGCATGGATCTCAAAGAC	NM_013693.3	116
	Reverse	GTGGGTGAGGAGCACGTAGT		
Sur2a	Forward	CCTTCGGCTCTCGACTTCTA	NM_021041.2	181
	Reverse	ACTCGACCCAAGCAAATTGT		
Nppa*	Forward	ATCTGCCCTCTTGAAAAGCA	NM_008725.3	213
	Reverse	ACACACCACAAGGGCTTAGG		
ActinB	Forward	GTCCACACCCGCCACC	NM_007393.5	168
	Reverse	ACCCATTCCCACCATCACAC		
Gapdh	Forward	TTCACCACCATGGAGAAGGC	NM_001289726.1	52
	Reverse	CCCTTTTGGCTCCACCCT		

**p16* sequence was obtained from Baker et al., 2018, and the *Nppa* sequence was obtained from Muñoz-Espín et al., 2018.

.

Results

1. Induction of cellular senescence in HL-1 cardiac myocyte cell line upon doxorubicin treatment

To investigate whether the selective elimination of senescent cells would prevent long-term associated cardiac pathologies to DOX, we first established an *in vitro* model using the HL-1 cardiac myocyte cell line (**Figure 18A**). HL-1 cells represent a cardiac myocyte cell line that can be repeatedly passaged, and have been previously used to induce a cardiomyocyte senescence model (Yu et al., 2020), as even immortalized, these cells maintain a cardiac-specific phenotype and allow to obtain reproducible experiments (Claycomb et al., 1998). We first performed a dose-response curve of DOX for 72 h and found that 100 nM treatment was enough to induce senescence in HL-1 cells without causing significant cell death, keeping cell viability up to 80% (**Figure 18B**). DOX-treated HL-1 cells showed increased lysosomal β-galactosidase (β-gal) activity, a typical marker of senescence activation (Dimri et al., 1995), evidenced by the increment in blue-stained cells observed in X-Gal staining assays *versus* untreated cells (**Figure 18C**). In line with these results, flow cytometry studies using the lipophilic β-galactosidase substrate 5-dodecanoylaminofluorescein di-β-D-galactopyranoside (C_{12}FDG) confirmed the accumulation of senescent population in DOX-treated HL-1 cardiomyocytes (3-fold) compared to non-treated cells (**Figure 18D**).

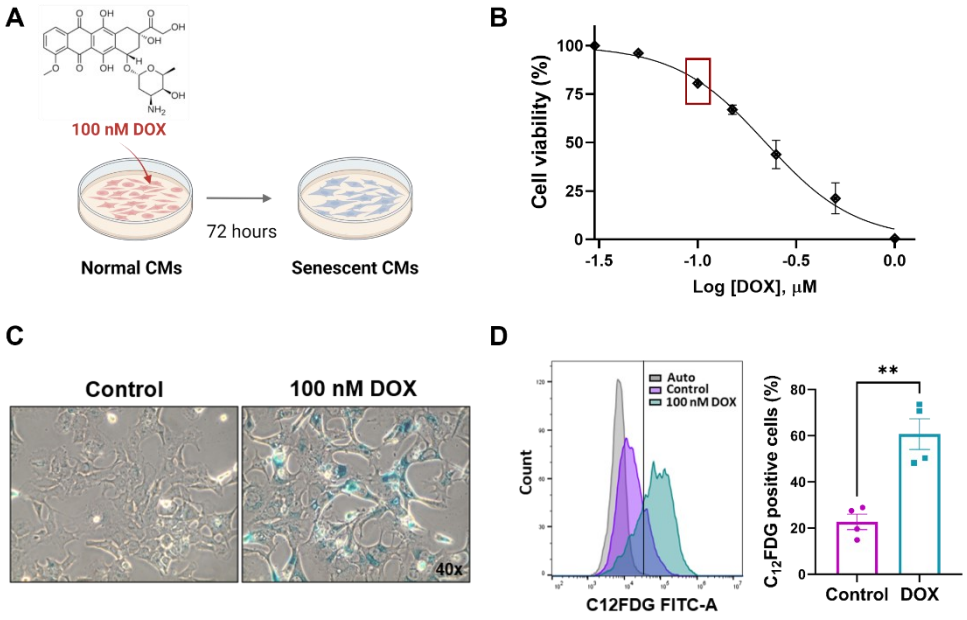

Figure 18. DOX treatment induces senescence-associated β-galactosidase (SA-β-gal) activity in HL-1 cells.
(A) Schematic representation of the *in vitro* model of senescence induction in HL-1 cardiomyocyte cells (CMs) upon DOX treatment, for 72 h. **(B)** Dose-response curve of DOX in HL-1 cells incubated with the indicated range of drug concentrations for 72 h (0 to 1 µM). Cell viability data shown are mean effect relative to vehicle-only control wells ± SEM (n=3). The red square indicates 100 nM DOX. **(C)** Representative bright-field images of SA-β-Gal staining of control and 100 nM DOX-treated HL-1 cells. Blue staining confirms high β-Gal at pH 6 upon DOX treatment. **(D)** Histogram and percentage of C_{12}FDG positive cells indicate β-Gal activity in control and DOX-treated cells by flow cytometry. Values are expressed as mean ± SEM and statistical significance was assessed by the two-tailed Student's t-test: **$p < 0.01$ (n=4).

Moreover, cell cycle analyses by flow cytometry after DOX treatment for 72 h showed that DOX-induced accumulation of cells in G2/M-phase, a hallmark of the cell cycle effect of DOX treatment (A. Shimizu et al., 1998) (**Figure 19A**). Additionally, the suppression of proliferation in HL-1 cells by

DOX treatment was confirmed by time-lapse imaging for 48 h (**Figure 19B**) and by crystal violet staining after one week in culture. For the later, we performed a proliferation arrest assay where the same initial number of DOX-treated or untreated cells were seeded, and cells stained with crystal violet after one week in culture. Lower levels of staining in the DOX-treated HL-1 cells were observed, indicative of decreased cellular proliferation confirming cell cycle arrest (**Figure 19C**). Immunostaining of the Ki67 proliferation marker demonstrated the stop of cellular proliferation for DOX-treated HL-1 cells also confirming cell cycle arrest (**Figure 19D**).

It is now well recognized that most stressors that induce cellular senescence activate either or both the p53/p21 or $p16^{Ink4a}$/retinoblastoma protein pathways to prevent entry into the cell cycle (B. D. Chang et al., 1999; Chicas et al., 2010). Hypo-phosphorylation in retinoblastoma (Rb) protein and upregulation of p53 and p21 were observed in extracts of DOX-treated HL-1 cells, as is expected for a senescent phenotype (**Figure 20A**). We also demonstrated the induction of β-galactosidase (β-gal) protein expression by western blot (**Figure 20A**). In our regard, the importance of β-gal up-expression is essential for validating our targeted strategies, as the proper performance of both, nanoparticles (**GalNP(Nav)**) and the prodrug (**Nav-Gal**) depends on this activity (*vide infra*). The up-expression of *p21* and *p53* and the SASP markers *Cxcl1* and *IL6* were also confirmed at mRNA levels in HL-1 in response to DOX exposure (**Figure 20B**).

These studies demonstrated that cell cycle exit, and senescence after DOX exposure are accompanied by the activation of the cell cycle inhibitors

p53/p21 and hypo-phosphorylation in retinoblastoma (Rb) protein, β-gal induction, and SASP expression.

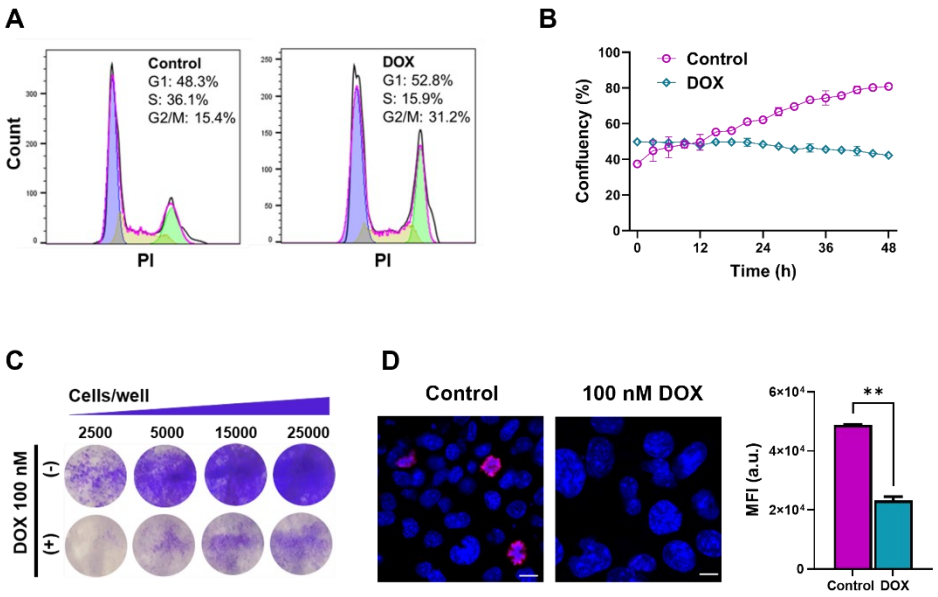

Figure 19. DOX induces cell cycle and proliferation arrest in HL-1 cells.
(A) Cell cycle distribution was measured using flow cytometry. Propidium iodide (PI) staining of control and 100 nM DOX-treated HL-1 cells. DOX-treated cells accumulate in cell cycle G2/M after 3 days of treatment. **(B)** Graphs represent confluency (%) of HL-1 control and DOX-treated cells followed by time-lapse imaging, showing suppression of proliferation in HL-1 cells by 100 nM DOX. **(C)** Cell proliferation arrest assay by crystal violet staining. The same number of control and DOX-treated cells were seeded with increasing cell numbers (2500; 5000; 15000; 25000) in a 24-well plate and were let to proliferate for one week. Cell cycle arrest was confirmed by crystal violet staining. **(D)** (Left) Representative immunofluorescence images of the cell proliferation marker Ki67 (red fluorescence) in control and DOX-treated HL-1 cells by confocal microscopy. The nucleus is stained with Hoechst 33342 (blue). Ki67 expression decreases upon DOX treatment. Scale bar, 10 µm. (Right) Quantification of mean fluorescence intensity of Ki67 red signal corresponding to 3 different fields. Bars represent the mean ± SEM and statistical significance was assessed by the two-tailed Student's t-test: **p <0.01.

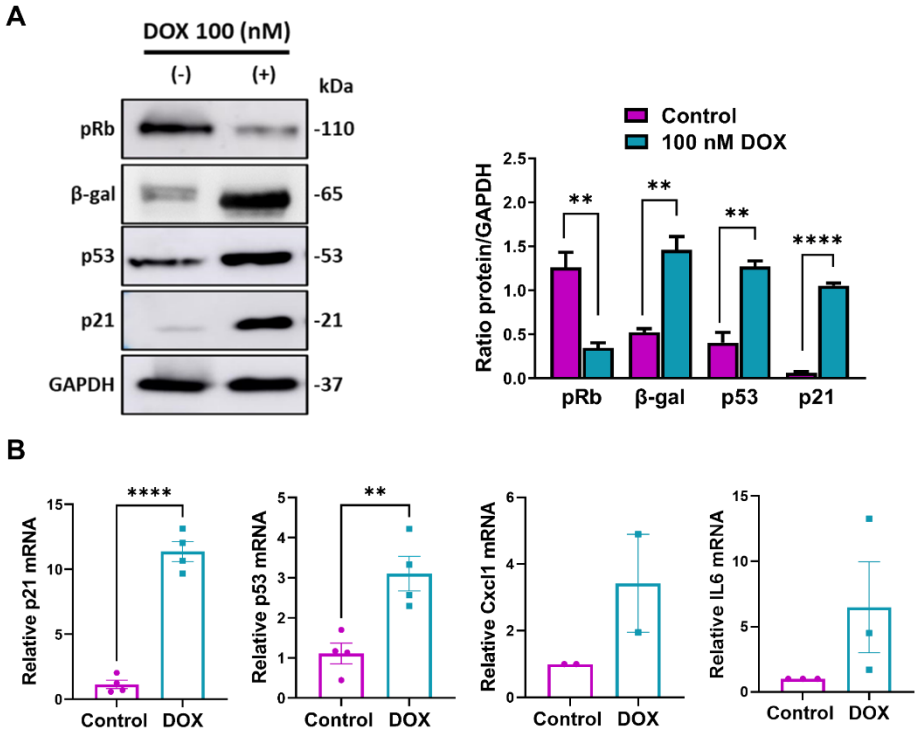

Figure 20. DOX induces the expression of senescent markers in HL-1 cells. **(A)** (Left) Representative western blot analysis showing the decrease in phospho-retinoblastoma (pRb) expression (110 kDa) and the increment in β-galactosidase (65 kDa), p53 (53 kDa) and p21 (21 kDa) protein expression for DOX-treated HL-1 cells. GAPDH (37 kDa) was included as a loading control. (Right) Quantification of ratio protein expression versus internal reference (GAPDH) in control and DOX-treated cells. Values are expressed as mean ± SEM and statistical significance was assessed by the two-tailed Student's t-test: *p<0.05; **p<0.01; ****p <0.0001 (n≥3). **(B)** mRNA expression levels of the senescence makers *p21* and *p53*, and the SASP markers, *Cxcl1* and *IL-6* in HL-1 control and DOX-treated cells, showing up-expression in DOX-treated cells. *Actb* was used for input normalization. Bars represent the mean ± SEM and statistical significance was assessed by the two-tailed Student's t-test: **p<0.01; ****p <0.0001 (n≥2).

Once the induction of cellular senescence in the HL-1 cardiac myocyte cell line upon DOX treatment was demonstrated, we evaluated the effectiveness of the senolytic navitoclax *in vitro.* As navitoclax is an inhibitor of the anti-apoptotic proteins Bcl-2, Bcl-xL, and Bcl-w, we first analyzed changes in Bcl-2 family proteins expression upon DOX treatment in HL-1 cardiomyocytes (**Figure 21**). We corroborated the upregulation of these anti-apoptotic proteins (**Figure 21A**), as well as the pro-apoptotic proteins Bim, Bok, and Bax, which were also upregulated in senescent HL-1 cells (**Figure 21B**). These results indicated dysregulation in apoptosis machinery after DOX exposure with high dependence on anti-apoptotic proteins for survival, which strongly suggests that navitoclax could be a suitable senolytic treatment in this model.

Next, we treated control and senescent HL-1 cells with increasing concentrations of navitoclax for 48 h (**Figure 22**). Navitoclax exhibited senolytic activity by selectively inducing apoptosis on senescent HL-1 cells (**Figure 22B**). The IC50 value was calculated for both control (IC50 = 8.43 µM) and senescent cells (IC50 = 0.37 µM), resulting in a senolytic index of 23 (**Table 7**). These results confirm that after induction of senescence by DOX in HL-1 myocytes, navitoclax exhibits senolytic activity. Besides, we performed an X-Gal staining including control and DOX-treated cells treated with navitoclax (IC50 for senescent cells: 0.37µM) (**Figure 22C**). These results confirm navitoclax treatment resulted in a reduction in the number of senescent cells but not control cells, which reinforces the role of navitoclax as a senolytic therapy.

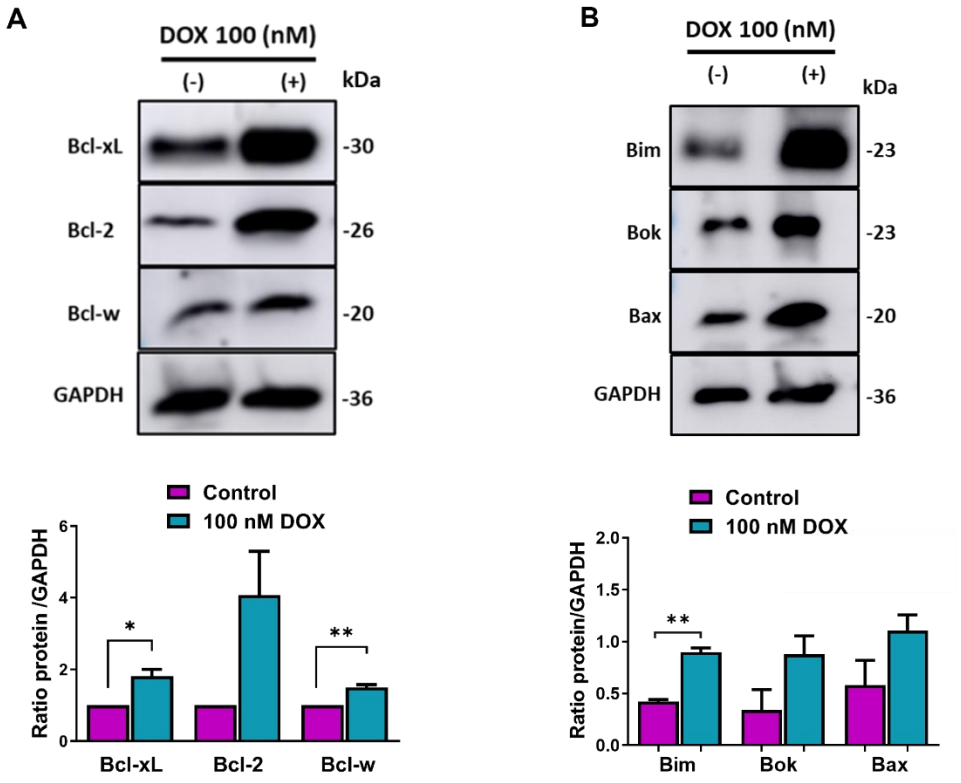

Figure 21. Protein profile expression of Bcl-2 family in HL-1 cells.
(A) Western blot analysis expression showing increased expression of anti-apoptotic proteins Bcl-xL (30 kDa), Bcl-2 (26 kDa), and Bcl-w (20 kDa) in DOX treated HL-1 cells. GAPDH (37 kDa) determination was included as a loading control. Quantification of ratio anti-apoptotic protein expression versus internal control (GAPDH) in control and DOX-treated cells. Values are expressed as mean ± SEM and statistical significance was assessed by the two-tailed Student's t-test: *p<0.05; **p <0.01 (n≥3). **(B)** Western blot analysis expression showing increased expression of pro-apoptotic members Bim (23 kDa), Bok (23 kDa), and Bax (20 kDa) in DOX-treated HL-1 cells. GAPDH (37 kDa) determination was included as a loading control. Quantification of the ratio of pro-apoptotic protein expression versus internal control (GAPDH) in control and DOX-treated cells. Values are expressed as mean ± SEM and statistical significance was assessed by the two-tailed Student's t-test: **p <0.01 (n=3).

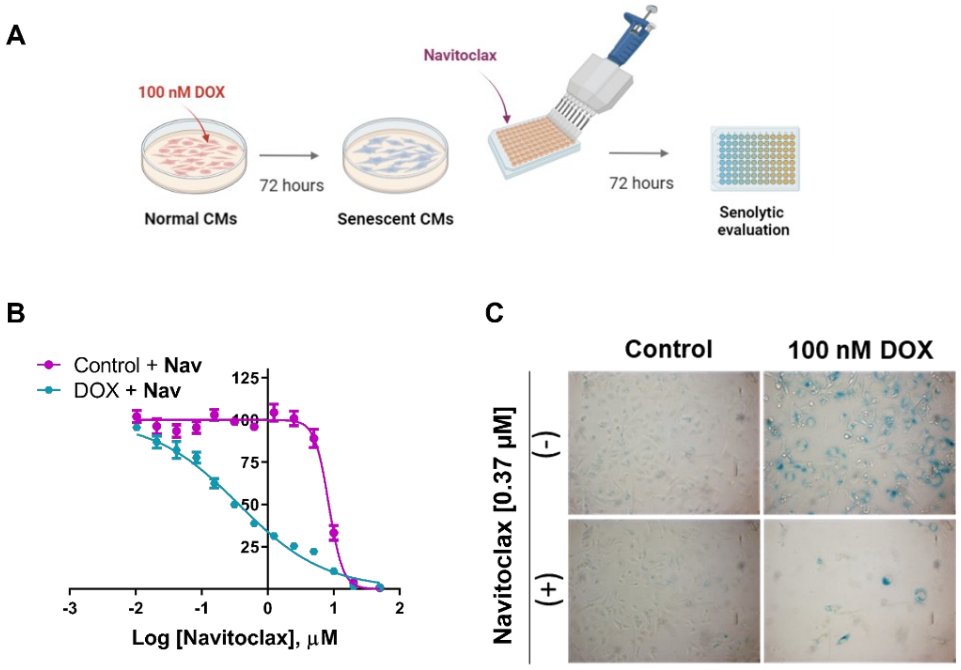

Figure 22. Navitoclax response.

(A) Schematic representation of the *in vitro* navitoclax effect evaluation in control and senescent HL-1 cardiomyocyte cells (CMs). **(B)** IC50 curves were obtained with increasing concentrations of free navitoclax (0.01 to 50 µM) for control and DOX-treated cells measured after 48 h of treatment by luminescent ATP detection. Values are expressed as mean ± SEM (n=8). **(C)** Representative bright-field images of SA-β-gal staining of control and 100 nM DOX-treated HL-1 cells non-treated (upper panels) or navitoclax treated for 48 h (bottom panels) at IC50 concentration for senescent cells (0.37 µM). Blue staining confirms high β-gal activity in DOX treatment. Navitoclax exposure resulted in a reduction in the number of senescent cells but not control, which reinforces the role of navitoclax as a senolytic therapy.

2. Synthesis of galactan-capped nanoparticles loaded with navitoclax (GalNP(nav))

Considering our purpose to overcome the toxicity limitations of navitoclax (e.g., hematological toxicities), we took advantage of the high lysosomal β-galactosidase (β-gal) activity present in senescent cells and encapsulated navitoclax in mesoporous silica nanoparticles capped with a hexa-galacto-oligosaccharide (galactan) to specifically target senescent cells and avoid cargo leakage (**Figure 23A**). We have previously reported the senolytic potential of these nanoparticles in models of dyskeratosis congenita, chemotherapy-treated xenografts, pulmonary fibrosis, and endothelial-induced senescence (Agostini et al., 2012; Estepa-Fernández et al., 2021; Galiana et al., 2020; Muñoz-Espín et al., 2018). The synthesis of the nanoparticles has been reported elsewhere (Galiana et al., 2020). In our case, the mesoporous silica nanoparticles (MSNs) are loaded with indocyanine green (ICG, for tracking purposes), or navitoclax (Nav, for treatment), and coated with galactan (solids **GalNP(ICG)** and **GalNP(Nav)**, respectively). When the galactan-gated nanodevices reach senescent cells, the lysosomal β-gal activity induces the hydrolysis of the cap with the subsequent preferential cargo release into senescent cells (**Figure 23B**) (Muñoz-Espín et al., 2018). To evaluate the biocompatibility of the mesoporous silica carrier in HL-1 cardiomyocytes, galactan-capped nanoparticles without cargo were also prepared (**GalNP**).

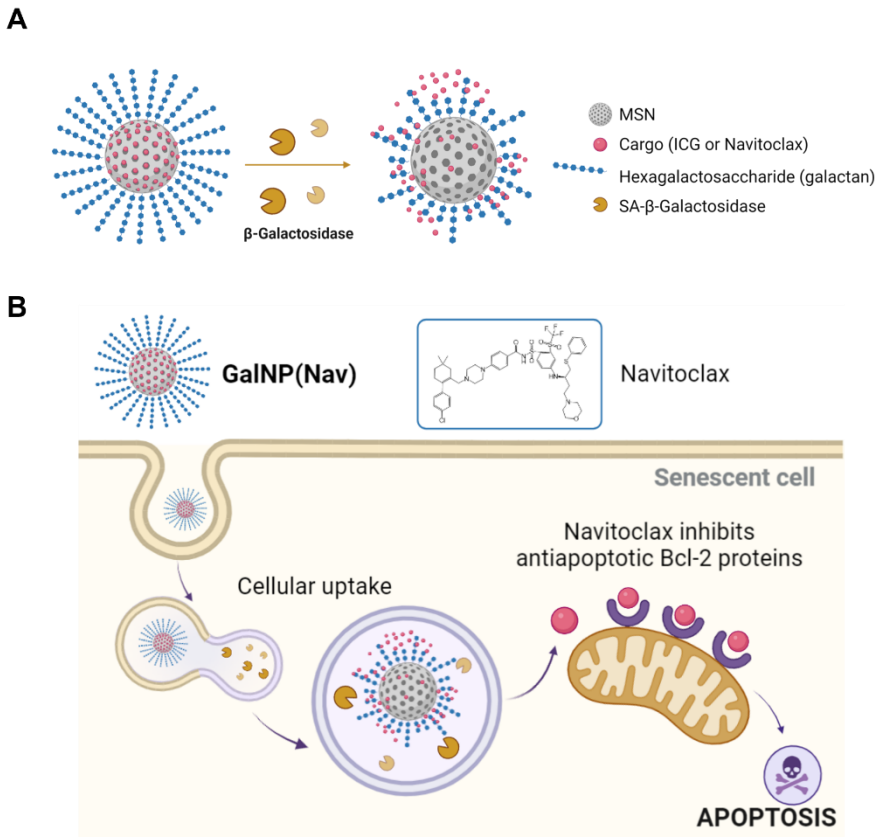

Figure 23. Schematic representation of galactan-capped nanoparticles.
(A) Scheme of mesoporous silica nanoparticles (MSNs) loaded with ICG or navitoclax, functionalized and capped with an oligosaccharide galactan that opens in response to β-galactosidase activity releasing its cargo. **(B)** The cellular uptake of **GalNP(Nav)** is mediated via endocytosis. In senescent cells, the high lysosomal β-galactosidase activity (SA-β-gal), allows the hydrolysis of the cap, and navitoclax is released into the cytoplasm and inhibits anti-apoptotic Bcl-2 proteins, which are overexpressed in senescent cells, driving specific apoptosis.

The nanoparticles were characterized by standard techniques (Agostini et al., 2012; Galiana et al., 2020) (**Figure 24**). TEM (**Figure 24A**) and Powder X-ray diffraction studies (**Figure 24B**) confirmed the presence

of the mesoporous structure of the starting nanoparticles as well as the spherical morphology and size of ca. 100 nm, which are maintained after the loading and functionalization processes. Starting MSNs exhibit a total specific surface area of 1228.80 m^2 g^{-1}, a pore volume of 0.93 cm^3 g^{-1}, and pore size of 3.18 nm (**Figure 24C, Table 4**). In contrast, data for functionalized nanoparticles **GalNP** (**Figure 24E**), and **GalNP(ICG)** (**Figure 24D**) showed a substantial reduction of specific surface areas, exhibiting a total specific surface area of 55.82 and 101.41 m^2 g^{-1}, and a pore volume of 0.12 and 0.05 cm^3 g^{-1}, respectively, which agrees with filled mesopores (**Table 4**).

Zeta potential was -27.1 mV for starting calcined MSNs which changed to -0.06 mV and 0.34 mV for final **GalNP(ICG)** and **GalNP(Nav)**, respectively (**Table 5**). Besides, the hydrodynamic diameter increased from 153.5 nm for the calcined MSNs to 244.5 nm and 284.8 nm for **GalNP(ICG)** and **GalNP(Nav)**, respectively (**Table 5**). In all cases, a single population distribution was observed in DLS for all solids suggesting no aggregation. From thermogravimetric and elemental analysis, the amounts of cargo (ICG or Nav) and galactan in final NPs were determined (**Table 6**).

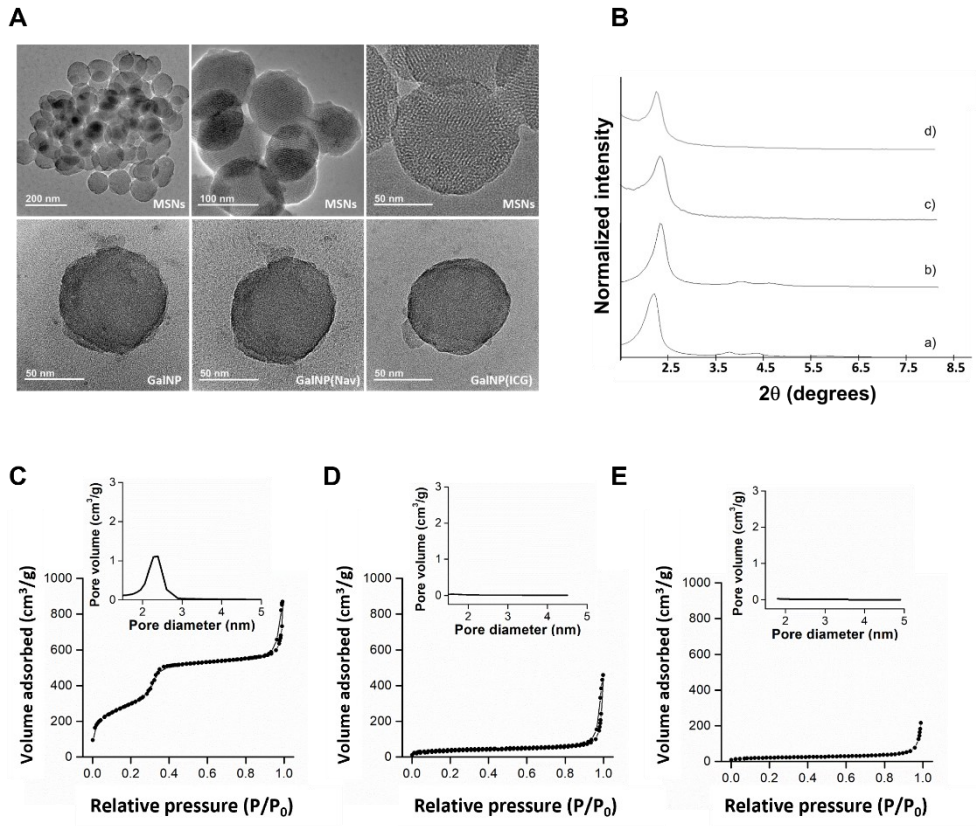

Figure 24. Characterization of the nanoparticles.
(A) (Upper panels) TEM analysis of calcined MSNs at increasing magnification. (Lower panels) TEM images of **GalNP** (left), **GalNP(Nav)** (central), and **GalNP(ICG)** (right). **(B)** Powder X-Ray diffraction patterns of (a) starting MSNs (b) calcined MSNs, (c) **GalNP(ICG)**, and (d) **GalNP**. **(C-E)** N_2 adsorption-desorption isotherms for **(C)** calcined MSNs, **(D) GalNP(ICG),** and **(E) GalNP.**

Table 4. BET-specific surface values, pore volumes, and pore sizes calculated from N_2 adsorption-desorption isotherms for indicated solids.

Solid	SBET [m^2g^{-1}]	Pore Volume [cm^3g^{-1}]	Pore Size [nm]
Calcined MSNs	1228.80	0.93	3.18
GalNP	55.82	0.12	--
GalNP(ICG)	101.41	0.05	--

Table 5. Hydrodynamic diameter and zeta potential of indicated solids.

Solid	Hydrodynamic particle diameter (nm)	Zeta Potential (mV)
Calcined MSNs	153.5 ± 4.0	-27.1 ± 0.5
GalNP	273.3 ± 3.9	0.03 ± 0.03
GalNP(ICG)	244.5 ± 4.1	-0.06 ± 0.04
GalNP(Nav)	284.8 ± 2.5	0.34 ± 0.02

Table 6. Amounts of gating oligosaccharide and cargo for nanodevices **GalNP(ICG)** and **GalNP(Nav)** in mg per g of solid.

Solid	$\alpha_{oligosaccharide}$ (mg/g solid)	α_{cargo} (mg/g solid)
GalNP(ICG)	100.7	43
GalNP(Nav)	167.7	54

Controlled cargo release of **GalNP(ICG)** and **GalNP(Nav)**, was also confirmed by delivery studies in the absence and the presence of the enzyme β-galactosidase (**Figure 25**). A clear cargo delivery was observed in the presence of the enzyme due to β-galactosidase-mediated hydrolysis of galactan and subsequent cargo release for **GalNP(ICG)** and **GalNP(Nav)**

(**Figure 25A** and **Figure 25B**, respectively). In contrast, in the absence of the enzyme, a flat baseline was observed indicating that cargo remained in the nanoparticles with no release. HL-1 cell viability studies under increasing concentrations of **GalNP** (0-2 mg/mL, filtered) demonstrated cell survival up to 90% after 72 h exposure, (**Figure 26**) confirming that the mesoporous silica carrier is not toxic.

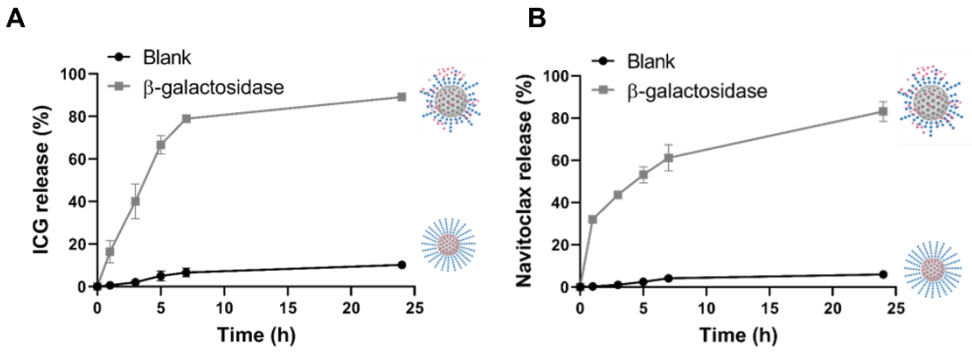

Figure 25. Cargo release and biocompatibility.
(A-B) Release profiles of ICG and navitoclax from **GalNP(ICG) (A)** and **GalNP(Nav) (B)**, respectively, in the absence (blank) or the presence of β-galactosidase from *Aspergillus oryzae* in water at pH 4.5. Data represent the means ± SEM (n=3).

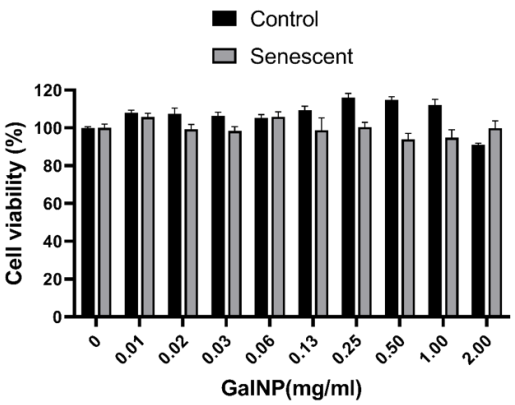

Figure 26. Cytotoxic profile of GalNP in HL-1 cells.
Cell viability of control and senescent HL-1 cells after treatment with **GalNP** at increasing concentrations (0-2 mg/mL, filtered) for 72 h.

3. Galactan-capped nanoparticles loaded with ICG deliver their cargo to senescent HL-1 cells versus non-senescent

Besides, **GalNP(ICG)** was used to follow the cell specific cargo release of the nanoparticles to senescent cells by confocal microscopy and flow cytometry. After 4 h of incubation, an increase in far-red fluorescence signal inside HL- 1 senescent cells was observed, indicative of nanoparticle internalization and fluorophore delivery (**Figure 27A**). In contrast, control cells showed negligible emission under similar exposure. Flow cytometry studies also showed a significant fluorescence increase in **GalNP(ICG)**-treated senescent HL-1 cells versus control cells (**Figure 27B**).

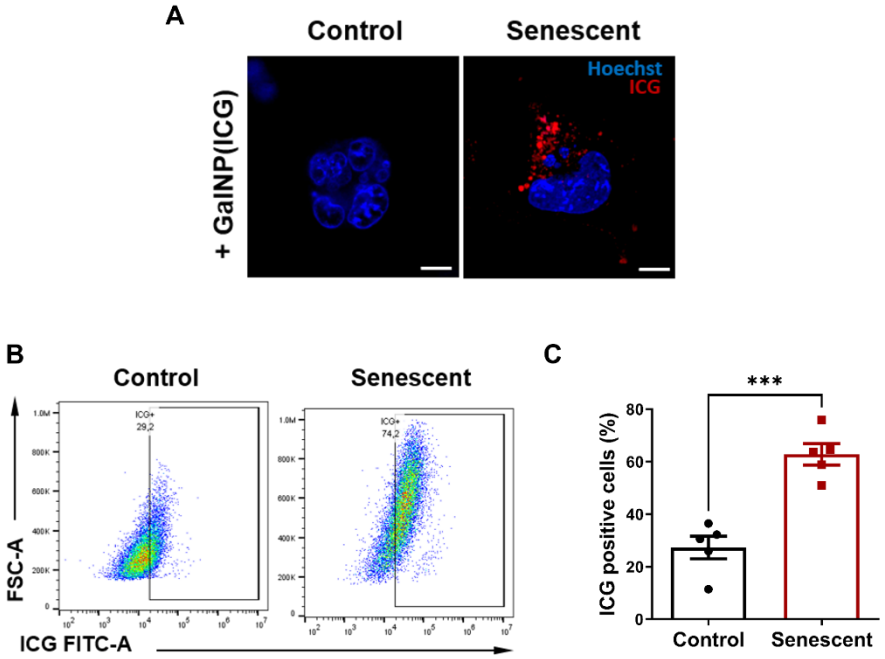

Figure 27. Cellular uptake of GalNP(ICG) by HL-1 cells.
(A) Confocal images of control and senescent cells incubated with **GalNP(ICG)** for 4 h (1 mg/mL, filtered). **GalNP(ICG)** are preferentially internalized by HL-1 senescent cells showing an increment in ICG release (red fluorescence). The nucleus is stained with Hoechst 33342 (blue). Scale bar, 10 µm. **(B)** Flow cytometry diagram of control and senescent cells incubated with **GalNP(ICG)** for 4 h (1 mg/mL, filtered). Increased signal for ICG indicates preferential uptake of nanoparticles with subsequent cargo release in senescent cells. **(C)** Percentage values of ICG positive cells obtained by flow cytometry were expressed as mean ± SEM and statistical significance was assessed by the two-tailed Student's t-test: ***p <0.001 (n=5).

4. Encapsulated navitoclax improves senolytic activity in senescent cardiac myocytes

Once demonstrated the targeted delivery of the nanoparticles to senescent HL-1 cells, we evaluated the senolytic activity of **GalNP(Nav)**. For this purpose, control and senescent cardiac myocytes were treated with increasing concentrations of **GalNP(Nav)** for 48 h (**Figure 28A**). Interestingly, we observed that HL-1 senescent cells treated with **GalNP(Nav)** showed higher sensitivity (IC50 of 0.16 μM), compared with control cells which remained viable in all the concentration range tested (up to 14 μM). The results confirmed a higher efficiency of the nanosenolytic compared with free navitoclax (see **Figure 22**) (nearly 4-fold), thus resulting **GalNP(Nav)** in a senolytic index of 86.7 (**Table 7, Figure 28B**). These results show the use of **GalNP(Nav)** improved the therapeutic outcome by reducing the dose of the drug and, consequently, protecting the non-senescent cells from apoptosis.

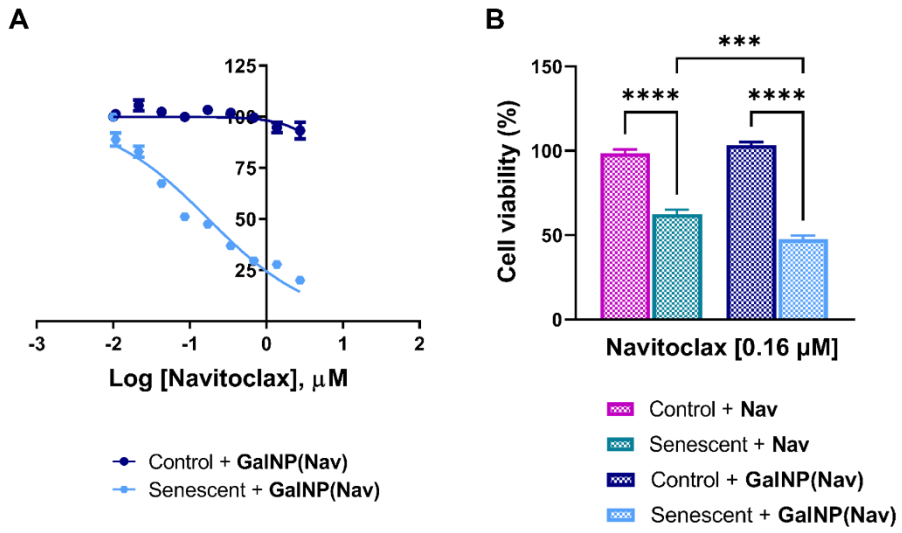

Figure 28. GalNP(Nav) improves senolytic activity in senescent HL-1 cardiac myocytes.

(A) IC50 curves obtained with increasing concentrations of **GalNP(Nav)** (corresponding to 0.01 to 2.7 µM of free navitoclax) for control and DOX-treated cells measured after 48 h of treatment by luminescent ATP detection. Values are expressed as mean ± SEM (n=5). **(B)** Comparison of the cytotoxic effect of free navitoclax versus **GalNP(Nav)** over control and senescent HL-1 cells at a concentration corresponding to the IC50 of senescent cells treated with **GalNP(Nav)**. Data represent means ± SEM for free navitoclax treated control and senescent cells (left), and **GalNP(Nav)** treated control and senescent cells (right). Statistical significance was determined by one-way ANOVA and Tukey post-test; ***$p < 0.001$; ****$p < 0.0001$ ($n \geq 5$).

5. Nav-Gal prodrug protects non-senescent cardiomyocyte cells from apoptosis

As an alternative to target navitoclax to senescent cells, we have previously described the preparation of the prodrug **Nav-Gal** (González-Gualda et al., 2020) based on the conjugation of navitoclax with an acetylated galactose (**Figure 29**). **Figure 30A-C** shows ^{1}H-NMR, COSY, and HRMS studies carried out on **Nav-Gal** to demonstrate the presence of the acetylgatactose units. **Nav-Gal** ^{1}H-NMR spectrum (**Figure 30A**) shows the presence of 4 singlets that integrate at 3 protons for each signal at 2.17 (s, 3H), 2.02 (s, 3H), 2.01 (s, 3H), and 2.00 (s, 3H). These values are characteristic of protons attached to alpha carbons relative to a carbonyl group and attributed to the 4 acetyl groups present on the galactose unit. Using two-dimensional homonuclear correlated spectroscopy (COSY), it was confirmed that these signals are linked to an adjacent carbon lacking protons (carbonyl carbon of the acetyl groups) (**Figure 30B**). Finally, the HRMS spectrum (**Figure 30C**) obtained indicates a charge mass ratio (m/z) in the molecular ion of 1304 that correlates with the M+H of the **Nav-Gal** molecule when galactose has acetyl groups.

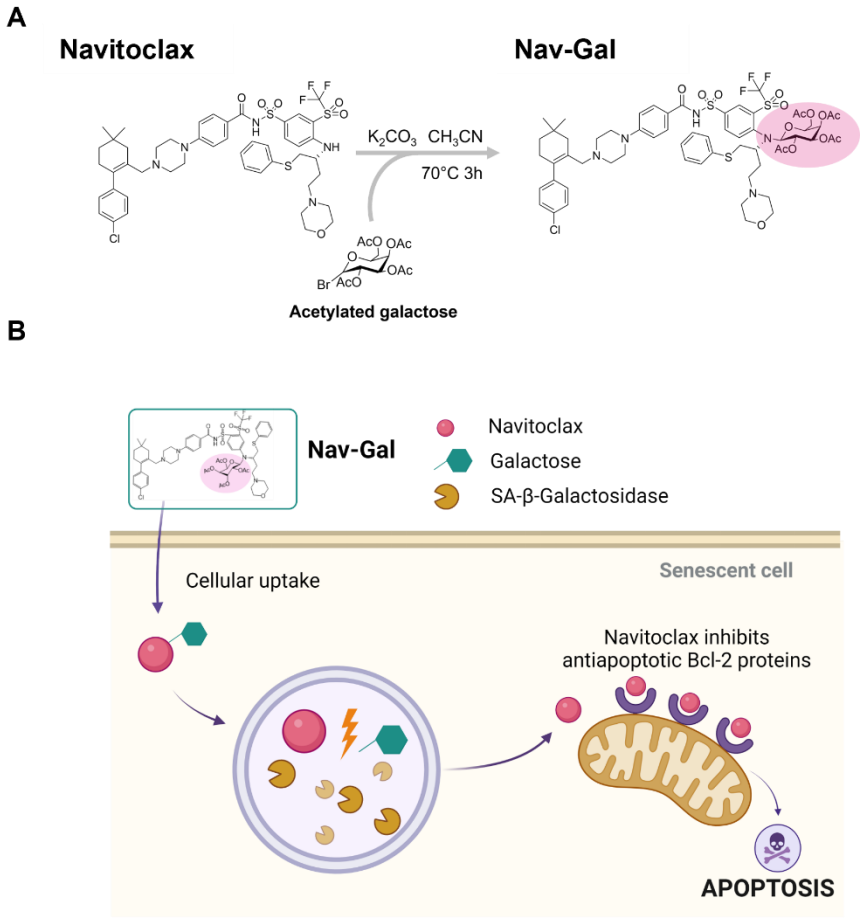

Figure 29. Schematic representation of Nav-Gal synthesis and mechanism of action.

(A) The synthetic route used for the galacto-conjugation of navitoclax with an acetylated galactose to obtain the **Nav-Gal** prodrug. **(B)** Nav-Gal is passively taken up by cells. In senescent cells, the high lysosomal β-galactosidase activity (SA-β-gal), allows the hydrolysis of either the cap or the cleavable galactose. Free navitoclax is released into the cytoplasm and inhibits anti-apoptotic Bcl-2 proteins, which are overexpressed in senescent cells, driving specific apoptosis.

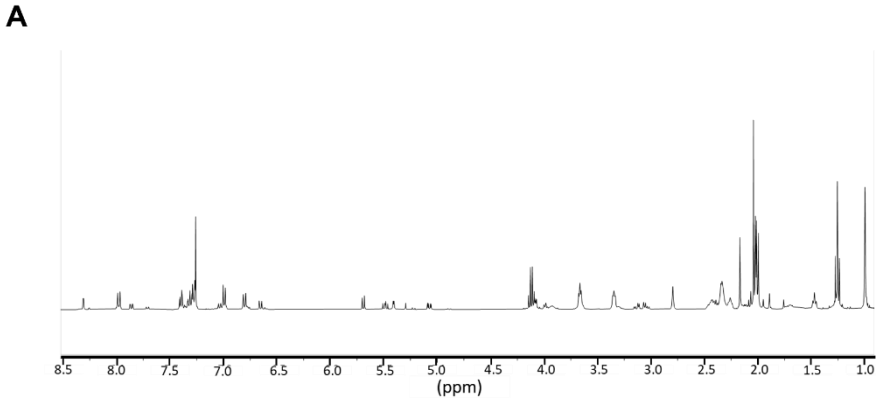
A
8.5
8.0
7.5
7.0
6.5
6.0
5.5
5.0
4.5
4.0
3.5
3.0
2.5
2.0
1.5
1.0
(ppm)

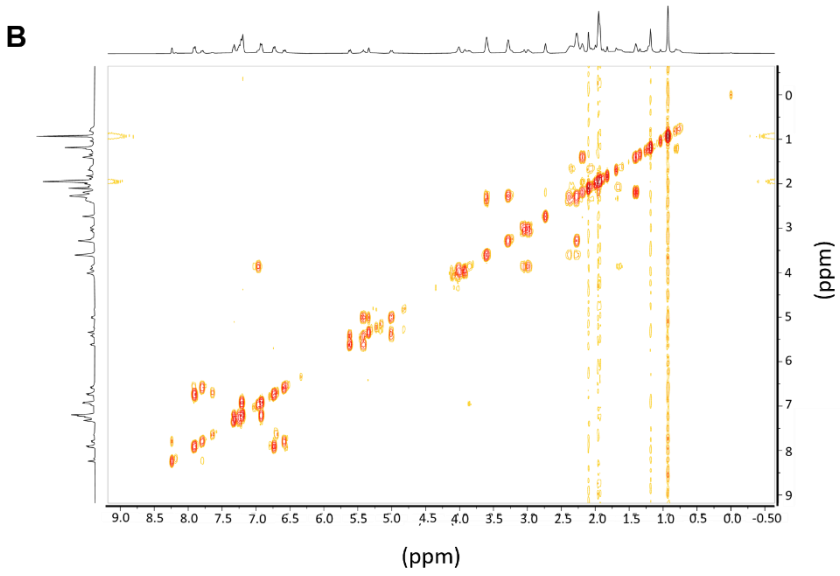
B
9.0
8.5
8.0
7.5
7.0
6.5
6.0
5.5
5.0
4.5
4.0
3.5
3.0
2.5
2.0
1.5
1.0
0.5
0.0
-0.50
(ppm)
0
1
2
3
4
5
6
7
8
9
(ppm)

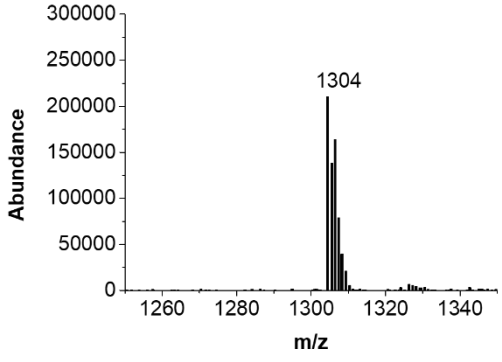
C
300000
250000
200000
150000
100000
50000
0
Abundance
1304
1260
1280
1300
1320
1340
m/z

Figure 30. Characterization of Nav-Gal prodrug.
(A) Chemical shifts of the signals of protons of Nav-Gal ^{1}H NMR (400 MHz, $CDCl_3$) δ 8.31 (d, J = 2.3 Hz, 1H), 7.98 (d, J = 9.1 Hz, 2H), 7.86 (dd, J = 9.1, 2.3 Hz, 1H), 7.41-7.26 (m, 5H), 7.04 6.97 (m, 4H), 6.80 (d, J = 9.3 Hz, 2H), 6.65 (d, J = 9.4 Hz, 1H), 5.69 (d, J = 8.2 Hz, 1H), 5.49 (dd, J = 10.4, 8.2 Hz, 1H), 5.41 (dd, J = 3.5, 1.1 Hz, 1H), 5.07 (dd, J = 10.4, 3.4 Hz, 1H), 4.08 (dd, J = 6.7, 4.7 Hz, 2H), 4.00 (dd, J = 6.5, 1.2 Hz, 1H), 3.70-3.60 (m, 4H), 3.39-3.32 (m, 4H), 3.19 – 3.00 (m, 3H), 2.80 (bs, 2H), 2.50-2.22 (m., 12H), 2.17 (s, 3H), 2.02 (s, 3H), 2.01 (s, 3H), 2.00 (s, 3H), 1.87 (bs, 2H), 1.77 – 1.65 (m, 2H), 1.47 (t, J = 6.4 Hz, 3H), 1.00 (s, 6H). **(B)** Homonuclear bidimensional correlated spectroscopy ^{1}H-^{1}H (2D) COSY NMR (400 MHz, CD_3Cl), signals outside of the diagonal arises from the protons that are coupled together in neighboring carbons**. (C)** HRMS of **Nav-Gal**, molecular ion (M) m/z theoretical value calculated 1303, m/z, observed correspond with M+H with a m/z value of 1304.

Nav-Gal prodrug was demonstrated to induce apoptosis preferentially in senescent cells, in a wide range of cell lines and models of TIS (González-Gualda et al., 2020). In HL-1, **Nav-Gal** showed an IC50 value of 2.1 µM for senescent HL-1 cell and 30.8 µM for non-senescent control cells (**Table 7**, **Figure 31A**). Albeit the senolytic index of **Nav-Gal** was slightly lower than that obtained for free navitoclax, **Nav-Gal** displays higher and remarkable protection on control cells even at high doses. For instance, at navitoclax concentrations of 10 µM, over 65% of control HL-1 cells are dead, whereas this value was only 15% for **Nav-Gal** (**Figure 31B**). These results evidence the efficacy of the prodrug in limiting the off-target effects derived from navitoclax and preventing non-senescent HL-1 cells from navitoclax cytotoxic activity.

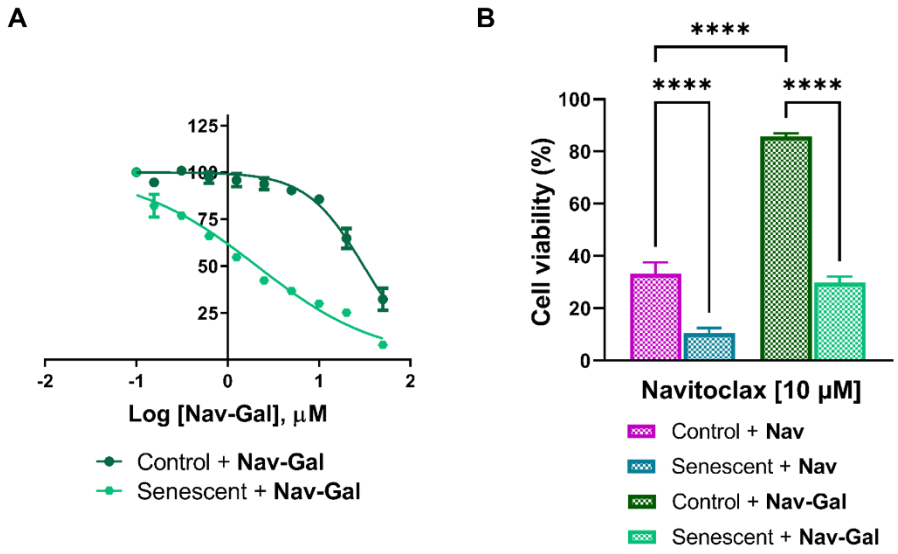

Figure 31. Gal-Nav improves senolytic activity over HL-1 senescent cells.
(A) IC50 curves were obtained with increasing concentrations of **Nav-Gal** (0.15 to 50 µM) for control and DOX-treated cells measured after 48 h of treatment by luminescent ATP detection. Values are expressed as mean ± SEM (n=3). **(B)** Comparison of the cytotoxic effect of free navitoclax and **Nav-Gal** over control and senescent HL-1 cells at 10 µM. Data represent means ± SEM for free navitoclax-treated control and senescent cells (left), and **Nav-Gal**-treated control and senescent (right). Statistical significance was determined by one-way ANOVA and Tukey post-test; ****$p < 0.0001$ ($n \geq 3$).

Table 7. IC50 values. IC50 (μM) values and senolytic index for different navitoclax-based treatments in HL-1 cells. The senolytic index is obtained as $IC50^{Control}/IC50^{Senescent.}$

Senolytic	Cells	IC50 (μM)	Senolytic index
Navitoclax	Control	8.43	23x
	Senescent	0.37	
GalNP(Nav)	Control	>14	>86.7x
	Senescent	0.16	
Nav-Gal	Control	30.76	14.7x
	Senescent	2.09	

6. Doxorubicin induces senescence accumulation in heart tissue and cardiac dysfunction in mice

Male mice appear to be more susceptible to anthracycline cardiac toxicity than female mice (Meiners et al., 2018). Furthermore, the mechanism behind this sexual dimorphism is unknown, and the sex-related changes in mice seem to be model-specific (Meiners et al., 2018; Zeiss et al., 2019). Thus, both male and female mice were included in this study. On the other hand, a single dose of 10 mg/kg DOX was previously demonstrated to induce senescence in the heart and correlated with cardiac dysfunction (Demaria et al., 2017). Nevertheless, a chronic treatment would be a more realistic approach considering the administration patterns used for patients (Lipshultz et al., 2018). Thus, we examined the effects of either a single dose of DOX (10 mg/kg, IP), henceforth referred to as DOX10, or the chronic injection of smaller doses 2 days/week at 2.5 mg/kg (accumulated dose, 20 mg/kg., IP), henceforth referred as DOX20, in male and female C57BL/6J mice (10-weeks). After 4 weeks of treatment, all mice were maintained free of

treatment until day 44 (**Figure 33**). During this time, the effect of DOX on cardiac function was assessed by echocardiography (Echo). The used parameters to assess left ventricular systolic functions are fractional shortening (FS) and ejection fraction (EF). FS indicates the change of left ventricular (LV) diameter during systolic contraction, and EF stands for the percentage of blood volume pumping capacity (Demaria et al., 2017) (**Figure 32**).

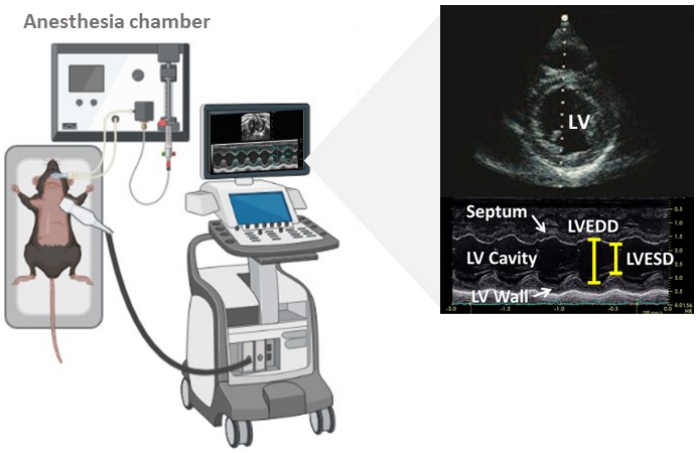

Figure 32. Schema of cardiac echography in mice.
Mice were lightly anesthetized in an anesthesia induction chamber and then placed on a specially designed stage with integrated electrocardiographic, cutaneous, temperature and respiratory monitors for imaging, while maintain anesthetized by facemask. Echocardiography was performed to evaluate the mice cardiac function. The used parameters to assess left ventricular systolic functions are fractional shortening (FS) and ejection fraction (EF) which were determined from the M-mode of the parasternal short-axis view. The caption represents the typical M-mode imaging. The left ventricular end-diastolic dimension (LVEDD) and left ventricular end-systolic dimension (LVESD) are measured to obtained FS and EF values by using Vivid Analysis software.

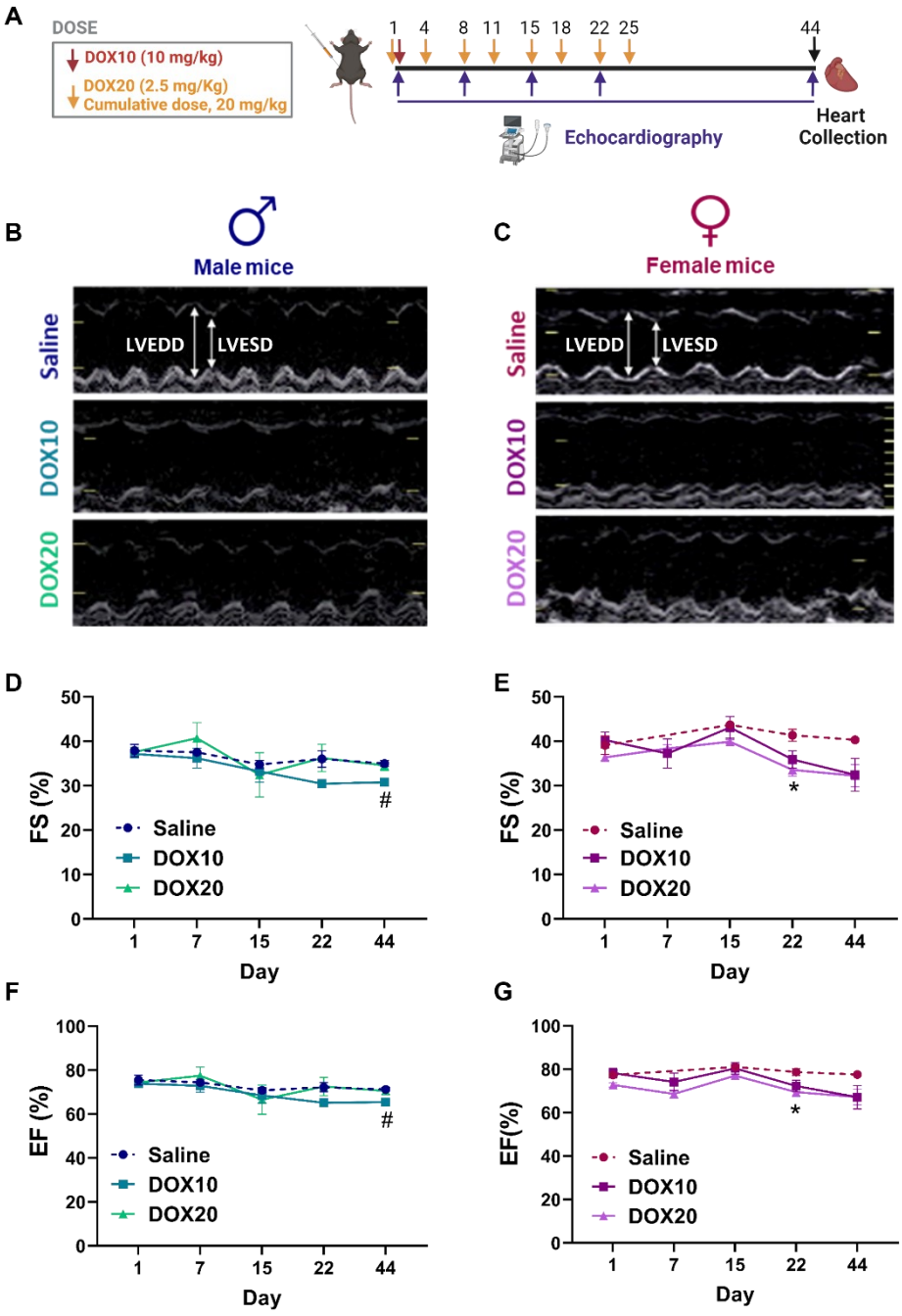
A
DOSE
DOX10 (10 mg/kg)
DOX20 (2.5 mg/Kg)
Cumulative dose, 20 mg/kg
1 4 8 11 15 18 22 25
44
Echocardiography
Heart Collection
B
Male mice
C
Female mice
Saline
DOX10
DOX20
LVEDD
LVESD
D
E
FS (%)
Saline
DOX10
DOX20
Day
F
G
EF (%)
EF(%)

Figure 33. Cardiac functionality of male and female mice after DOX administration.
(A) Experimental design: wild-type male and female C57BL/6J mice (10 weeks old) were treated with saline or doxorubicin (IP) in a unique administration (10 mg/kg body weight, DOX10) or in a chronic regime (cumulative dose, 20 mg/kg body weight, DOX20), 2 injections per week for 4 weeks (n=3). Echocardiography analyses were performed weekly to follow the cardiac dysfunction of mice. Hearts were collected at the endpoint of the experiment (day 44). In advance, the graph representing male results is shown in blue colors, and female results are shown in violet colors **(B-C)** Representative echocardiographic analysis on male **(B)** and female **(C)** mice, respectively, in each experimental condition at day 44 (LVEDD = left ventricular end-diastolic dimension; LVESD = left ventricular end-systolic dimension). After injection with DOX, a decrease in LV contraction is observed. **(D-E)** Changes in fractional shortening (FS) values were obtained for male **(D)** and female **(E)** animals during the curse of the experimental. For male mice, a decrease in FS was observed in the DOX10 group versus saline-treated mice at day 44. For female mice, a decrease in FS value was observed for animals in both experimental groups, DOX10 and DOX20 versus saline-treated mice. **(F-G)** Changes in ejection fraction (EF) in male **(F)** and female **(G)** mice during the curse of the experimental. Data represent means of 3 different independent measures represented for each animal ± SEM (n=3). Statistical significance was determined by one-way ANOVA and Tukey post-test; #$p<0.05$ (DOX10 vs Saline-group, for male) and *$p<0.05$ (DOX20 vs Saline-group, for female).

The echocardiographic evaluations are shown in **Figure 33**. Representative echocardiographic images are shown in **Figure 33B**, for male, and **Figure 33C**, for female. Graph data revealed a significant decrease in FS and EF in DOX10-treated mice (single dose of DOX), regardless of sex. In the case of the chronic regime (DOX20), only female mice showed a decrease in heart function (**Figure 33E** and **Figure 33G**), which is observable from day 22 after treatment (**Figure 34**). Cardiac function remained stable in control mice over the time course of this study.

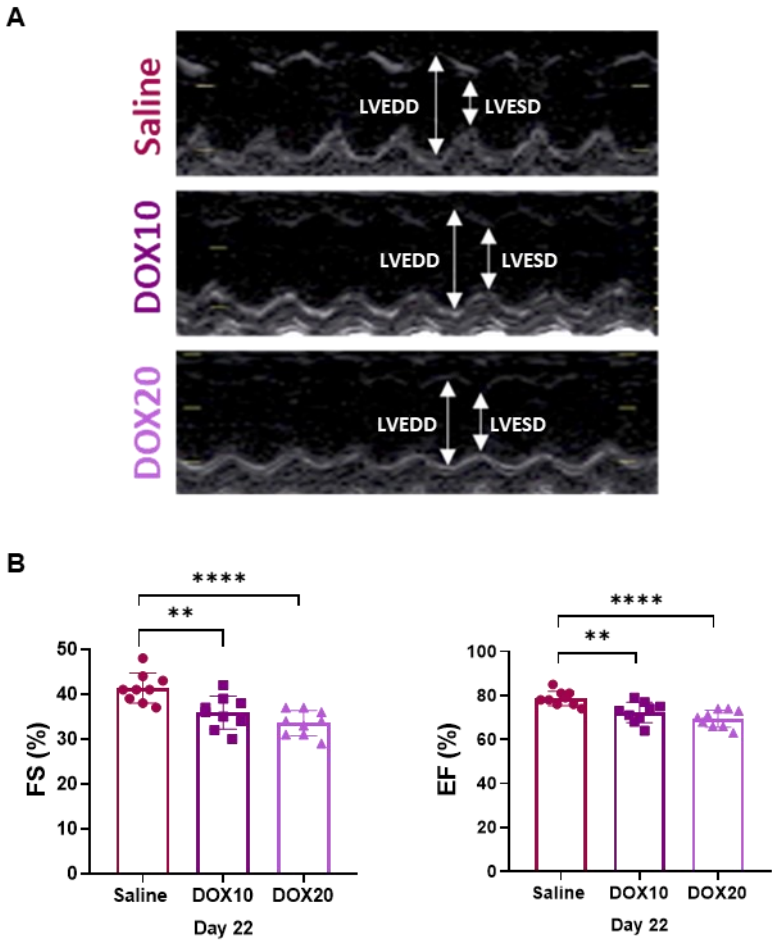

Figure 34. Cardiac functionality in female mice at day 22.
(A) Representative echocardiographic analysis of female mice in each experimental condition at day 22. (LVEDD = left ventricular end-diastolic dimension; LVESD = left ventricular end-systolic dimension). After injection with DOX, a decrease in LV contraction is observed. **(B)** Graphs indicating values of FS and EF at day 22 respectively. Data represent means ± SD. The mean of 3 different independent measures is represented for each animal (n=3). Statistical significance was determined by one-way ANOVA and Tukey post-test; **p < 0.01; ****p < 0.0001.

Importantly, DOX did not cause weight loss in female mice in any administration regime. In contrast, a significant decay in weight loss was observed for male mice at both doses (**Figure 35**). Of note, no animal died during the experiment due to DOX administration.

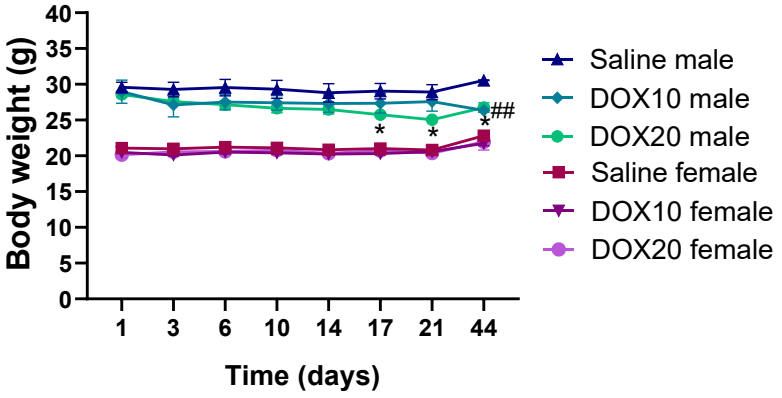

Figure 35. Body weight during experimental.
Date for male (blue tones) and female (violet tones) mice during 44 days of the experiment. Loss of weight was observed for males treated with DOX from day 17. Non-changes were observed in female mice. Values are expressed as mean ± SD (n=3). Statistical significance was assessed by the two-tailed Student's t-test: *p < 0.05 (male: DOX20 vs Saline); ## p < 0.001 (male: DOX10 vs Saline).

To assess the gene expression of senescence and cardiotoxicity markers in this mice model, we collected the hearts of the animals at the endpoint. We first evaluated the difference between sexes and found a similar trend expression in these markers in both male and female animals. Therefore, we consider all the data for statistical analysis. We evaluated the gene expression of the classical hallmarks of cellular senescence, *p16*, *p21*, and *p53*, and the well-established SASP factors, *Ccl8*, *IL-1α*, and *TNFα* (**Figure**

36 and **Figure 38**) (M. S. Chen et al., 2022; Hudgins et al., 2018). We observed an increased expression of *p16*, *p21*, and *p53* in the heart tissue of DOX20-treated mice, but no significant changes were found in DOX10 compared to controls (**Figure 36**). Moreover, immunostaining analysis showed an increased expression of p21 in the heart tissue of the female DOX20 group compared to controls (**Figure 37**). The expression profile of the SASP factors markers (*Ccl8*, *IL-1α*, and *TNFα*) indicated the upregulation in the DOX20 group, which strengthens the induction of senescence in this model (**Figure 38**).

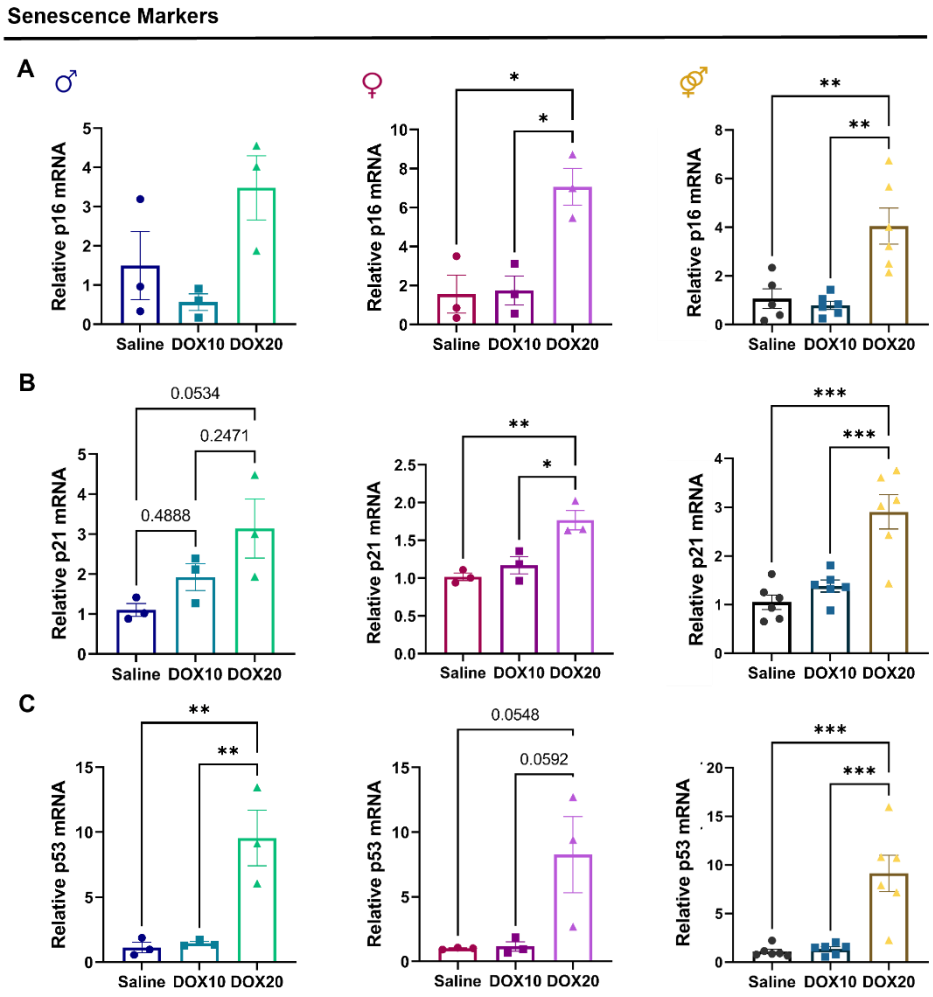

Figure 36. Expression of senescence markers in the heart after doxorubicin administration.

(A) mRNA expression levels of the senescent makers, *p16* **(A)**, *p21* **(B)**, and *p53* **(C)**, in heart tissue of mice; (left) for male, (middle) for female mice, (right) mixed sexes. *Actb* and *Gapdh* were used for input normalization. Values are relative to control mice and are expressed as mean ± SEM. Statistical significance was determined by one-way ANOVA and Tukey post-test; *p<0.05; **p<0.01; ***p<0.001 (n=3, heart per sex-differentiated graphs and n≥5, heart mixed sex groups).

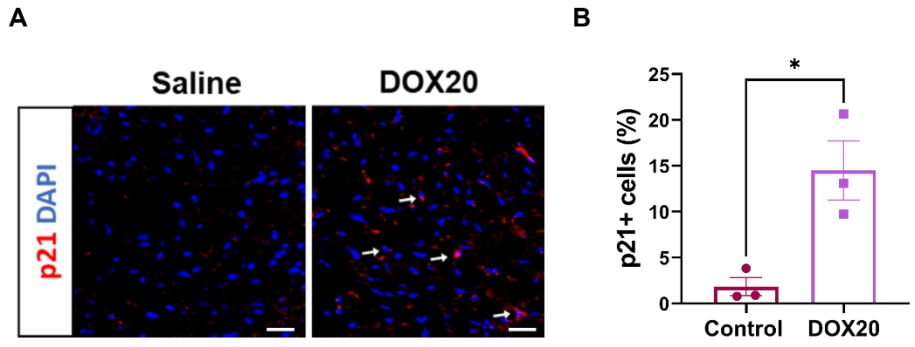

Figure 37. Immunostaining of p21 positive cells in heart tissue.
(A) Representative confocal images of heart tissue sections from female animals treated with saline or chronic administration of DOX (20 mg/kg). p21 expression (white arrows) is overexpressed in DOX-treated mice (red signal). DAPI (blue signal) is counterstained for the nucleus. Scale bar, 20 µm. **(B)** Quantification of the total number of p21-positive cells. Fields were selected for covering most of the total heart area. Data represent means ± SEM per animal and statistical significance was assessed by the two-tailed Student's t-test: *p <0.05 (n=3, heart per group).

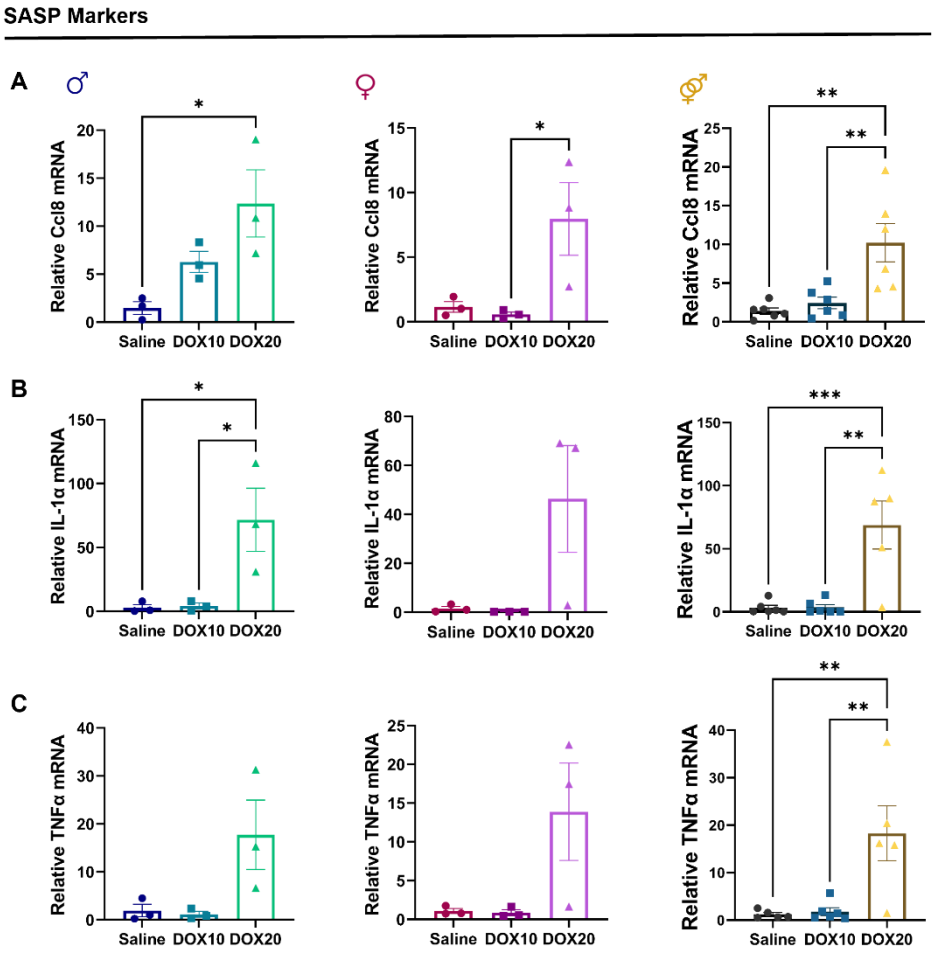

Figure 38. Expression of SASP markers in the heart after doxorubicin administration.

(A) mRNA expression levels of the senescent makers, *Ccl8* **(A)**, *IL-1α* **(B)**, and *TNFα* **(C)**, and in heart tissue of mice; (left) for male, (middle) for female mice, (right) mixed sexes. *Actb* and *Gapdh* were used for input normalization. Values are relative to control mice and are expressed as mean ± SEM. Statistical significance was determined by one-way ANOVA and Tukey post-test; *p<0.05; **p<0.01; ***p<0.001 (n=3, heart per sex-differentiated graphs and n≥5, heart mixed sex groups).

We next measured the expression of different cardiac injury markers in the heart. *Sur2a* is a marker of cardiac stress tolerance, which decreases in cardiac aging (Baker et al., 2016), and high levels of *Nppa,* reflect cardiac hypertrophy and are a marker associated with heart failure (Gallo et al., 2020; Muñoz-Espín et al., 2018). In line with this, we observed a significant decrease in *Sur2a* expression in DOX20-treated mice but not in the DOX10 group. Significant induction of *Nppa* was observed for DOX20-treated mice (**Figure 39**). Altogether, the results indicate that both male and female mice treated with chronic administration of DOX expressed senescence and cardiotoxicity markers in heart tissue. Therefore, we did not observe significative sex-differentiation in the DOX-induced senescence phenotype under our administration regimen.

Despite no differences were observed in senescence and cardiotoxicity markers in heart tissue from both males and females treated with chronic regime, females were selected for further studies considering the significant differences in cardiac function. Besides, the evaluation of cardiotoxicity in females could be a key point as anthracyclines are the backbone of chemotherapy-based regimens for breast and ovarian neoplasms (M. Zhao et al., 2017).

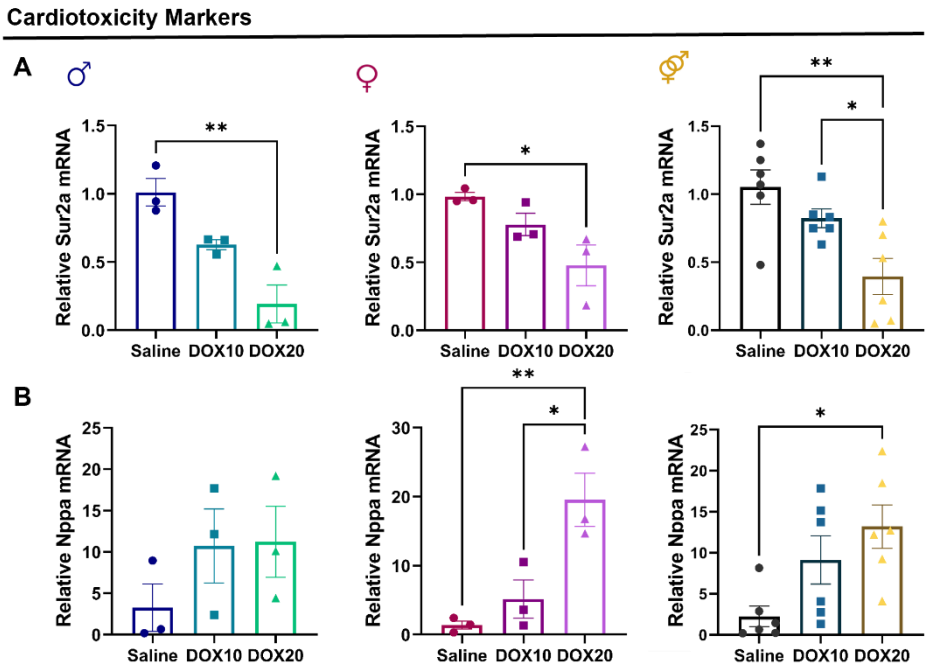

Figure 39. Expression of cardiotoxicity markers in the heart after DOX administration and body weight of mice.

(A-B) mRNA expression levels of cardiotoxicity markers, *Sur2a* **(A)** and *Nppa* **(B)**, in heart tissue of mice; (left) for male, (middle) for female mice, (right) mixed sexes. *Actb* and *Gapdh* were used for input normalization. Values are relative to control mice and are expressed as mean ± SEM. Statistical significance was determined by one-way ANOVA and Tukey post-test; *p<0.05; **p<0.01; ***p<0.001 (n=3, heart per sex-differentiated graphs and n≥5, heart mix sex groups).

7. Navitoclax-based therapies restore cardiac function in a doxorubicin-induced cardiotoxicity mouse model

Navitoclax in different formulations was then tested in the DOX-induced cardiotoxicity model described in the previous section. Female mice were treated with either saline (control) or DOX on days 1 and 4 every week, for 4 weeks (accumulative dose, 20 mg/kg). Senolytic treatment with either free navitoclax (50 mg/kg/day, OG), **GalNP(Nav)** (0.025 mg/day, IP) or **Nav-Gal** (67 mg/kg/day, IP) were administered for 2 consecutive days following DOX administration (**Figure 40**).

According to the results above, we found a decline in cardiac function expressed by a decrease in FS and EF percentages for DOX-treated groups during the experimental which were found significant at day 15 (**Figure 40D and Figure 40E**). At the endpoint, while FS and EF progressively declined in DOX-treated mice, a protective effect in cardiac function was observed from all three navitoclax formulations (**Figure 41B and 41C**). Representative M-mode echocardiography images from the mice groups under study are shown in **Figure 41A**.

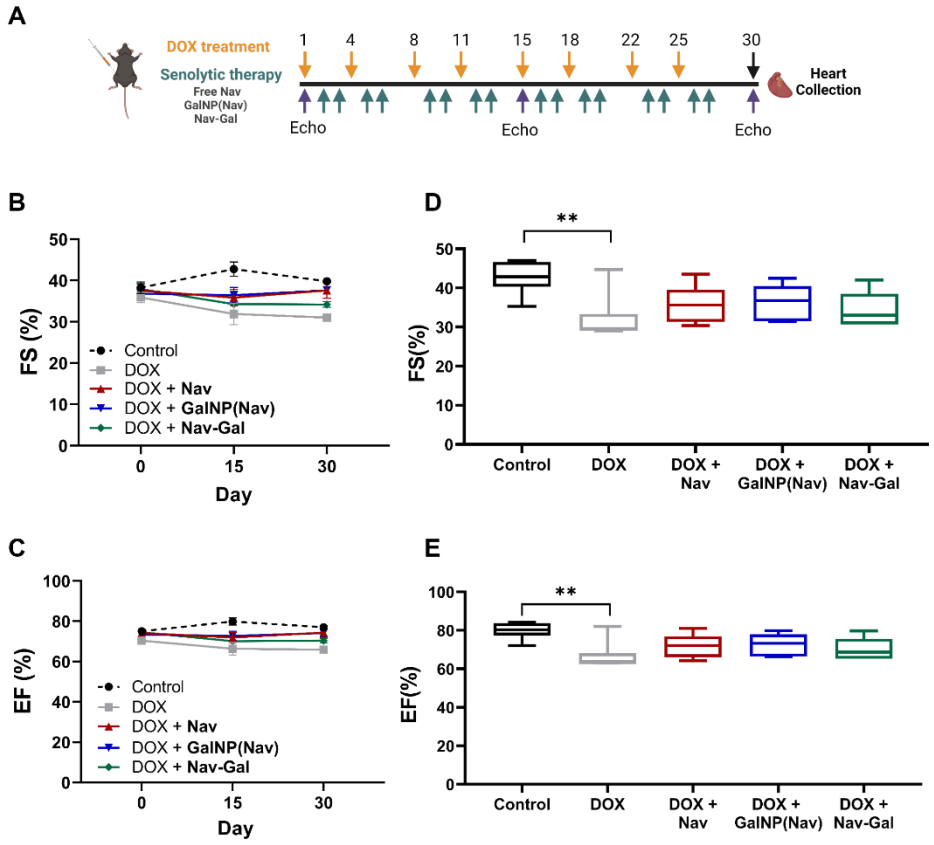

Figure 40. Cardiac functionality of mice after DOX administration and senolytic treatment.

(A) Experimental design: wild-type female C57BL/6J mice (10 weeks old) were treated with doxorubicin (IP) in a chronic regime (cumulative dose, 20 mg/kg body weight), 2 injections per week for 4 weeks. Senolytic treatment with either free navitoclax (50 mg/kg/day, OG), **GalNP(Nav)** (0.025 mg/day, IP) or **Nav-Gal** (67 mg/kg/day, IP) were administered for 2 consecutive days following DOX administration. Echocardiography analyses were performed every 15 days to follow the cardiac dysfunction of mice. Hearts were collected at the endpoint of the experiment (day 30). C57BL/6J mice in each experimental condition (n=6) as described: Control (black), DOX (grey), DOX + Nav (red), DOX + **GalNP(Nav)** (blue) or DOX + **Nav-Gal** (green). **(B-C)** Changes in fractional shortening (FS) **(B)** and ejection fraction (EF) **(C)** in mice during the curse of experimental. Data

represent means ± SEM. Mean of 3 different independent measures is represented for each animal (n≥5). **(D-E)** Graphs indicating values of FS **(D)** and EF **(E)** at day 15 for all experimental groups. At this point, a significant decrease in FS and EF values was observed for DOX-treated mice. Statistical significance was determined by one-way ANOVA and Tukey post-test; **p<0.01 (n≥5).

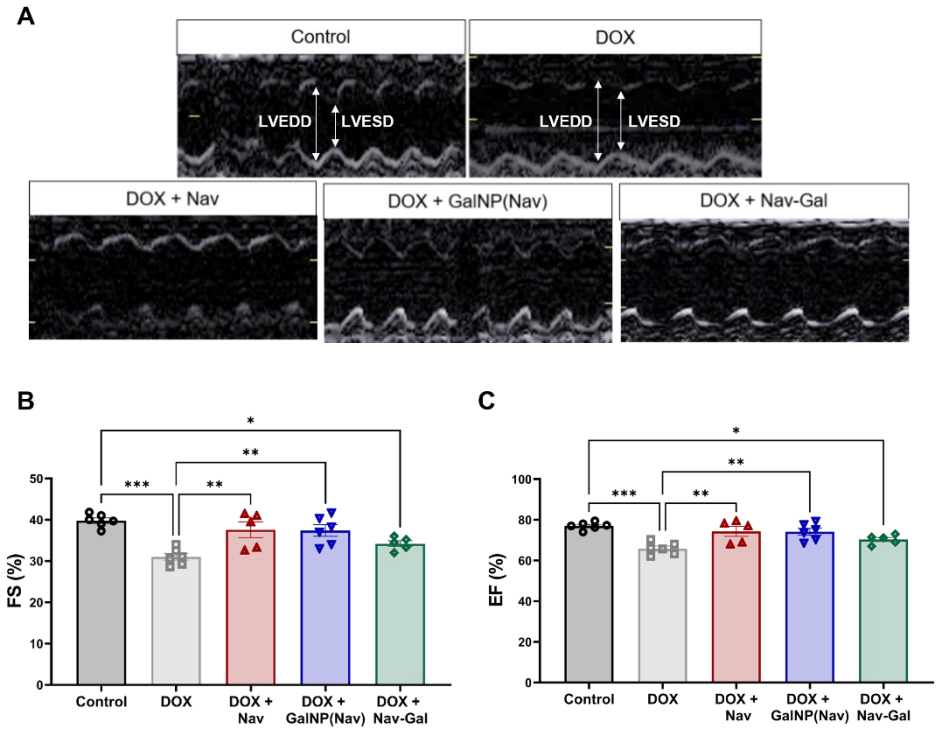

Figure 41. Cardiac functionality of mice after DOX administration and senolytic treatment at endpoint.

C57BL/6J mice in each experimental condition (n=6) as described: Control (black), DOX (grey), DOX + Nav (red), DOX + **GalNP(Nav)** (blue) or DOX + **Nav-Gal** (green). **(A)** Representative echocardiographic analysis of mice in each experimental condition displaying changes in left ventricle (LV) systolic function at day 30. After injection with DOX, a decrease in LV contraction is observed which is attenuated upon senolytic treatment. **(B-C)** Fractional shortening (FS) **(B)**, and ejection fraction (EF) **(C)** values were obtained for animals at the experimental endpoint (day 30). A decrease in FS and EF values was observed for animals in the DOX group and FS

and EF increase upon administration of senolytic treatment. Data represent the means of 3 different independent measures for each animal ± SEM (n≥5). Statistical significance was determined by one-way ANOVA and Tukey post-test; *p<0.05; **p<0.01; ***p<0.001.

According to our previous results, the expression of the senescence markers *p16, p21*, and *p53* were upregulated in cardiac tissue after DOX treatment compared to control mice. Interestingly, the expression of these senescence markers was alleviated upon senolytic treatment, regardless of the therapeutic strategy used (free navitoclax, **GalNP(Nav),** or **Nav-Gal)** (**Figure 42**). These results were further corroborated in heart tissue by p21 and p53 immunofluorescence (**Figure 43**), where it was found that the induction of both markers in heart tissue after DOX treatment was reverted upon senolytic administration. Besides, a decrease in mRNA expression levels of the cardiotoxicity marker *Sur2a* upon DOX treatment was prevented upon senolytic treatment (**Figure 42D**). Furthermore, histopathologic analyses revealed that DOX-treated animals exhibited an increase in cardiomyocyte cross-sectional area, which was attenuated upon senolytic treatment (**Figure 43**).In addition, no evidence of losing weight, or renal or hepatic damage was observed in any of the groups treated with free navitoclax, **GalNP(Nav),** or **Nav-Gal**, as evaluated by serum markers (**Figure 44**).

Altogether, these data support the role of senescence in cardiac dysfunction following DOX treatment and demonstrate that senolytic treatment with different formulations of navitoclax (free, encapsulated, or as a pro-drug) restores cardiac function in mice.

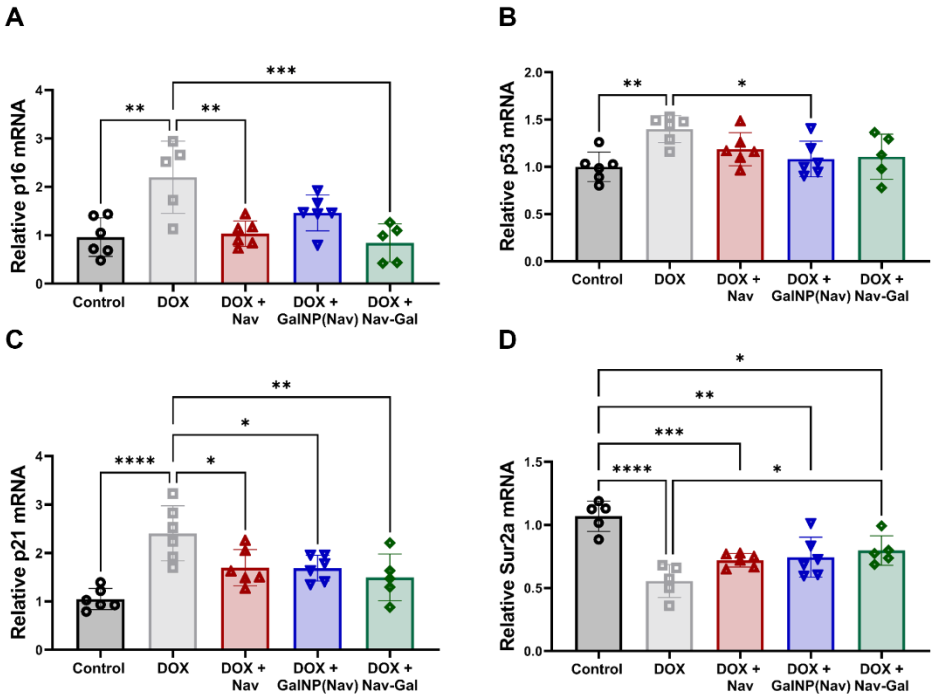

Figure 42. Gene expression of senescence and cardiotoxicity markers in heart mice.

mRNA expression of the senescence markers *p16* **(A)**, *p21***(B)**, *p53* **(C)**, and *Sur2a* **(D)**, in the hearts of mice in each experimental condition: Control (saline, black), DOX (grey), DOX + Nav (red), DOX + **GalNP(Nav)** (blue) or DOX + **Nav-Gal** (green). *Actb* and *Gapdh* were used for input normalization. Values are expressed as mean ± SEM (n≥5). Statistical significance was determined by one-way ANOVA and Tukey post-test; *p<0.05; **p<0.01; ***p<0.001; ****p<0.0001.

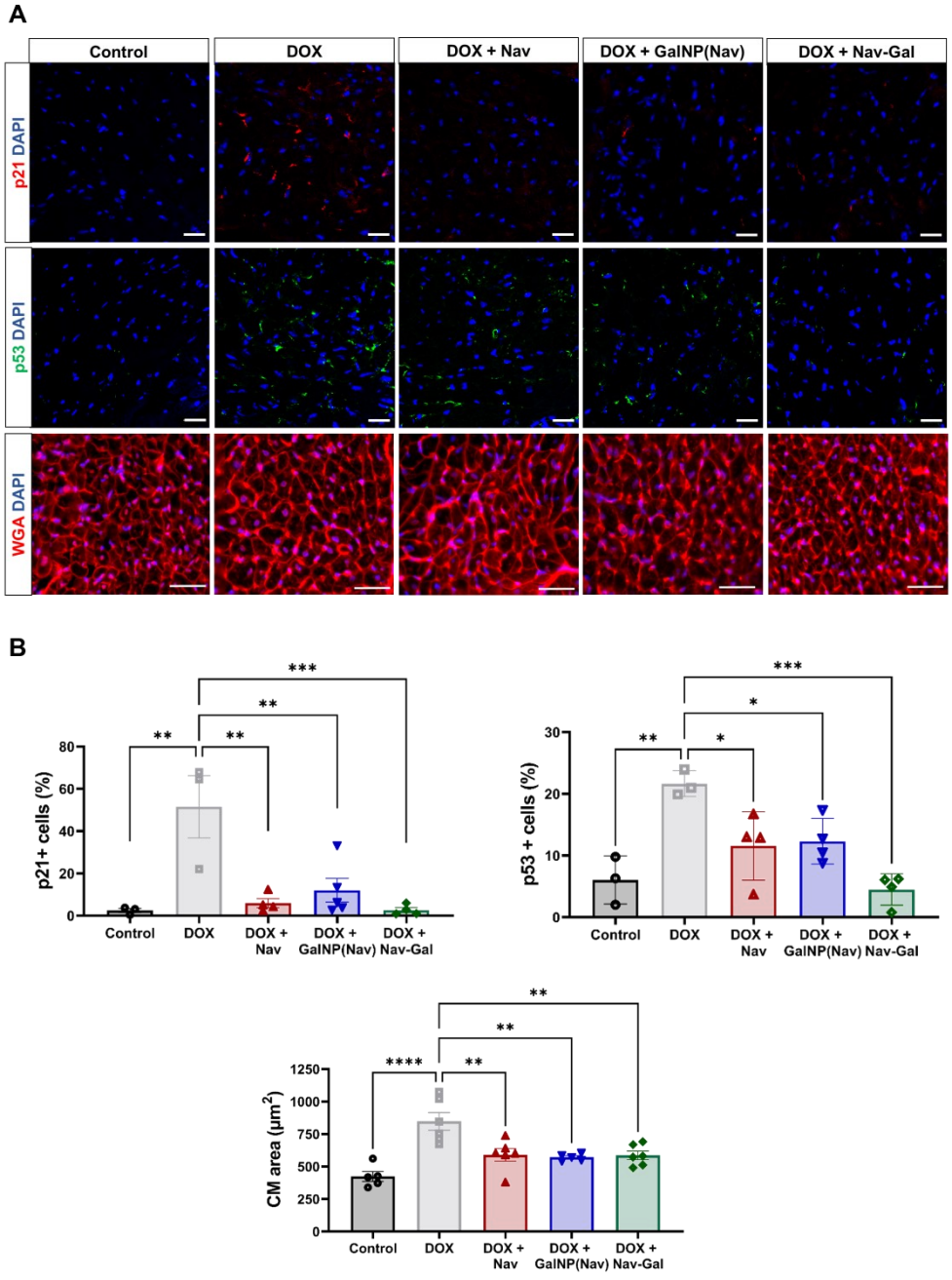

Figure 43. Immunofluorescence of senescence markers and hypertrophy of cardiomyocytes in the heart.

(A) Representative images were obtained for the detection of p21 (red signal) and p53 (green signal) on heart tissue slices. DAPI stains the nucleus (blue). DOX treatment upregulates the expression of both markers in heart tissue indicating accumulation of senescent cells. Upon administration of senolytic treatment, this upregulation is reverted. Scale bar, 20 μm. Representative WGA-Alexa Fluor 647 conjugate-stained heart sections. WGA staining (red) of cardiomyocytes (CM) cross-sectional area. DAPI stains the nucleus (blue). Scale bar, 50 μm. **(B)** The graphs indicate the percentage of p21-positive cells and p53-positive cells in hearts, and quantification of CM cross-sectional area from animals in each experimental condition: Control (saline, black), DOX (grey), DOX + Nav (red), DOX + **GalNP(Nav)** (blue) or DOX + **Nav-Gal** (green). Fields for quantification were selected for covering most of the total heart area. Data represent means ± SEM per animal and statistical significance was determined by one-way ANOVA and Tukey post-test; *$p<0.05$; **$p<0.01$; ***$p<0.001$; ****$p<0.0001$ ($n\geq3$ hearts per group).

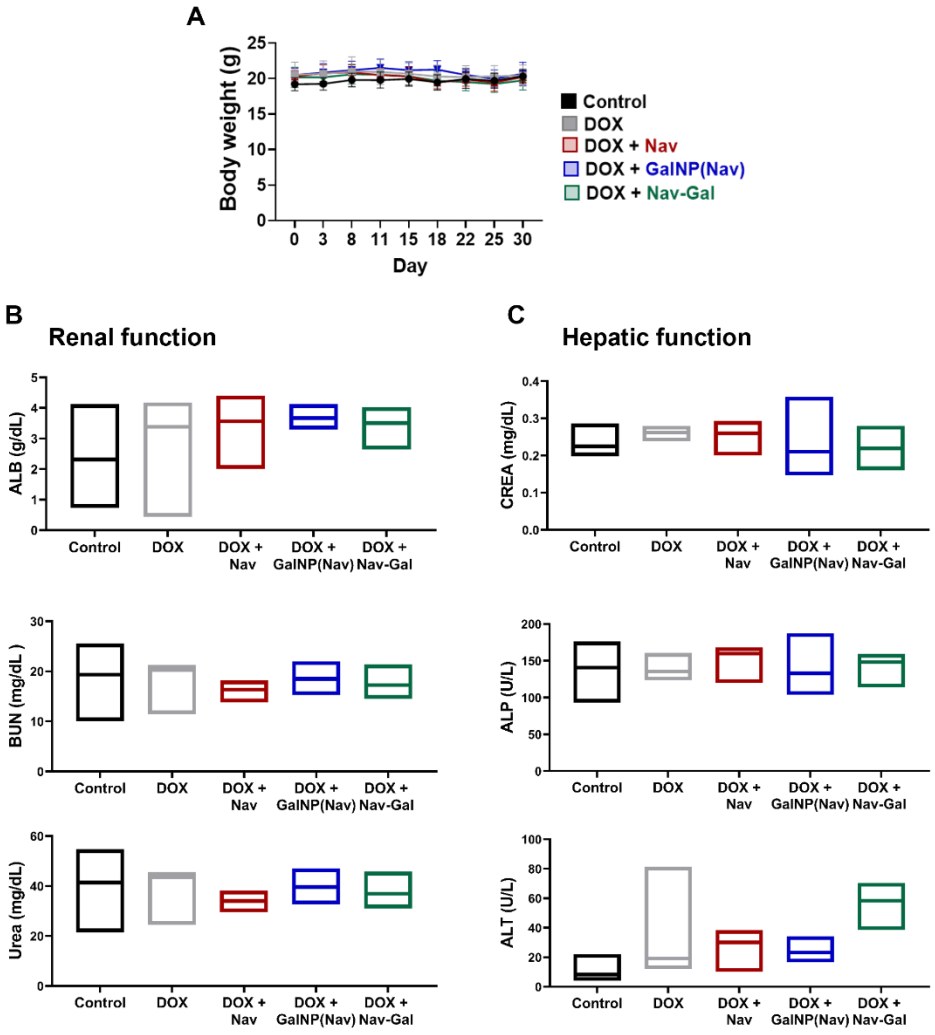

Figure 44. Body weight, renal and hepatic function after senolytic treatment. C57BL/6J mice in each experimental condition: Control (black), DOX (grey), DOX + Nav (red), DOX + **GalNP(Nav)** (blue) or DOX + **Nav-Gal** (green). **(A)** Bodyweight mice during 30 days of experimental. Non-changes were observed in any experimental group. **(B-C)** Analysis of renal **(B)** and hepatic **(C)** function of mice at the end of the treatment. ALB, albumin; BUN, blood urea nitrogen; Urea; CREA, creatinin; ALP, alkaline phosphatase; ALT, alanine transaminase.

Discussion

1. Validation of senolytic therapy in senescent cardiomyocytes *in vitro*.

Cardiotoxicity induced by doxorubicin (DOX) is considered an extremely serious adverse effect of oncologic treatment due to the development of irreversible heart failure (HF) (Oliveira et al., 2014; Santos et al., 2018; Timm et al., 2020). Although the molecular mechanism of DOX-induced cardiotoxicity stays not fully understood, new clinical evidence and experimental studies have linked cellular senescence, senescent cell accumulation, and the release of SASP components with DOX-related cardiac pathologies (Mehdizadeh et al., 2021; Mitry et al., 2020; Piegari et al., 2013). In this thesis project, we demonstrate for the first time that the senolytic treatment based on the use of the senolytic navitoclax in different formulations improves cardiac function thereby alleviating cardiotoxicity associated with DOX administration.

Considering the implication of cardiomyocyte cells (CMs) in senescence-related pathologies, we evaluated the effect of DOX therapy in these cells *in vitro*. Although primarily isolated CMs seem to exhibit the best similarity to *in vivo* features, their use in culture is limited as they do not proliferate long (Häseli et al., 2020). An alternative for *in vitro* drug evaluation is the HL-1 cardiomyocyte cell line (Claycomb et al., 1998). These cells, even immortalized, maintain a cardiac-specific phenotype and have been previously used as an experimental model for cardiomyocyte-induced senescence (Yu et al., 2020). We treated HL-1 cells with low-dose DOX (100 nM) since it has been shown that cardiac cells undergo a senescence program rather than apoptotic damage under these conditions (Piegari et al., 2013;

Spallarossa et al., 2009). Indeed, we corroborated that cells maintained their viability without drastic cell death induction but manifested stress-induced premature senescence characterized by the expression of major markers of cellular senescence (González-Gualda et al., 2021). We found increased lysosomal β-galactosidase (SA-β-gal) activity and the accumulation of cell cycle-suppressing proteins such as hypo-phosphorylated retinoblastoma (pRb), p53 and p21. The proliferative arrest was extensively demonstrated and it was associated with a change in the phenotype to enlarger, flattered and vacuolated cells (Piegari et al., 2013). The gene expression of well-established SASP factors, *IL6* and *Cxcl1*, also increased in senescent CMs (Coppé et al., 2010). Of note, these factors were previously found to be elevated in old mice whole hearts (Ock et al., 2016), but not in purified old CMs, which seems to express a noncanonical SASP characterized by enhanced expression of *Edn3*, *TGFb2*, and *Gdf15* (Anderson et al., 2019). Nevertheless, as the expression of SASP factors in HL-1 cardiomyocyte upon DOX has never been characterized, and they are highly dependent on stress-inductor and cell type, our results here cannot be discussed with previous literature but they do indicate the stimulation of a secretory environment further reinforcing the senescence phenotype (Coppé et al., 2010).

Senolytic therapies are not exempt from off-target toxicities in normal cells, thus, specifically targeting senescent cells remains a considerable challenge (Raffaele et al., 2022). In particular, the use of navitoclax, one of the most recognized senolytics drugs, is associated with hematological toxicity, causing severe thrombocytopenia and neutropenia (Cang et al., 2015; Rudin et al., 2012). Nevertheless, the safety and potency of existing senolytics can be improved by molecular engineering and drug delivery approaches. To

reduce these side effects, our group has worked for years on the design of different targeted strategies based on navitoclax: (i) encapsulated navitoclax in mesoporous silica capped with a hexa-galacto-oligosaccharide (**GalNP(Nav)**); and a navitoclax prodrug consisting of navitoclax functionalized with a tetraacetylgalactose group (**Nav-Gal**) (González-Gualda et al., 2020; Muñoz-Espín et al., 2018). These strategies have been extensively validated in chemotherapy-induced senescence cancer models and fibrosis models where the presence of senescent cells is highly elevated. Nevertheless, their efficacy has never been evaluated in cardiac senescence tissue. Therefore, taking advance of these previously developed systems, we evaluated in our study not only free navitoclax treatment but also these two targeted therapies. Both targeted therapies rely on the high level of lysosomal β-gal activity in senescent cells (Dimri et al., 1995). Our group has previously demonstrated that encapsulated navitoclax in mesoporous silica nanoparticles (MSNs) capped with galactan effectively releases the cargo within senescent cells (Galiana et al., 2020; Muñoz-Espín et al., 2018). The treatment of senescent HL-1 cells with **GalNP(Nav)** increases the senolytic index of free navitoclax, in agreement with previous reports in chemotherapy-induced senescence tumor models (Estepa-Fernández et al., 2021; Galiana et al., 2020; Muñoz-Espín et al., 2018). Despite these promising results and the emergent interest in nanomedicine applications, the clinical translation of nanotechnologies is still challenging due to an incomplete understanding of nano-bio interactions and scalable manufacturing (Shi et al., 2017). As an alternative to nanotechnology, we developed a prodrug consisting of functionalized navitoclax with a cleavable acetylated galactose, obtaining the product **Nav-Gal** (González-Gualda et al., 2020). This prodrug was

previously validated in tumor models of chemotherapy-induced senescence and demonstrated improved selective senolytic activity (González-Gualda et al., 2020). The senolytic index of **Nav-Gal** for HL-1 cells was slightly lower than that obtained for free navitoclax. However, the advantage of **Nav-Gal** relies on the remarkably low toxicity towards non-senescent HL-1 cells. Observed differences between navitoclax, **GalNP(Nav)**, and **Nav-Gal** *in vitro* are likely due to the built-in mechanism for the targeted therapy, which requires previous processing and activation by lysosomal β-gal activity, meaning that navitoclax and its targeted-based therapies might have different pharmacokinetics and pharmacodynamics. It is worth noting that the *in vitro* assays do not always fully recapitulate what happens *in vivo* due to the complexity of living organisms, therefore animal models continue to be an essential tool for studying cardiac senescence.

2. Doxorubicin-induced cardiotoxicity correlates with cardiac senescence

Some considerations should be taken into account before selecting the mouse models as cardiac responses vary between mice strain, sex, and age (Podyacheva et al. 2021). The first experimental study showing the beneficial effect of senescence clearance in a model of DOX-induced cardiotoxicity was carried out by Demaria and co-workers, using the transgenic p16-3MR mouse model, in which p16-positive cells are selectively cleared after administration of ganciclovir. However, as it is based on a genetically engineered mouse model, pharmacological therapy would be more realistic for clinical translation (Demaria et al., 2017). For this purpose, we tried to remain as much as possible in the previous mice model of DOX-induced cardiac

senescence (Demaria et al., 2017). Accordingly, we selected the C57BL/6J strain to maintain the same genetic background as the transgenic model. Of note, as senescence accumulates in tissue with age, distinguishing the contribution of DOX in terms of senescence induction from an aged model, could be problematic. Therefore, we followed again Demaria's work and selected 10-week-old animals for our experiments. Furthermore, male mice appear to be more susceptible to anthracycline cardiac toxicity than female mice, nevertheless, the mechanism behind this sexual dimorphism is unknown, and the sex-related changes in mice seem to be model-specific (Meiners et al., 2018; Zeiss et al., 2019). Conversely, in clinical practice, women seem to be significantly more susceptible than men, although this sex disparity is not entirely clear (Oliveira et al., 2014). Thus, both male and female mice were included in this study.

For determining the contribution of senescent cells to short-term chemotherapy toxicity, we selected two different dose regimens. On one hand, Demaria demonstrated that a single dosage of 10 mg/kg DOX was enough to induce senescence in heart tissue, and it was therefore considered in our evaluations (Demaria et al., 2017). Nevertheless, a chronic treatment would be a more realistic approach considering the administration patterns used for patients (Lipshultz et al., 2018). Therefore, we selected a regime of cumulative dose of 20 mg/kg administered in 8 different doses for 4 weeks (IP). Initial attempts to establish DOX cardiomyopathy models predominantly used intravenous (IV) administration. However, in the context of handling many animals, the intraperitoneal (IP) method of DOX was accepted into practice as both methods had similar results (Johansen 1981).

By using a combination of different markers, we proved that treatment with DOX efficiently induces the expression of classical hallmarks of cellular senescence and cardiotoxicity factors throughout the heart of C57BL6/J mice treated with a cumulative dose. As we did not find changes in gene expression due to sex, we considered data from males and females in a unique cohort. Only biological replicates were excluded from qPCR analysis if the mRNA quality value was not applicable. The increased expression of $p16^{INK4a}$ is a robust senescence marker in numerous mouse and human tissues and we also found its expression was upregulated in mice treated with an accumulative dose of DOX at day 44. Nevertheless, that expression was not observed in mice treated with an acute dose, in controversial to previous results (Demaria et al., 2017). The differences might be due to the fact that the mice used by Demaria had a modified genetic background under the control of the senescence-sensitive $p16^{INK4a}$ promoter, while we used wild-type animals in our study. A similar trend was observed for both *p53* and *p21* and some components of the SASP, *Ccl8*, *IL-1α*, and *TNFα,* further demonstrating that senescence occurs only upon chronic administration of DOX. In heart of aged animals, the fold change expression of *Ccl8* and *TNFα* was also detected (Hoshino et al., 2013; Hudgins et al., 2018). On their behalf, cardiotoxicity markers *Sur2a* and *Nppa* also expressed cardiotoxicity in our model. In particular, *Sur2a* is a marker of cardiac stress tolerance, which decreases in cardiac aging (Baker et al., 2016). *Nppa* is part of a larger transcriptional program involving natriuretic peptides, which is associated with cardiac hypertrophy, which, in turn, is a compensatory response to DOX-induced cardiomyocyte death (Gallo et al., 2020; Muñoz-Espín et al., 2018).

DOX-induced cardiotoxicity is characterized by progressive left ventricular (LV) ejection fraction (LVEF or EF) decline. This reduced systolic function, if disregarded and not treated, may progressively lead to heart failure (Nousiainen et al., 2002). EF refers to the fraction of heart volume pumped during each heart contraction, and a different variant, fractional shortening (FS), indicates the change of left ventricular diameter during systolic contraction (Demaria et al., 2017). These key functional variables are measured via echocardiography (Echo) and are currently used to diagnose myocardial dysfunction in mice models and patients (Cardinale et al., 2015; Podyacheva et al., 2021; Scherrer-Crosbie et al., 2008). As cardiac dimensions vary between sexes, in our study results from male and female mice were analyzed separately.

To evaluate this animal model of DOX-induced cardiotoxicity, we performed Echo scans on all animals twice a week for 44 days. We found a decrease in cardiac function, in only a single-dose of DOX-treated mice, regardless of sex, observed from day 22. These data seem to be in line with the one obtained by Demaria, where the cardiac dysfunction was only detectable 4 weeks after DOX treatment, but not earlier. These small differences in time might be due in part as Demaria *et al* only performed the Echo scans on days 15 and 30, but this dysfunction might have been observed some days before the endpoint (Demaria et al., 2017). In the case of the chronic regime, we found systolic dysfunction preferentially in female mice, observable from the second week after treatment (day 15) and increasing until the final time point (day 44). Here, we observed the systolic function of animals decreased upon DOX treatment as previously described (Demaria et al., 2017).

Considering the significant differences in cardiac function observed during the experimental animal model along with the *ex vivo* senescence evaluation, female mice treated in chronic regimes were selected for further investigation. Besides, the evaluation of cardiotoxicity in females could be a key point as anthracyclines are the backbone of chemotherapy-based regimens for breast and ovarian neoplasms.

3. Senolysis therapy alleviates DOX-induced cardiotoxicity

To further evaluate the senolytic therapy in our model of cardiotoxicity, mice were administered with concomitant treatment of DOX and free navitoclax, galacto-functionalized navitoclax-loaded MSNs (**GalNP(Nav)**), or prodrug (**Nav-Gal**), respectively. After 4 weeks of treatment, results showed a reduced accumulation of senescence in the heart following senolytic administration, demonstrated by the expression of the senescent markers *p16*, *p21*, and *p53.* Cardiac *Sur2a* expression decreased upon DOX treatment, but no such decline was observed upon senolytic treatment, suggesting that cardiac stress tolerance was preserved. Of note, the senescent cell clearance correlated with a preserved cardiac function, which was already observed 2 weeks after DOX treatment. At the final point, after senolytic treatment, systolic dysfunction was considerably improved, reversing the trend for a progressive loss post-DOX treatment. Remarkably, this decay was prevented in all mice groups receiving the senolytic administration, regardless of the strategy. This cardiac recovery indicated that clearance of senescent cells reduced the adverse cardiotoxicity in terms of functionality changes. The importance of this outcome can be seen in

previous reports showing that DOX-treated patients recovering from cardiac dysfunction were less likely to suffer adverse cardiac events, in comparison with those who did not normalize LVEF (Cardinale et al., 2015). Furthermore, we found that cardiomyocytes from mice treated with DOX exhibit dilated phenotype in the heart in accordance with previous studies (Jafarinezhad et al., 2019; Meléndez et al., 2020). Cardiac aging is characterized by a loss of cardiomyocytes, observed at the histological level, due to decreasing ability to replace apoptotic cells and thereby inducing hypertrophy of the remaining cardiomyocytes. Our results are in line with previous reports using the INK-ATTAC transgenic strategy in aged mice, where the removal of $p16^{Ink4a}$-positive cells, blunted cardiomyocyte hypertrophy, preserved cardiac stress tolerance, and reduced expression of inflammatory factors in the heart (Baker et al., 2016). Accordingly, our data indicate that DOX induces a senescent phenotype similar to that observed in aged heart tissue and that the administration of navitoclax alleviates some of the associated symptoms. Nevertheless, different experimental studies showed cardiomyocyte atrophy, but no hypertrophy, as a subclinical myocardial effect of anthracycline-induced cardiotoxicity (D. S. Chen et al., 2022; Ferreira de Souza et al., 2018). The reasons for such discrepancies remain unclear and will require further research to clarify. A likely explanation for this discrepancy include the use of different animal models, the use of various morphologic evaluation methods and time points, or even the administration of different chemotherapy regimens for treating cancer in humans (Park et al., 2020).

Regarding senolytic therapy, the therapeutic windows of the different navitoclax-based strategies can be discussed. The administration of **Nav-Gal**

was molar equivalent to navitoclax, and we observed similar therapeutical behavior. In the case of **GalNP(Nav)**, the use of a nanocarrier increases the bioavailability of the drug in the target organ, reducing doses. Thus, we observed similar results when compared to its free counterparts even when a 40x lower dose was administered when using **GalNP(Nav)**. Regardless of the strategy, expression levels of different markers were comparable to those observed in healthy mice after senolytic treatment.

Although senolytics are specific for senescent cells, they can also affect other cell types leading to off-target effects. It is known the main associated adverse side effect of navitoclax is thrombocytopenia, as the drug can act on the BCL-2 homologs including BCL-xL, highly expressed by platelets (H. Zhang et al., 2007). Therefore, navitoclax can trigger apoptosis and a reduced platelet population (Kaefer et al., 2014). Although several studies reported that thrombocytopenia was fully reversed upon cessation of drug use, it should be taken into account that navitoclax is usually administered in combination with chemotherapeutic drugs for cancer treatment (Rudin et al., 2012; H. Zhang et al., 2007). Thus, the bone marrow platelet population may already be compromised either by the presence of tumor cells in this tissue or by the effect of other drugs. Therefore, avoiding this off-target effect would be highly requested (Kaefer et al., 2014). Previous studies carried out in our group on the use of **GalNP(Nav)** and **Nav-Gal** on senescent cancer mouse models, demonstrated these strategies protected from a significant reduction in platelet counts associated to free navitoclax in treated mice and human and murine blood samples (González-Gualda et al., 2020; Muñoz-Espín et al., 2018). Notably, wild-type C57BL/6J mice treated for 10 consecutive days with **Nav-Gal** resulted in less thrombocytopenia

compared to free navitoclax treatment (González-Gualda et al., 2020). In conclusion, the main advantage of using the targeting strategies resides in the prevention of the off-target effects associated with the free drug administration, which is highly desirable for clinical applications. Nonetheless, because clinical studies might be simpler to conduct, it will be likely for the prodrug formulation to reach clinical applications first. Nevertheless, note that silica nanoparticles have already reached clinical trials evaluation and thus the use of MSNs in clinics could be expected in a near future (Bukara et al., 2016; Janjua et al., 2021).

Before senolytics reach clinical translation, some considerations should be made regarding the possible benefits and risks of the therapy. For instance, it would be of interest to assess the effect of different administration regimens, taking into consideration the dose, administration timing, and long-term outcomes since it might be possible that the effects of senolytic therapy are beneficial in the short term but have consequences later in life. A set of guidelines have been developed for clinical trials involving senolytics (Burd et al., 2016; J. Justice et al., 2016).

Attending to animal experimentation, some limitations of the current treatment strategy can be discussed. Although DOX-induced cardiotoxicity has been extensively studied in the literature, there is no experimental consensus for the chronic DOX cardiomyopathy model showing good reproducibility. The different protocols vary in mice strains, drug dose, administration regimen, and different endpoints evaluations, thus hampering the comparison of results between studies (Podyacheva et al., 2021). However, the criteria for assessing myocardial damage while administering

DOX do not differ significantly and include functional assessment by echocardiography and assessment of markers of myocardial damage as natriuretic peptides. Also, myocardial tissue is used for histological examination or analysis of the expression of proteins and RNA (Podyacheva et al., 2021). Therefore, we followed this criterion to validate our experimental approach as a proper cardiotoxicity mouse model to evaluate cardiac senescence. It is worth noting that an important criterion for the model quality is the animal survival rate. For that, animals were carefully monitored during and after treatment and no harmful symptoms were found. Interestingly, no mouse died due to the DOX treatment, which is the main concern in research on DOX-induced cardiotoxicity models (Mizuta et al., 2020). None of them died due to the administration of senolytic drugs either. Only one mouse died in the middle of the experiment due to technical issues related to IP administration.

Besides, in this study, neither the kinetics of senescence accumulation after DOX treatment nor the dynamics of senescence elimination were evaluated. To optimize treatment regimes, exhaustive studies of the kinetics of accumulation and elimination may be necessary. Nevertheless, a major obstacle to progress in this research area is the lack of real-time methods to monitor senescence *in vivo*. In this regard, our group has previously designed different molecular probes to detect cellular senescence in mice bearing tumor xenografts. Further studies in this field would be crucial for monitoring different senescence-related diseases as well as senolytic therapy (Lozano-Torres et al., 2017, 2020; Lozano-Torres, Blandez, et al., 2021; Lozano-Torres, Rojas-Vázquez, et al., 2021).

For a comprehensive understanding of senescence after DOX treatment, it would be interesting to establish a longer period of evaluation due to the importance of SASP in propagating senescence, which might contribute to cardiotoxicity. In fact, we did find slight differences between the initial experimental study, which lasted 44 days, and the senolytic experiments, which lasted 30 days. Although senescence induction was demonstrated in both experiments, the fold change in expression levels was consistently higher with time, indicating the significance of longer periods to reinforce senescence.

A major weakness not only in our work but also in the available literature on cellular senescence in the heart is that most studies have reported tissue-level properties and have not defined the role of senescence in the different cell types, whose contributions to associated cardiac diseases may differ significantly. Thus, still is unknown which cardiac cell type being most susceptible to senescence during aging-related diseases and which one drives cardiac diseases. Previous studies have attributed the beneficial effect of clearing senescent cells in murine aging hearts to proliferation-competent cells rather than cardiomyocytes (Baker et al., 2016). Additionally, a different study in a myocardial ischemia-reperfusion injury (IRI) model demonstrated that short-term navitoclax treatment induced apoptosis approximately in 90% of interstitial cells, with cardiomyocytes making up the remaining 10%. These data suggest that cardiomyocytes might not be the most important senescent cell type to target to improve remodeling and function post-IRI. Furthermore, this senescent cell clearance did not stimulate a regenerative response (Dookun et al., 2020). Further studies using animal models where senescent

cells can be cleared in a cell-type-specific manner might be of interest to formally evaluate senescence implications.

A different concern relates to the potential therapeutic benefits of targeting cardiac cellular senescence. With age, a higher residual level of senescence accumulates in the heart tissue. Along with the fact that cardiac stem cell function declines with age if too many cardiac cells are cleared and not replaced, cardiac function may deteriorate further causing a worsening outcome (Kirkland et al., 2017; Richardson et al., 2015; Short et al., 2019). Particularly, this is important in models of cardiac senescence as the regenerative potential of the heart is limited compared to other cell populations (Bergmann et al., 2015). Nevertheless, in aged mice, previous reports demonstrate that navitoclax improved cardiac function and remodeling following myocardial infarction (Walaszczyk et al., 2019), and similar results were obtained even after only a dose of D+Q (Y. Zhu et al., 2015). Our study demonstrates that, even in short term, senolytic therapy leads to very positive effects after clearing DOX-induced senescence in the heart. Thus, these findings suggest that the elimination of senescent cardiac cells is a potentially beneficial therapeutic strategy. Also, regenerative responses in cardiomyocytes were found following senolytic treatment in aged mice (Anderson et al., 2019; Lewis-McDougall et al., 2019). Currently, it remains unclear whether senescent cell removal can improve established heart failure or merely blunt development (Childs et al., 2018). In addition, as aforementioned, navitoclax and our targeted therapeutical approach act systemically. Thus, it is difficult to dissect whether navitoclax was improving the cardiac function directly or was just improving the overall health of the

mice, possibly by reducing inflammation systemically or improving vascular health.

Several animal models have been used to study the mechanisms underlying cardiac senescence in DOX-treated mice. According to our results, previous DOX-treated mice had increased cardiac levels of p53, which was associated with the repression of the promoter PGC1α, a master regulator of mitochondrial function. In p53- deficient mice, this expression is rescued, suggesting a direct role of cellular senescence in mitochondrial dysfunction upon DOX therapy (Hoshino et al., 2013; Sahin et al., 2011). Furthermore, in an *in vitro* study, inhibition of the SASP product PAI1 decreased ROS generation in DOX-treated cardiomyocytes and endothelial cells limiting the senescence phenotype (Ghosh et al., 2016).

After carefully evaluating previous results in senolytic therapy and DOX-induced senescence, we suggest that the therapeutic effect of navitoclax (regardless of the formulation used) could be explained as follows: i) DOX produces DNA damage and oxidative stress which induces the accumulation of damaged cells in the heart and leads to senescence; ii) accumulated senescent cells release SASPs factors promoting a proinflammatory microenvironment and accelerated aging, and lead to myocardial dysfunction; iii) senolysis acts as an adjuvant therapy favoring senescent cells elimination and preventing from the associated cardiotoxicity; iv) the eradication of senescent cells might also mitigate the senescent secretome (SASP), avoiding bystander effect; v) selective elimination of senescent cells with senolytic alleviate cardiac deterioration by DOX and might promote the regenerative

capacity of the heart. Nevertheless, additional studies in preclinical models are required to conclusively demonstrate the feasibility of this proposal.

As the therapy evaluated in mice models does not always recapitulate what happens in humans, it is highly requested to validate if the senolytic therapy could be an actual alternative for treating DOX-associated cardiotoxicity. This translation to humans would reduce the incidence of HF and adverse cardiotoxic effects in patients, improving their quality of life. Furthermore, this should be in correlation with the identification of novel markers of senescence to improve the diagnosis and prognosis. Therefore, it would be interesting to study an extensive SASP array associated with DOX-induced senescence. Nevertheless, this requires thorough investigation and characterization as these factors are difficult to be directly linked to a specific cell type (Coppé et al., 2010). This would be important to validate senescence biomarkers to diagnose and predict patients most at risk of HF or stratify regeneration therapies to patients with the lowest senescence levels which are most likely to have successful results (Althubiti et al., 2014).

Altogether, we report here the first demonstration that systemic administration of navitoclax in different formulations is effective in clearing senescent cells in the heart and correlates with the prevention of cardiac dysfunction in a mouse model of doxorubicin-induced cardiotoxicity. These results evidence the potential of using these new senolytic therapies to alleviate cardiac dysfunction, thus limiting the cardiotoxicity induced in DOX-treated patients. Selective elimination of senescent cells with senolytics could become a promising next-generation therapy to address an unmet medical need in cardiac pathologies. The study also supports that the

combination of senolytics with anticancer agents used in clinics might reduce accelerated aging processes and adverse side effects induced by chemotherapy in patients in different tissues and organs. Although more research is needed in this field, these preliminary results might open the door to a new era of interventional research and clinical care that will improve the lives of cancer survivors across their lifespan.

Conclusions

The general conclusions of this PhD project are:

1. We have evidenced that doxorubicin led to chemotherapy-induced senescence in cardiomyocytes and the heart of treated mice leading to cardiotoxicity.
2. We have demonstrated the beneficial effect of combined doxorubicin with senolytic therapies to improve cardiotoxicity-associated side effects.
3. We report here the first demonstration that systemic administration of navitoclax is effective in clearing senescent cells in the heart and correlates with the prevention of cardiac dysfunction in a mouse model of doxorubicin-induced cardiotoxicity.
4. We have evaluated the efficacy of targeted mesoporous silica nanoparticles loaded with navitoclax and a prodrug of navitoclax to improve the therapeutic profile of the free drug.
5. Selective elimination of senescent cells could become a promising next-generation therapy to limit the cardiotoxicity induced in DOX-treated patients.

Taken together, the results evidence the potential of using these new senolytic therapies to alleviate cardiac dysfunction and address an unmet medical need in chemotherapy-induced cardiac pathologies.

References

Abdelgawad, I. Y., Sadak, K. T., … Zordoky, B. N. (2021). Molecular mechanisms and cardiovascular implications of cancer therapy-induced senescence. *Pharmacol. Ther.*, *221*, 107751. doi: 10.1016/j.pharmthera.2020.107751

Acosta, J. C., Banito, A., … Gil, J. (2013). A complex secretory program orchestrated by the inflammasome controls paracrine senescence. *Nat. Cell Biol.*, *15*(8), 978–990. doi: 10.1038/NCB2784

Agostini, A., Mondragón, L., … Murguía, J. R. (2012). Targeted Cargo Delivery in Senescent Cells Using Capped Mesoporous Silica Nanoparticles. *Angew. Chemie Int. Ed.*, *51*(42), 10556–10560. doi: 10.1002/anie.201204663

Aguayo-Mazzucato, C., Andle, J., … Bonner-Weir, S. (2019). Acceleration of β Cell Aging Determines Diabetes and Senolysis Improves Disease Outcomes. *Cell Metab.*, *30*(1), 129-142.e4. doi: 10.1016/J.CMET.2019.05.006

Althubiti, M., Lezina, L., … Macip, S. (2014). Characterization of novel markers of senescence and their prognostic potential in cancer. *Cell Death Dis.*, *5*(11), e1528. doi: 10.1038/cddis.2014.489

Altieri, P., Barisione, C., … Ameri, P. (2016). Testosterone antagonizes doxorubicin-induced senescence of cardiomyocytes. *J. Am. Heart Assoc.*, *5*(1). doi: 10.1161/JAHA.115.002383

Anderson, R., Lagnado, A., … Walaszczyk, A. (2019). Length-independent telomere damage drives post-mitotic cardiomyocyte senescence. *EMBO J.*, e100492. doi: 10.15252/embj.2018100492

Anderson, R., Richardson, G. D., & Passos, J. F. (2018). Mechanisms driving the ageing heart. *Exp. Gerontol.*, *109*, 5–15. doi: 10.1016/j.exger.2017.10.015

Anselmo, A. C., Mitragotri, | Samir, … Paulson, J. A. (2021). Nanoparticles in the clinic: An update post COVID-19 vaccines. *Bioeng. Transl. Med.*, *6*(3), 1–20. doi: 10.1002/btm2.10246

Aznar, E., Marcos, M. D., … Guillem, C. (2009). pH- and Photo-Switched Release of Guest Molecules from Mesoporous Silica Supports. *J. Am. Chem. Soc.*, *131*(19), 6833–6843. doi: 10.1021/JA810011P

Aznar, E., Oroval, M., … Sancenón, F. (2016). Gated Materials for On-Command Release of Guest Molecules. *Chem. Rev.*, *116*(2), 561–718. doi: 10.1021/acs.chemrev.5b00456

Baar, M. P., Brandt, R. M. C. C., … de Keizer, P. L. J. J. (2017). Targeted Apoptosis of Senescent Cells Restores Tissue Homeostasis in Response to Chemotoxicity and Aging. *Cell*, *169*(1), 132-147.e16. doi: 10.1016/J.CELL.2017.02.031

Baker, D. J., Childs, B. G., … van Deursen, J. M. (2016). Naturally occurring

p16(Ink4a)-positive cells shorten healthy lifespan. *Nature*, *530*(7589), 184–189. doi: 10.1038/nature16932

Baker, D. J., Wijshake, T., … van Deursen, J. M. (2011). Clearance of p16Ink4a-positive senescent cells delays ageing-associated disorders. *Nature*, *479*(7372), 232–236. doi: 10.1038/nature10600

Barrett, E. P., Joyner, L. G., & Halenda, P. P. (1951). The Determination of Pore Volume and Area Distributions in Porous Substances. I. Computations from Nitrogen Isotherms. *J. Am. Chem. Soc.*, *73*(1), 373–380. doi: 10.1021/ja01145a126

Basisty, N., Kale, A., … Schilling, B. (2020). A proteomic atlas of senescence-associated secretomes for aging biomarker development. *PLoS Biol.*, *18*(1), e3000599. doi: 10.1371/JOURNAL.PBIO.3000599

Beauséjour, C. M., Krtolica, A., … Campisi, J. (2003). Reversal of human cellular senescence: roles of the p53 and p16 pathways. *EMBO J.*, *22*(16), 4212–4222. doi: 10.1093/EMBOJ/CDG417

Beltrami, A. P., Barlucchi, L., … Anversa, P. (2003). Adult cardiac stem cells are multipotent and support myocardial regeneration. *Cell*, *114*(6), 763–776. doi: 10.1016/S0092-8674(03)00687-1

Bergmann, O., Zdunek, S., … Frisén, J. (2015). Dynamics of Cell Generation and Turnover in the Human Heart. *Cell*, *161*(7), 1566–1575. doi: 10.1016/J.CELL.2015.05.026

Bernardos, A., Aznar, E., … Soto, J. (2008). Controlled release of vitamin B2 using mesoporous materials functionalized with amine-bearing gate-like scaffoldings. *J. Control. Release*, *131*(3), 181–189. doi: 10.1016/J.JCONREL.2008.07.037

Birch, J. & Gil, J. (2020). Senescence and the SASP: Many therapeutic avenues. *Genes Dev.*, *34*(23–24), 1565–1576. doi: 10.1101/gad.343129.120

Blasco, M. A., Lee, H. W., … Greider, C. W. (1997). Telomere shortening and tumor formation by mouse cells lacking telomerase RNA. *Cell*, *91*(1), 25–34. doi: 10.1016/S0092-8674(01)80006-4

Bobo, D., Robinson, K. J., … Corrie, S. R. (2016). Nanoparticle-Based Medicines: A Review of FDA-Approved Materials and Clinical Trials to Date. *Pharm. Res.*, *33*(10), 2373–2387. doi: 10.1007/S11095-016-1958-5

Bringas, E., Köysüren, Ö., … Stroeve, P. (2012). Triggered release in lipid bilayer-capped mesoporous silica nanoparticles containing SPION using an alternating magnetic field. *Chem. Commun.*, *48*(45), 5647–5649. doi: 10.1039/C2CC31563G

Brunauer, S., Emmett, P. H., & Teller, E. (1938). Adsorption of Gases in Multimolecular Layers. *J. Am. Chem. Soc.*, *60*(2), 309–319. doi: 10.1021/JA01269A023

Bukara, K., Schueller, L., … Kiekens, F. (2016). Ordered mesoporous silica to enhance the bioavailability of poorly water-soluble drugs: Proof of concept in man. *Eur. J. Pharm. Biopharm.*, *108*, 220–225. doi: 10.1016/j.ejpb.2016.08.020

Burd, C. E., Gill, M. S., … Kirkland, J. L. (2016). Barriers to the Preclinical Development of Therapeutics that Target Aging Mechanisms. *Journals Gerontol. - Ser. A Biol. Sci. Med. Sci.*, *71*(11), 1388–1394. doi: 10.1093/gerona/glw112

Cai, Q., Luo, Z. S., … Cui, F. Z. (2001). Dilute Solution Routes to Various Controllable Morphologies of MCM-41 Silica with a Basic Medium†. *Chem. Mater.*, *13*(2), 258–263. doi: 10.1021/CM990661Z

Cai, Y., Zhou, H., … Deng, H. (2020). Elimination of senescent cells by β-galactosidase-targeted prodrug attenuates inflammation and restores physical function in aged mice. *Cell Res.*, *30*(7), 574–589. doi: 10.1038/s41422-020-0314-9

Campisi, J. (2001). Cellular senescence as a tumor-suppressor mechanism. *Trends Cell Biol.*, *11*(11). doi: 10.1016/S0962-8924(01)02151-1

Campisi, J. & d'Adda di Fagagna, F. (2007). Cellular senescence: When bad things happen to good cells. *Nat. Rev. Mol. Cell Biol.*, *8*(9), 729–740. doi: 10.1038/nrm2233

Cang, S., Iragavarapu, C., … Liu, D. (2015). ABT-199 (venetoclax) and BCL-2 inhibitors in clinical development. *J. Hematol. Oncol.*, *8*(1), 129. doi: 10.1186/s13045-015-0224-3

Canino, C., Mori, F., … Cioce, M. (2012). SASP mediates chemoresistance and tumor-initiating-activity of mesothelioma cells. *Oncogene*, *31*(26), 3148–3163. doi: 10.1038/ONC.2011.485

Cardinale, D., Colombo, A., … Cipolla, C. M. (2015). Early detection of anthracycline cardiotoxicity and improvement with heart failure therapy. *Circulation*, *131*(22), 1981–1988. doi: 10.1161/CIRCULATIONAHA.114.013777

Carvalho, C., Santos, R., … Moreira, P. (2009). Doxorubicin: the good, the bad and the ugly effect. *Curr. Med. Chem.*, *16*(25), 3267–3285. doi: 10.2174/092986709788803312

Castillo, R. R., Lozano, D., … Vallet-Regí, M. (2019). Advances in mesoporous

silica nanoparticles for targeted stimuli-responsive drug delivery: an update. *Expert Opin. Drug Deliv.*, *16*(4), 415–439. doi: 10.1080/17425247.2019.1598375

Casula, A., Llopis-Lorente, A., … Caltagirone, C. (2017). A new class of silica-supported chromo-fluorogenic chemosensors for anion recognition based on a selenourea scaffold. *Chem. Commun.*, *53*(26), 3729–3732. doi: 10.1039/C7CC01214D

Cauda, V., Argyo, C., & Bein, T. (2010). Impact of different PEGylation patterns on the long-term bio-stability of colloidal mesoporous silica nanoparticles †. *J. Mater. Chem.*, *20*(39), 8693–8699. doi: 10.1039/c0jm01390k

Cesselli, D., Beltrami, A. P., … Leri, A. (2011). Effects of age and heart failure on human cardiac stem cell function. *Am. J. Pathol.*, *179*(1), 349–366. doi: 10.1016/J.AJPATH.2011.03.036

Chan, H. B. S., Budd, P. M., & De Naylor, T. V. (2001). Control of mesostructured silica particle morphology. *J. Mater. Chem.*, *11*(3), 951–957. doi: 10.1039/B005713O

Chang, B. D., Xuan, Y., … Roninson, I. B. (1999). Role of p53 and p21waf1/cip1 in senescence-like terminal proliferation arrest induced in human tumor cells by chemotherapeutic drugs. *Oncogene*, *18*(34), 4808–4818. doi: 10.1038/SJ.ONC.1203078

Chang, J., Wang, Y., … Zhou, D. (2016). Clearance of senescent cells by ABT263 rejuvenates aged hematopoietic stem cells in mice. *Nat. Med.*, *22*(1), 78–83. doi: 10.1038/NM.4010

Chaudhury, K., Kumar, V., … RoyChoudhury, S. (2014). Regenerative nanomedicine: current perspectives and future directions. *Int. J. Nanomedicine*, *9*(1), 4153. doi: 10.2147/IJN.S45332

Chen, C., Geng, J., … Qu, X. (2011). Polyvalent nucleic acid/mesoporous silica nanoparticle conjugates: dual stimuli-responsive vehicles for intracellular drug delivery. *Angew. Chem. Int. Ed. Engl.*, *50*(4), 882–886. doi: 10.1002/ANIE.201005471

Chen, D. S., Yan, J., & Yang, P. Z. (2022). Cardiomyocyte Atrophy, an Underestimated Contributor in Doxorubicin-Induced Cardiotoxicity. *Front. Cardiovasc. Med.*, *9*. doi: 10.3389/FCVM.2022.812578

Chen, M. S., Lee, R. T., & Garbern, J. C. (2022). Senescence mechanisms and targets in the heart. *Cardiovasc. Res.*, *118*(5), 1173–1187. doi: 10.1093/cvr/cvab161

Chicas, A., Wang, X., … Lowe, S. W. (2010). Dissecting the unique role of the retinoblastoma tumor suppressor during cellular senescence. *Cancer Cell*,

17(4), 376–387. doi: 10.1016/j.ccr.2010.01.023

Childs, B. G., Baker, D. J., … van Deursen, J. M. (2014). Senescence and apoptosis: dueling or complementary cell fates? *EMBO Rep.*, *15*(11), 1139–1153. doi: 10.15252/embr.201439245

Childs, B. G., Baker, D. J., … Van Deursen, J. M. (2016). Senescent intimal foam cells are deleterious at all stages of atherosclerosis. *Science*, *354*(6311), 472–477. doi: 10.1126/SCIENCE.AAF6659

Childs, B. G., Durik, M., … Van Deursen, J. M. (2015). Cellular senescence in aging and age-related disease: from mechanisms to therapy. *Nat. Med.*, *21*(12), 1424. doi: 10.1038/NM.4000

Childs, B. G., Li, H., … van Deursen, J. M. (2018). Senescent cells : a therapeutic target for cardiovascular disease. *J. Clin. Invest.*, *128*(4), 1217–1228. doi: 10.1172/JCI95146

Chimenti, C., Kajstura, J., … Anversa, P. (2003). Senescence and death of primitive cells and myocytes lead to premature cardiac aging and heart failure. *Circ. Res.*, *93*(7), 604–613. doi: 10.1161/01.RES.0000093985.76901.AF

Choi, Y. H. & Han, H. K. (2018). Nanomedicines: current status and future perspectives in aspect of drug delivery and pharmacokinetics. *J. Pharm. Investig.*, *48*(1), 43–60. doi: 10.1007/S40005-017-0370-4

Choi, Y. L., Jaworski, J., … Jung, J. H. (2011). Controlled release using mesoporous silica nanoparticles functionalized with 18-crown-6 derivative. *J. Mater. Chem.*, *21*(22), 7882–7885. doi: 10.1039/C1JM11334H

Chomczynski, P. & Sacchi, N. (1987). Single-step method of RNA isolation by acid guanidinium thiocyanate-phenol-chloroform extraction. *Anal. Biochem.*, *162*(1), 156–159. doi: 10.1006/abio.1987.9999

Chung, Y. H., Beiss, V., … Steinmetz, N. F. (2020). COVID-19 Vaccine Frontrunners and Their Nanotechnology Design. *ACS Nano*, *14*(10), 12522–12537. doi: 10.1021/ACSNANO.0C07197

Claycomb, W. C., Lanson, N. A., … Izzo, N. J. (1998). HL-1 cells: A cardiac muscle cell line that contracts and retains phenotypic characteristics of the adult cardiomyocyte. *Proc. Natl. Acad. Sci. U. S. A.*, *95*(6), 2979–2984. doi: 10.1073/pnas.95.6.2979

Coll, C., Mondragón, L., … Pérez-Payá, E. (2011). Enzyme-mediated controlled release systems by anchoring peptide sequences on mesoporous silica supports. *Angew. Chemie - Int. Ed.*, *50*(9), 2138–2140. doi: 10.1002/anie.201004133

Collado, M. & Serrano, M. (2010). Senescence in tumours: evidence from mice and

humans. *Nat. Rev. Cancer*, *10*(1), 51–57. doi: 10.1038/NRC2772

Coppé, J. P., Desprez, P. Y., … Campisi, J. (2010). The senescence-associated secretory phenotype: the dark side of tumor suppression. *Annu. Rev. Pathol.*, *5*(1), 99–118. doi: 10.1146/ANNUREV-PATHOL-121808-102144

Coppé, J. P., Patil, C. K., … Campisi, J. (2008). Senescence-associated secretory phenotypes reveal cell-nonautonomous functions of oncogenic RAS and the p53 tumor suppressor. *PLoS Biol.*, *6*(12). doi: 10.1371/journal.pbio.0060301

Corma, A., Kan, Q., … Rey, F. (1997). Synthesis of MCM-41 with Different Pore Diameters without Addition of Auxiliary Organics. *Chem. Mater.*, *9*(10), 2123–2126. doi: 10.1021/CM970203V

Correia-Melo, C., Marques, F. D., … Passos, J. F. (2016). Mitochondria are required for pro-ageing features of the senescent phenotype. *EMBO J.*, *35*(7), 724–742. doi: 10.15252/EMBJ.201592862

Cui, S., Xue, L., … Chen, Y. (2018). Postinfarction Hearts Are Protected by Premature Senescent Cardiomyocytes Via GATA4-Dependent CCN1 Secretion. *J. Am. Hear. Assoc. Cardiovasc. Cerebrovasc. Dis.*, *7*(18). doi: 10.1161/JAHA.118.009111

Dai, D. F., Chen, T., … Rabinovitch, P. S. (2010). Age-dependent cardiomyopathy in mitochondrial mutator mice is attenuated by overexpression of catalase targeted to mitochondria. *Aging Cell*, *9*(4), 536–544. doi: 10.1111/J.1474-9726.2010.00581.X

Davaapil, H., Brockes, J. P., & Yun, M. H. (2017). Conserved and novel functions of programmed cellular senescence during vertebrate development. *Development*, *144*(1), 106–114. doi: 10.1242/DEV.138222

De Angelis, A., Urbanek, K., … Berrino, L. (2016). Doxorubicin cardiotoxicity and target cells: a broader perspective. *Cardiooncology*, *2*(1). doi: 10.1186/S40959-016-0012-4

Debacq-Chainiaux, F., Erusalimsky, J. D., … Toussaint, O. (2009). Protocols to detect senescence-associated beta-galactosidase (SA-betagal) activity, a biomarker of senescent cells in culture and in vivo. *Nat. Protoc.*, *4*(12), 1798–1806. doi: 10.1038/nprot.2009.191

Demaria, M., O'Leary, M. N., … Campisi, J. (2017). Cellular Senescence Promotes Adverse Effects of Chemotherapy and Cancer Relapse. *Cancer Discov.*, *7*(2), 165–176. doi: 10.1158/2159-8290.CD-16-0241

Demaria, M., Ohtani, N., … Campisi, J. (2014). An essential role for senescent cells in optimal wound healing through secretion of PDGF-AA. *Dev. Cell*, *31*(6), 722–733. doi: 10.1016/J.DEVCEL.2014.11.012

Demirci, D., Dayanc, B., … Senturk, S. (2021). The jekyll and hyde of cellular senescence in cancer. *Cells*, *10*(2), 1–24. doi: 10.3390/cells10020208

Dewilde, S., Carroll, K., … Sawyer, J. (2020). Evaluation of the cost-effectiveness of dexrazoxane for the prevention of anthracycline-related cardiotoxicity in children with sarcoma and haematologic malignancies: A European perspective. *Cost Eff. Resour. Alloc.*, *18*(1), 1–10. doi: 10.1186/S12962-020-0205-4

Dimri, G. P., Lee, X., … Campisi, J. (1995). A biomarker that identifies senescent human cells in culture and in aging skin in vivo. *Proc. Natl. Acad. Sci. U. S. A.*, *92*(20), 9363–9367. doi: 10.1073/PNAS.92.20.9363

Din, S., Konstandin, M. H., … Sussman, M. A. (2014). Metabolic dysfunction consistent with premature aging results from deletion of Pim kinases. *Circ. Res.*, *115*(3), 376–387. doi: 10.1161/CIRCRESAHA.115.304441

Doan, L., Paine, P., … Quarta, M. (2020). *Targeted senolytic prodrug is well tolerated and results in amelioration of frailty, muscle regeneration and cognitive functions in geriatric mice*. doi: 10.21203/rs.3.rs-92962/v1

Dookun, E., Walaszczyk, A., … Richardson, G. D. (2020). Clearance of senescent cells during cardiac ischemia–reperfusion injury improves recovery. *Aging Cell*, *19*(10), 1–15. doi: 10.1111/acel.13249

Ekpenyong-Akiba, A. E., Canfarotta, F., … Macip, S. (2019). Detecting and targeting senescent cells using molecularly imprinted nanoparticles. *Nanoscale Horizons*, *4*(3), 757–768. doi: 10.1039/C8NH00473K

Ekpenyong-Akiba, A. E., Poblocka, M., … Macip, S. (2020). Amelioration of age-related brain function decline by Bruton's tyrosine kinase inhibition. *Aging Cell*, *19*(1). doi: 10.1111/ACEL.13079

Estepa-Fernández, A., Alfonso, M., … Martínez-Máñez, R. (2021). Senolysis Reduces Senescence in Veins and Cancer Cell Migration. *Adv. Ther.*, *2100149*, 1–15. doi: 10.1002/adtp.202100149

Estepa-Fernández, A., García-Fernández, A., … Martínez-Máñez, R. (2022). Combination of palbociclib with navitoclax based-therapies enhances in vivo antitumoral activity in triple-negative breast cancer. *Pharmacol. Res.*, *187*, 106628. doi: 10.1016/j.phrs.2022.106628

Estepa-Fernández, A., García-Fernández, A., … Martínez-Máñez, R. (2023). Engineering nanoparticle communication in living systems by stigmergy: An application to enhance antitumor therapy in triple-negative breast cancer. *Nano Today*, *48*, 101692. doi: 10.1016/j.nantod.2022.101692

Evangelou, K., Lougiakis, N., … Gorgoulis, V. G. (2017). Robust, universal

biomarker assay to detect senescent cells in biological specimens. *Aging Cell*, *16*(1), 192–197. doi: 10.1111/acel.12545

Ewer, M. S. & Ewer, S. M. (2015). Cardiotoxicity of anticancer treatments. *Nat. Rev. Cardiol.*, *12*(9), 547–558. doi: 10.1038/NRCARDIO.2015.65

Faget, D. V., Ren, Q., & Stewart, S. A. (2019). Unmasking senescence: context-dependent effects of SASP in cancer. *Nat. Rev. Cancer*, *19*(8), 439–453. doi: 10.1038/S41568-019-0156-2

Farokhzad, O. C. & Langer, R. (2009). Impact of nanotechnology on drug delivery. *ACS Nano*, *3*(1), 16–20. doi: 10.1021/NN900002M

Farr, J. N., Xu, M., … Khosla, S. (2017). Targeting cellular senescence prevents age-related bone loss in mice. *Nat. Med.*, *23*(9), 1072. doi: 10.1038/NM.4385

Ferreira de Souza, T., Quinaglia A.C. Silva, T., … Coelho-Filho, O. R. (2018). Anthracycline Therapy Is Associated With Cardiomyocyte Atrophy and Preclinical Manifestations of Heart Disease. *JACC. Cardiovasc. Imaging*, *11*(8), 1045. doi: 10.1016/J.JCMG.2018.05.012

Feynman, R. P. (1960). There's Plenty of Room at the Bottom. *Eng. Sci.*, *23*, 22–36.

Fozzard, H. A. & Sheets, M. F. (1985). Cellular mechanism of action of cardiac glycosides. *J. Am. Coll. Cardiol.*, *5*(5 Suppl A), 10A-15A. doi: 10.1016/S0735-1097(85)80458-7

Frescas, D., Roux, C. M., … Gudkov, A. V. (2017). Senescent cells expose and secrete an oxidized form of membrane-bound vimentin as revealed by a natural polyreactive antibody. *Proc. Natl. Acad. Sci. U. S. A.*, *114*(9), E1668–E1677. doi: 10.1073/PNAS.1614661114

Fuhrmann-Stroissnigg, H., Ling, Y. Y., … Robbins, P. D. (2017). Identification of HSP90 inhibitors as a novel class of senolytics. *Nat. Commun.*, *8*(1). doi: 10.1038/S41467-017-00314-Z

Fumagalli, M., Rossiello, F., … Di Fagagna, F. D. A. (2012). Telomeric DNA damage is irreparable and causes persistent DNA-damage-response activation. *Nat. Cell Biol.*, *14*(4), 355–365. doi: 10.1038/NCB2466

Galiana, I., Lozano-Torres, B., … Orzáez, M. (2020). Preclinical antitumor efficacy of senescence-inducing chemotherapy combined with a nanoSenolytic. *J. Control. Release*, *323*(10), 624–634. doi: 10.1016/j.jconrel.2020.04.045

Gallo, S., Spilinga, M., … Crepaldi, T. (2020). Activation of the MET receptor attenuates doxorubicin-induced cardiotoxicity in vivo and in vitro. *Br. J. Pharmacol.*, *177*(13), 3107. doi: 10.1111/BPH.15039

Galvis, D., Walsh, D., … Rankin, J. (2019). A dynamical systems model for the

measurement of cellular senescence. *J. R. Soc. Interface*, *16*(159). doi: 10.1098/RSIF.2019.0311

García-fernández, A., Aznar, E., … Sancenón, F. (2020). New Advances in In Vivo Applications of Gated Mesoporous Silica as Drug Delivery Nanocarriers. *Small*, *16*(3), 1–62. doi: 10.1002/smll.201902242

Ge, M., Hu, L., … He, Y. (2021). Senolytic targets and new strategies for clearing senescent cells. *Mech. Ageing Dev.*, *195*, 111468. doi: 10.1016/J.MAD.2021.111468

Genchi, G. G., Marino, A., … Ciofani, G. (2017). Remote Control of Cellular Functions: The Role of Smart Nanomaterials in the Medicine of the Future. *Adv. Healthc. Mater.*, *6*(9). doi: 10.1002/ADHM.201700002

Georgakopoulou, E., Tsimaratou, K., … Gorgoulis, V. (2012). Specific lipofuscin staining as a novel biomarker to detect replicative and stress-induced senescence. A method applicable in cryo-preserved and archival tissues. *Aging (Albany. NY).*, *5*(1), 37–50. doi: 10.18632/aging.100527

Ghosh, A. K., Rai, R., … Vaughan, D. E. (2016). A small molecule inhibitor of PAI-1 protects against doxorubicin-induced cellular senescence. *Oncotarget*, *7*(45), 72443–72457. doi: 10.18632/oncotarget.12494

Giménez, C., De La Torre, C., … Amor??s, P. (2015). Gated mesoporous silica nanoparticles for the controlled delivery of drugs in cancer cells. *Langmuir*, *31*(12), 3753–3762. doi: 10.1021/acs.langmuir.5b00139

González-Gualda, E., Baker, A. G., … Muñoz-Espín, D. (2021). A guide to assessing cellular senescence in vitro and in vivo. *FEBS J.*, *288*(1), 56–80. doi: 10.1111/FEBS.15570

González-Gualda, E., Pàez-Ribes, M., … Muñoz-Espín, D. (2020). Galacto-conjugation of Navitoclax as an efficient strategy to increase senolytic specificity and reduce platelet toxicity. *Aging Cell*, *Apr;19*(4), e13142. doi: 10.1111/acel.13142

Gorgoulis, V., Adams, P. D., … Demaria, M. (2019). Cellular Senescence: Defining a Path Forward. *Cell*, *179*(4), 813–827. doi: 10.1016/j.cell.2019.10.005

Gude, N. A., Broughton, K. M., … Sussman, M. A. (2018). Cardiac ageing: extrinsic and intrinsic factors in cellular renewal and senescence. *Nat. Rev. Cardiol. 2018 159*, *15*(9), 523–542. doi: 10.1038/s41569-018-0061-5

Guerrero, A., Guiho, R., … Gil, J. (2020). Galactose-modified duocarmycin prodrugs as senolytics. *Aging Cell*, *Apr;19*(4), e13133. doi: 10.1111/acel.13133

Hampel, B., Malisan, F., … Jansen-Dürr, P. (2004). Differential regulation of apoptotic cell death in senescent human cells. *Exp. Gerontol.*, *39*(11–12), 1713–1721. doi: 10.1016/J.EXGER.2004.05.010

Häseli, S., Deubel, S., … Ott, C. (2020). Cardiomyocyte Contractility and Autophagy in a Premature Senescence Model of Cardiac Aging. *Oxid. Med. Cell. Longev.*, *2020*. doi: 10.1155/2020/8141307

Hayflick, L. (1965). The limited in vitro lifetime of human diploid cell strains. *Exp. Cell Res.*, *37*(3), 614–636. doi: 10.1016/0014-4827(65)90211-9

Hayflick, L. & Moorhead, P. S. (1961). The serial cultivation of human diploid cell strains. *Exp. Cell Res.*, *25*(3), 585–621. doi: 10.1016/0014-4827(61)90192-6

He, Y., Zhang, X., … Zhou, D. (2020). Using proteolysis-targeting chimera technology to reduce navitoclax platelet toxicity and improve its senolytic activity. *Nat. Commun. 2020 111*, *11*(1), 1–14. doi: 10.1038/s41467-020-15838-0

Herbig, U., Jobling, W. A., … Sedivy, J. M. (2004). Telomere shortening triggers senescence of human cells through a pathway involving ATM, p53, and p21(CIP1), but not p16(INK4a). *Mol. Cell*, *14*(4), 501–513. doi: 10.1016/S1097-2765(04)00256-4

Hernandez-Segura, A., de Jong, T. V., … Demaria, M. (2017). Unmasking Transcriptional Heterogeneity in Senescent Cells. *Curr. Biol.*, *27*(17), 2652–2660. doi: 10.1016/j.cub.2017.07.033

Hernandez-Segura, A., Nehme, J., & Demaria, M. (2018). Hallmarks of Cellular Senescence. *Trends Cell Biol.*, *28*(6), 436–453. doi: 10.1016/j.tcb.2018.02.001

Herranz, N. & Gil, J. (2018). Mechanisms and functions of cellular senescence. *J. Clin. Invest.*, *128*(4), 1238–1246. doi: 10.1172/JCI95148

Hewitt, G., Jurk, D., … Passos, J. F. (2012). Telomeres are favoured targets of a persistent DNA damage response in ageing and stress-induced senescence. *Nat. Commun.*, *3*. doi: 10.1038/NCOMMS1708

Hickson, L. J., Langhi Prata, L. G. P., … Kirkland, J. L. (2019). Senolytics decrease senescent cells in humans: Preliminary report from a clinical trial of Dasatinib plus Quercetin in individuals with diabetic kidney disease. *EBioMedicine*, *47*, 446–456. doi: 10.1016/j.ebiom.2019.08.069

Hildebrand, D. G., Lehle, S., … Schulze-Osthoff, K. (2013). α-Fucosidase as a novel convenient biomarker for cellular senescence. *Cell Cycle*, *12*(12), 1922–1927. doi: 10.4161/cc.24944

Hoffmann, F., Cornelius, M., … Fröba, M. (2006). Silica-based mesoporous

organic-inorganic hybrid materials. *Angew. Chemie - Int. Ed.*, *45*(20), 3216–3251. doi: 10.1002/anie.200503075

Hoshino, A., Mita, Y., … Matoba, S. (2013). Cytosolic p53 inhibits Parkin-mediated mitophagy and promotes mitochondrial dysfunction in the mouse heart. *Nat. Commun.*, *4*(1), 1–12. doi: 10.1038/ncomms3308

Hudgins, A. D., Tazearslan, C., … Suh, Y. (2018). Age- and Tissue-Specific Expression of Senescence Biomarkers in Mice. *Front. Genet.*, *9*(59). doi: 10.3389/fgene.2018.00059

Jafarinezhad, Z., Rafati, A., … Karbalay-Doust, S. (2019). Cardioprotective effects of curcumin and carvacrol in doxorubicin-treated rats: Stereological study. *Food Sci. Nutr.*, *7*(11), 3581. doi: 10.1002/FSN3.1210

Janjua, T. I., Cao, Y., … Popat, A. (2021). Clinical translation of silica nanoparticles. *Nat. Rev. Mater. 2021 612*, *6*(12), 1072–1074. doi: 10.1038/s41578-021-00385-x

Januzzi, J. L., Packer, M., … Solomon, S. D. (2018). IGFBP7 (Insulin-Like Growth Factor-Binding Protein-7) and Neprilysin Inhibition in Patients With Heart Failure. *Circ. Heart Fail.*, *11*(10), e005133. doi: 10.1161/CIRCHEARTFAILURE.118.005133

Jeon, O. H., Kim, C., … Elisseeff, J. H. (2017). Local clearance of senescent cells attenuates the development of post-traumatic osteoarthritis and creates a pro-regenerative environment. *Nat. Med.*, *23*(6), 775–781. doi: 10.1038/NM.4324

Jia, K., Dai, Y., … Jin, Q. (2020). Senolytic Agent Navitoclax Inhibits Angiotensin II-Induced Heart Failure in Mice. *J. Cardiovasc. Pharmacol.*, *76*(4), 452–460. doi: 10.1097/FJC.0000000000000878

Jia, L., Zhang, W., … Du, J. (2017). Haplodeficiency of Ataxia Telangiectasia Mutated Accelerates Heart Failure After Myocardial Infarction. *J. Am. Heart Assoc.*, *6*(7). doi: 10.1161/JAHA.117.006349

Jurk, D., Wang, C., … von Zglinicki, T. (2012). Postmitotic neurons develop a p21-dependent senescence-like phenotype driven by a DNA damage response. *Aging Cell*, *11*(6), 996–1004. doi: 10.1111/J.1474-9726.2012.00870.X

Justice, J., Miller, J. D., … Kirkland, J. L. (2016). Frameworks for Proof-of-Concept Clinical Trials of Interventions That Target Fundamental Aging Processes. *Journals Gerontol. - Ser. A Biol. Sci. Med. Sci.*, *71*(11), 1415–1423. doi: 10.1093/gerona/glw126

Justice, J. N., Nambiar, A. M., … Kirkland, J. L. (2019). Senolytics in idiopathic pulmonary fibrosis: Results from a first-in-human, open-label, pilot study. *EBioMedicine*, *40*, 554–563. doi: 10.1016/j.ebiom.2018.12.052

Kaefer, A., Yang, J., … Xiong, H. (2014). Mechanism-based pharmacokinetic/pharmacodynamic meta-analysis of navitoclax (ABT-263) induced thrombocytopenia. *Cancer Chemother. Pharmacol.*, *74*(3), 593–602. doi: 10.1007/S00280-014-2530-9

Kalkavan, H. & Green, D. R. (2018). MOMP, cell suicide as a BCL-2 family business. *Cell Death Differ.*, *25*(1), 46–55. doi: 10.1038/CDD.2017.179

Katz, M. L., Robinson, W. G., … Bieri, J. G. (1984). Lipofuscin accumulation resulting from senescence and vitamin E deficiency: Spectral properties and tissue distribution. *Mech. Ageing Dev.*, *25*(1–2), 149–159. doi: 10.1016/0047-6374(84)90137-4

Khan, Z. H., Kumar, A., … Husain, M. (2016). Introduction to nanomaterials. In Advanced Structured Materials (Vol. 79, pp. 1–23). doi: 10.1007/978-81-322-2668-0_1

Kikuchi, K., Holdway, J. E., … Poss, K. D. (2010). Primary contribution to zebrafish heart regeneration by gata4(+) cardiomyocytes. *Nature*, *464*(7288), 601–605. doi: 10.1038/NATURE08804

Kile, B. T. (2014). The role of apoptosis in megakaryocytes and platelets. *Br. J. Haematol.*, *165*(2), 217–226. doi: 10.1111/bjh.12757

Kim, H. N., Chang, J., … Almeida, M. (2017). DNA damage and senescence in osteoprogenitors expressing Osx1 may cause their decrease with age. *Aging Cell*, *16*(4), 693–703. doi: 10.1111/ACEL.12597

Kim, T. W., Kim, H. J., … Kim, J. R. (2008). Identification of replicative senescence-associated genes in human umbilical vein endothelial cells by an annealing control primer system. *Exp. Gerontol.*, *43*(4), 286–295. doi: 10.1016/J.EXGER.2007.12.010

Kirkland, J. L., Tchkonia, T., … Robbins, P. D. (2017). The Clinical Potential of Senolytic Drugs. *J. Am. Geriatr. Soc.*, *65*(10), 2297–2301. doi: 10.1111/jgs.14969

Kirschner, K., Rattanavirotkul, N., … Chandra, T. (2020). Functional heterogeneity in senescence. *Biochem. Soc. Trans.*, *48*(3), 765–773. doi: 10.1042/BST20190109

Knaś, M., Zalewska, A., … Zwierz, K. (2012). The profile of lysosomal exoglycosidases in replicative and stress-induced senescence in early passage human fibroblasts. *Folia Histochem. Cytobiol.*, *50*(2), 220–227. doi: 10.5603/FHC.2012.0031

Kobler, J., Möller, K., & Bein, T. (2008). Colloidal Suspensions of Functionalized Mesoporous Silica Nanoparticles. *ACS Nano*, *2*(4), 791–799. doi:

10.1021/NN700008S

Korolchuk, V. I., Miwa, S., … von Zglinicki, T. (2017). Mitochondria in Cell Senescence: Is Mitophagy the Weakest Link? *EBioMedicine*, *21*, 7–13. doi: 10.1016/J.EBIOM.2017.03.020

Kosugi, R., Shioi, T., … Izumi, T. (2006). Angiotensin II receptor antagonist attenuates expression of aging markers in diabetic mouse heart. *Circ. J.*, *70*(4), 482–488. doi: 10.1253/CIRCJ.70.482

Kuilman, T., Michaloglou, C., … Peeper, D. S. (2010). The essence of senescence. *Genes Dev.*, *24*(22), 2463–2479. doi: 10.1101/GAD.1971610

Kulkarni, J. A., Thomson, S. B., … Leavitt, B. R. (2020). Spontaneous, solvent-free entrapment of siRNA within lipid nanoparticles. *Nanoscale*, *12*(47), 23959–23966. doi: 10.1039/D0NR06816K

Kurz, D. J., Decary, S., … Erusalimsky, J. D. (2000). Senescence-associated (beta)-galactosidase reflects an increase in lysosomal mass during replicative ageing of human endothelial cells. *J. Cell Sci.*, *113 (Pt 20)*(20), 3613–3622. doi: 10.1242/JCS.113.20.3613

Laflamme, M. A. & Murry, C. E. (2011). Heart regeneration. *Nature*, *473*(7347), 326–335. doi: 10.1038/NATURE10147

Lee, B. Y., Han, J. A., … Hwang, E. S. (2006). Senescence-associated beta-galactosidase is lysosomal beta-galactosidase. *Aging Cell*, *5*(2), 187–195. doi: 10.1111/J.1474-9726.2006.00199.X

Leri, A., Franco, S., … Blasco, M. A. (2003). Ablation of telomerase and telomere loss leads to cardiac dilatation and heart failure associated with p53 upregulation. *EMBO J.*, *22*(1), 131–139. doi: 10.1093/EMBOJ/CDG013

Lewinska, A., Adamczyk-Grochala, J., … Pazik, R. (2020). AMPK-mediated senolytic and senostatic activity of quercetin surface functionalized Fe 3 O 4 nanoparticles during oxidant-induced senescence in human fibroblasts. *Redox Biol.*, *28*. doi: 10.1016/J.REDOX.2019.101337

Lewis-McDougall, F. C., Ruchaya, P. J., … Ellison-Hughes, G. M. (2019). Aged-senescent cells contribute to impaired heart regeneration. *Aging Cell*, *18*(3), e12931. doi: 10.1111/acel.12931

Li, J., Li, S. H., … Li, R. K. (2019). Long-term repopulation of aged bone marrow stem cells using young Sca-1 cells promotes aged heart rejuvenation. *Aging Cell*, *18*(6). doi: 10.1111/ACEL.13026

Li, Q., Cheng, L., … Ma, X. (2019). Efficacy and Safety of Bcl-2 Inhibitor Venetoclax in Hematological Malignancy: A Systematic Review and Meta-

Analysis of Clinical Trials. *Front. Pharmacol.*, *10*(JUN). doi: 10.3389/FPHAR.2019.00697

Li, S., Sun, M., … Kuang, H. (2020). Chiral Cu x Co y S Nanoparticles under Magnetic Field and NIR Light to Eliminate Senescent Cells. *Angew. Chem. Int. Ed. Engl.*, *59*(33), 13915–13922. doi: 10.1002/ANIE.202004575

Li, X., Liu, M., … Zhang, P. (2017). Cardiac complications in cancer treatment – A review. *Hell. J. Cardiol.*, *58*(3), 190–193. doi: 10.1016/j.hjc.2016.12.003

Lin, Q., Huang, Q., … Zhu, L. (2010). Anticancer drug release from a mesoporous silica based nanophotocage regulated by either a one- or two-photon process. *J. Am. Chem. Soc.*, *132*(31), 10645–10647. doi: 10.1021/JA103415T

Lipshultz, S. E. & Herman, E. H. (2018). Anthracycline cardiotoxicity: The importance of horizontally integrating pre-clinical and clinical research. *Cardiovasc. Res.*, *114*(2), 205–209. doi: 10.1093/cvr/cvx246

Lipshultz, S. E., Scully, R. E., … Colan, S. D. (2010). Assessment of dexrazoxane as a cardioprotectant in doxorubicin-treated children with high-risk acute lymphoblastic leukaemia: long-term follow-up of a prospective, randomised, multicentre trial. *Lancet. Oncol.*, *11*(10), 950–961. doi: 10.1016/S1470-2045(10)70204-7

Liu, Z., Davis, C., … Dai, H. (2008). Circulation and long-term fate of functionalized, biocompatible single-walled carbon nanotubes in mice probed by Raman spectroscopy. *Proc. Natl. Acad. Sci.*, *105*(5), 1410 LP – 1415. doi: 10.1073/pnas.0707654105

Llopis-Lorente, A., Lozano-Torres, B., … Sancenón, F. (2017). Mesoporous silica materials for controlled delivery based on enzymes. *J. Mater. Chem. B*, *5*(17), 3069–3083. doi: 10.1039/C7TB00348J

Lombardo, D., Kiselev, M. A., & Caccamo, M. T. (2019). Smart Nanoparticles for Drug Delivery Application: Development of Versatile Nanocarrier Platforms in Biotechnology and Nanomedicine. *J. Nanomater.*, *2019*. doi: 10.1155/2019/3702518

López-Otín, C., Blasco, M. A., … Kroemer, G. (2013). The hallmarks of aging. *Cell*, *153*(6), 1194. doi: 10.1016/j.cell.2013.05.039

Lozano-Torres, B., Blandez, J. F., … Martínez-Máñez, R. (2020). Real-Time In Vivo Detection of Cellular Senescence through the Controlled Release of the NIR Fluorescent Dye Nile Blue. *Angew. Chem. Int. Ed. Engl.*, *59*(35), 15152–15156. doi: 10.1002/ANIE.202004142

Lozano-Torres, B., Blandez, J. F., … Martínez-Máñez, R. (2021). A Two-Photon Probe Based on Naphthalimide-Styrene Fluorophore for the In Vivo Tracking

of Cellular Senescence. *Anal. Chem.*, *93*(5), 3052–3060. doi: 10.1021/ACS.ANALCHEM.0C05447

Lozano-Torres, B., Galiana, I., … Sancenón, F. (2017). An OFF-ON Two-Photon Fluorescent Probe for Tracking Cell Senescence in Vivo. *J. Am. Chem. Soc.*, *139*(26), 8808–8811. doi: 10.1021/JACS.7B04985

Lozano-Torres, B., Rojas-Vázquez, S., … Martinez-Manez, R. (2021). *A renal clearable uorogenic probe for in vivo detection of cellular senescence*. doi: 10.21203/rs.3.rs-418261/v1

Lu, M., Qu, A., … Xu, C. (2020). Mitochondria-Targeting Plasmonic Spiky Nanorods Increase the Elimination of Aging Cells in Vivo. *Angew. Chemie Int. Ed.*, *59*(22), 8698–8705. doi: 10.1002/ANIE.202002576

Maejima, Y., Adachi, S., … Isobe, M. (2008). Induction of premature senescence in cardiomyocytes by doxorubicin as a novel mechanism of myocardial damage. *Aging Cell*, *7*(2), 125–136. doi: 10.1111/j.1474-9726.2007.00358.x

Marcotte, R., Lacelle, C., & Wang, E. (2004). Senescent fibroblasts resist apoptosis by downregulating caspase-3. *Mech. Ageing Dev.*, *125*(10–11), 777–783. doi: 10.1016/J.MAD.2004.07.007

Masaldan, S., Clatworthy, S. A. S., … Cater, M. A. (2018). Iron accumulation in senescent cells is coupled with impaired ferritinophagy and inhibition of ferroptosis. *Redox Biol.*, *14*, 100–115. doi: 10.1016/J.REDOX.2017.08.015

Mauro, A. G., Bonaventura, A., … Toldo, S. (2019). NLRP3 Inflammasome in Acute Myocardial Infarction. *J. Cardiovasc. Pharmacol.*, *74*(3), 175–187. doi: 10.1097/FJC.0000000000000717

McGowan, J. V, Chung, R., … Yellon, D. M. (2017). Anthracycline Chemotherapy and Cardiotoxicity. *Cardiovasc. Drugs Ther.*, *31*(1), 63–75. doi: 10.1007/s10557-016-6711-0

Mehdizadeh, M., Aguilar, M., … Nattel, S. (2021). The role of cellular senescence in cardiac disease: basic biology and clinical relevance. *Nat. Rev. Cardiol.*, *0123456789*(4), 250–264. doi: 10.1038/s41569-021-00624-2

Meiners, B., Shenoy, C., & Zordoky, B. N. (2018). Clinical and preclinical evidence of sex-related differences in anthracycline-induced cardiotoxicity. *Biol. Sex Differ.*, *9*(1), 38. doi: 10.1186/s13293-018-0198-2

Meléndez, G. C., Vasu, S., … Jordan, J. H. (2020). Myocardial Extracellular and Cardiomyocyte Volume Expand After Doxorubicin Treatment Similar to Adjuvant Breast Cancer Therapy. *JACC. Cardiovasc. Imaging*, *13*(4), 1084–1085. doi: 10.1016/J.JCMG.2019.10.020

Meyer, K., Hodwin, B., … Sarikas, A. (2016). Essential Role for Premature Senescence of Myofibroblasts in Myocardial Fibrosis. *J. Am. Coll. Cardiol.*, *67*(17), 2018–2028. doi: 10.1016/J.JACC.2016.02.047

Mitry, M. A., Laurent, D., … Edwards, J. G. (2020). Accelerated cardiomyocyte senescence contributes to late-onset doxorubicin-induced cardiotoxicity. *Am. J. Physiol. Physiol.*, *318*(2), C380–C391. doi: 10.1152/ajpcell.00073.2019

Mizuta, Y., Tokuda, K., … Akahoshi, T. (2020). Sodium thiosulfate prevents doxorubicin-induced DNA damage and apoptosis in cardiomyocytes in mice. *Life Sci.*, *257*(June), 118074. doi: 10.1016/j.lfs.2020.118074

Morin, D., Long, R., … Ghaleh, B. (2019). Hsp22 overexpression induces myocardial hypertrophy, senescence and reduced life span through enhanced oxidative stress. *Free Radic. Biol. Med.*, *137*, 194–200. doi: 10.1016/J.FREERADBIOMED.2019.04.035

Morsli, S., Doherty, G. J., & Muñoz-Espín, D. (2022). Activatable senoprobes and senolytics: Novel strategies to detect and target senescent cells. *Mech. Ageing Dev.*, *202*, 111618. doi: 10.1016/j.mad.2021.111618

Muñoz-Espín, D., Rovira, M., … Serrano, M. (2018). A versatile drug delivery system targeting senescent cells. *EMBO Mol. Med.*, *10*(9), e9355. doi: 10.15252/emmm.201809355

Muñoz-Espín, D. & Serrano, M. (2014). Cellular senescence: from physiology to pathology. *Nat. Rev. Mol. Cell Biol. 2014 157*, *15*(7), 482–496. doi: 10.1038/nrm3823

Myrianthopoulos, V., Evangelou, K., … Gorgoulis, V. G. (2019). Senescence and senotherapeutics: a new field in cancer therapy. *Pharmacol. Ther.*, *193*, 31–49. doi: 10.1016/j.pharmthera.2018.08.006

Nair, N. & Gongora, E. (2016). Heart failure in chemotherapy-related cardiomyopathy: Can exercise make a difference? *BBA Clin.*, *6*, 69. doi: 10.1016/J.BBACLI.2016.06.001

Narita, M. M., Nũnez, S., … Lowe, S. W. (2003). Rb-mediated heterochromatin formation and silencing of E2F target genes during cellular senescence. *Cell*, *113*(6), 703–716. doi: 10.1016/s0092-8674(03)00401-x

Navya, P. N., Kaphle, A., & Daima, H. K. (2018). Nanomedicine in sensing, delivery, imaging and tissue engineering: advances, opportunities and challenges. *SPR Nanosci.*, *5*, 30–56. doi: 10.1039/9781788013871-00030

Naylor, R. M., Baker, D. J., & Van Deursen, J. M. (2013). Senescent cells: a novel therapeutic target for aging and age-related diseases. *Clin. Pharmacol. Ther.*, *93*(1), 105–116. doi: 10.1038/CLPT.2012.193

Nelson, G., Wordsworth, J., … von Zglinicki, T. (2012). A senescent cell bystander effect: senescence-induced senescence. *Aging Cell*, *11*(2), 345–349. doi: 10.1111/J.1474-9726.2012.00795.X

Nousiainen, T., Jantunen, E., … Hartikainen, J. (2002). Early decline in left ventricular ejection fraction predicts doxorubicin cardiotoxicity in lymphoma patients. *Br. J. Cancer*, *86*(11), 1697. doi: 10.1038/SJ.BJC.6600346

Ock, S., Lee, W. S., … Kim, J. (2016). Deletion of IGF-1 receptors in cardiomyocytes attenuates cardiac aging in male mice. *Endocrinology*, *157*(1), 336–345. doi: 10.1210/en.2015-1709

Octavia, Y., Tocchetti, C. G., … Moens, A. L. (2012). Doxorubicin-induced cardiomyopathy: From molecular mechanisms to therapeutic strategies. *J. Mol. Cell. Cardiol.*, *52*(6), 1213–1225. doi: 10.1016/j.yjmcc.2012.03.006

Ogrodnik, M., Miwa, S., … Jurk, D. (2017). Cellular senescence drives age-dependent hepatic steatosis. *Nat. Commun.*, *8*. doi: 10.1038/NCOMMS15691

Oldershaw, R., Owens, W. A., … Meeson, A. (2019). Human Cardiac-Mesenchymal Stem Cell-Like Cells, a Novel Cell Population with Therapeutic Potential. *Stem Cells Dev.*, *28*(9), 593–607. doi: 10.1089/SCD.2018.0170

Oliveira, G. H., Qattan, M. Y., … Park, S. J. (2014). Advanced heart failure therapies for patients with chemotherapy-induced cardiomyopathy. *Circ. Hear. Fail.*, *7*(6), 1050–1058. doi: 10.1161/CIRCHEARTFAILURE.114.001292

Orlic, D., Kajstura, J., … Anversa, P. (2001). Bone marrow cells regenerate infarcted myocardium. *Nature*, *410*(6829), 701–705. doi: 10.1038/35070587

Ovadya, Y. & Krizhanovsky, V. (2018). Strategies targeting cellular senescence. *J. Clin. Invest.*, *128*(4), 1247. doi: 10.1172/JCI95149

Paez-Ribes, M., González-Gualda, E., … Muñoz-Espín, D. (2019). Targeting senescent cells in translational medicine. *EMBO Mol. Med.*, *11*(12). doi: 10.15252/EMMM.201810234

Pan, J., Li, D., … Meng, A. (2017). Inhibition of Bcl-2/xl With ABT-263 Selectively Kills Senescent Type II Pneumocytes and Reverses Persistent Pulmonary Fibrosis Induced by Ionizing Radiation in Mice. *Int. J. Radiat. Oncol. Biol. Phys.*, *99*(2), 353–361. doi: 10.1016/J.IJROBP.2017.02.216

Park, C. J., Branch, M. E., … Meléndez, G. C. (2020). The Role of Cardiac MRI in Animal Models of Cardiotoxicity: Hopes and Challenges. *J. Cardiovasc. Transl. Res.*, *13*(3), 367–376. doi: 10.1007/s12265-020-09981-8

Passos, J. F., Nelson, G., … Von Zglinicki, T. (2010). Feedback between p21 and reactive oxygen production is necessary for cell senescence. *Mol. Syst. Biol.*,

6, 347. doi: 10.1038/MSB.2010.5

Passos, J. F., Saretzki, G., … Von Zglinicki, T. (2007). Mitochondrial dysfunction accounts for the stochastic heterogeneity in telomere-dependent senescence. *PLoS Biol.*, *5*(5), 1138–1151. doi: 10.1371/JOURNAL.PBIO.0050110

Pelaz, B., Alexiou, C., … Parak, W. J. (2017). Diverse Applications of Nanomedicine. *ACS Nano*, *11*(3), 2313–2381. doi: 10.1021/ACSNANO.6B06040

Pham, L. M., Kim, E. C., … Kim, J. O. (2021). Targeting and clearance of senescent foamy macrophages and senescent endothelial cells by antibody-functionalized mesoporous silica nanoparticles for alleviating aorta atherosclerosis. *Biomaterials*, *269*. doi: 10.1016/J.BIOMATERIALS.2021.120677

Piegari, E., De Angelis, A., … Rossi, F. (2013). Doxorubicin induces senescence and impairs function of human cardiac progenitor cells. *Basic Res. Cardiol.*, *108*(2), 334. doi: 10.1007/s00395-013-0334-4

Pinto, A. R., Ilinykh, A., … Tallquist, M. D. (2016). Revisiting Cardiac Cellular Composition. *Circ. Res.*, *118*(3), 400–409. doi: 10.1161/CIRCRESAHA.115.307778

Podyacheva, E. Y., Kushnareva, E. A., … Toropova, Y. G. (2021). Analysis of models of doxorubicin-induced cardiomyopathy in rats and mice. A modern view from the perspective of the pathophysiologist and the clinician. *Front. Pharmacol.*, *12*(June), 1–12. doi: 10.3389/fphar.2021.670479

Qu, A., Wu, X., … Xu, C. (2020). An NIR-Responsive DNA-Mediated Nanotetrahedron Enhances the Clearance of Senescent Cells. *Adv. Mater.*, *32*(14). doi: 10.1002/ADMA.202000184

Raffaele, M., Phd, V., … Raffaele, M. (2022). *The costs and benefits of senotherapeutics for human health*. doi: 10.1016/S2666-7568(21)00300-7

Raman, N. K., Anderson, M. T., & Brinker, C. J. (1996). Template-Based Approaches to the Preparation of Amorphous, Nanoporous Silicas. *Chem. Mater.*, *8*(8), 1682–1701. doi: 10.1021/CM960138

Rawat, P. S., Jaiswal, A., … Navik, U. (2021). Doxorubicin-induced cardiotoxicity: An update on the molecular mechanism and novel therapeutic strategies for effective management. *Biomed. Pharmacother.*, *139*. doi: 10.1016/J.BIOPHA.2021.111708

Rayess, H., Wang, M. B., & Srivatsan, E. S. (2012). Cellular senescence and tumor suppressor gene p16. *Int. J. Cancer*, *130*(8), 1715–1725. doi: 10.1002/IJC.27316

Richardson, G. D., Laval, S., & Owens, W. A. (2015). Cardiomyocyte Regeneration in the mdx Mouse Model of Nonischemic Cardiomyopathy. *Stem Cells Dev.*, *24*(14), 1672–1680. doi: 10.1089/scd.2014.0495

Ritschka, B., Storer, M., … Keyes, W. M. (2017). The senescence-associated secretory phenotype induces cellular plasticity and tissue regeneration. *Genes Dev.*, *31*(2), 172–183. doi: 10.1101/gad.290635.116

Roos, C. M., Zhang, B., … Miller, J. D. (2016). Chronic senolytic treatment alleviates established vasomotor dysfunction in aged or atherosclerotic mice. *Aging Cell*, *15*(5), 973–977. doi: 10.1111/acel.12458

Rudin, C. M., Hann, C. L., … Gandhi, L. (2012). Phase II Study of Single-Agent Navitoclax (ABT-263) and Biomarker Correlates in Patients with Relapsed Small Cell Lung Cancer. *Clin. Cancer Res.*, *18*(11), 3163 LP – 3169. doi: 10.1158/1078-0432.CCR-11-3090

Rufini, A., Tucci, P., … Melino, G. (2013). Senescence and aging: the critical roles of p53. *Oncogene 2013 3243*, *32*(43), 5129–5143. doi: 10.1038/onc.2012.640

Ryu, S. J., Oh, Y. S., & Park, S. C. (2007). Failure of stress-induced downregulation of Bcl-2 contributes to apoptosis resistance in senescent human diploid fibroblasts. *Cell Death Differ.*, *14*(5), 1020–1028. doi: 10.1038/SJ.CDD.4402091

Saha, A. K., Zhen, M. Y. S., … Ramasubramanian, A. K. (2020). Design Considerations and Assays for Hemocompatibility of FDA-Approved Nanoparticles. *Semin. Thromb. Hemost.*, *46*(5), 637–652. doi: 10.1055/S-0039-1688491

Sahin, E., Colla, S., … DePinho, R. A. (2011). Telomere dysfunction induces metabolic and mitochondrial compromise. *Nature*, *470*(7334), 359. doi: 10.1038/NATURE09787

Sahin, E. & Depinho, R. A. (2010). Linking functional decline of telomeres, mitochondria and stem cells during ageing. *Nature*, *464*(7288), 520–528. doi: 10.1038/NATURE08982

Saleh, T., Tyutynuk-Massey, L., … Gewirtz, D. A. (2018). Non-Cell Autonomous Effects of the Senescence-Associated Secretory Phenotype in Cancer Therapy. *Front. Oncol.*, *0*(MAY), 164. doi: 10.3389/FONC.2018.00164

Santos, D. S. dos & Goldenberg, R. C. dos S. (2018). Doxorubicin-Induced Cardiotoxicity: From Mechanisms to Development of Efficient Therapy. In Cardiotoxicity (pp. 3–24). doi: 10.5772/intechopen.79588

Sawicki, K. T., Sala, V., … Ghigo, A. (2021). Preventing and Treating Anthracycline Cardiotoxicity: New Insights. *Annu Rev Pharmacol Toxicol.*, *61*(6), 309–332.

doi: 10.1146/annurev-pharmtox-030620-104842.

Schafer, M. J., White, T. A., … LeBrasseur, N. K. (2017). Cellular senescence mediates fibrotic pulmonary disease. *Nat. Commun.*, *8*. doi: 10.1038/ncomms14532

Scherrer-Crosbie, M. & Thibault, H. B. (2008). Echocardiography in Translational Research: Of Mice and Men. *J. Am. Soc. Echocardiogr.*, *21*(10), 1083. doi: 10.1016/J.ECHO.2008.07.001

Serrano, M., Lin, A. W., … Lowe, S. W. (1997). Oncogenic ras provokes premature cell senescence associated with accumulation of p53 and p16INK4a. *Cell*, *88*(5), 593–602. doi: 10.1016/S0092-8674(00)81902-9

Serrano, M., Orzáez, M., … Sancenón, F. (2019). The chemistry of senescence. *Nat. Rev. Chem.*, *3*(7), 426–441. doi: 10.1038/s41570-019-0108-0

Sharpless, N. E. & Sherr, C. J. (2015). Forging a signature of in vivo senescence. *Nat. Rev. Cancer*, *15*(7), 397–408. doi: 10.1038/NRC3960

Shay, J. W. & Wright, W. E. (2000). Hayflick, his limit, and cellular ageing. *Nat. Rev. Mol. Cell Biol. 2000 11*, *1*(1), 72–76. doi: 10.1038/35036093

Shi, J., Kantoff, P. W., … Farokhzad, O. C. (2017). Cancer nanomedicine: progress, challenges and opportunities. *Nat. Rev. Cancer*, *17*(1), 20–37. doi: 10.1038/nrc.2016.108

Shimizu, I. & Minamino, T. (2019). Cellular senescence in cardiac diseases. *J. Cardiol.*, *74*(4), 1–7. doi: 10.1016/j.jjcc.2019.05.002

Shin, M. D., Shukla, S., … Steinmetz, N. F. (2020). COVID-19 vaccine development and a potential nanomaterial path forward. *Nat. Nanotechnol.*, *15*(8), 646–655. doi: 10.1038/S41565-020-0737-Y

Short, S., Fielder, E., … von Zglinicki, T. (2019). Senolytics and senostatics as adjuvant tumour therapy. *EBioMedicine*, *41*, 683–692. doi: 10.1016/J.EBIOM.2019.01.056

Silber, J. H., Cnaan, A., … Zhao, H. (2004). Enalapril to prevent cardiac function decline in long-term survivors of pediatric cancer exposed to anthracyclines. *J. Clin. Oncol.*, *22*(5), 820–828. doi: 10.1200/JCO.2004.06.022

Šimůnek, T., Štěrba, M., … Gerši, V. (2009). Anthracycline-induced cardiotoxicity: overview of studies examining the roles of oxidative stress and free cellular iron. *Pharmacol. Rep.*, *61*(1), 154–171. doi: 10.1016/S1734-1140(09)70018-0

Soto-gamez, A. & Demaria, M. (2017). Therapeutic interventions for aging: the case of cellular senescence. *Drug Discov. Today*, *22*(5), 786–795. doi: 10.1016/j.drudis.2017.01.004

Spallarossa, P., Altieri, P., … Brunelli, C. (2009). Doxorubicin induces senescence or apoptosis in rat neonatal cardiomyocytes by regulating the expression levels of the telomere binding factors 1 and 2. *Am. J. Physiol. Heart Circ. Physiol.*, *297*(6). doi: 10.1152/AJPHEART.00068.2009

Stein, A., Melde, B. J., & Schroden, R. C. (2000). Hybrid Inorganic–Organic Mesoporous Silicates—Nanoscopic Reactors Coming of Age. *Adv. Mater.*, *12*(19), 1403–1419. doi: 10.1002/1521-4095(200010)12:19<1403::AID-ADMA1403>3.0.CO;2-X

Stober, W., Fink, A., & Ernst Bohn, D. (1968). Controlled Growth of Monodisperse Silica Spheres in the Micron Size Range 1. *J. Colloid Interface Sci.*, *26*, 62–69.

Storer, M., Mas, A., … Keyes, W. M. (2013). Senescence is a developmental mechanism that contributes to embryonic growth and patterning. *Cell*, *155*(5), 1119. doi: 10.1016/J.CELL.2013.10.041

Swain, S. M., Whaley, F. S., & Ewer, M. S. (2003). Congestive heart failure in patients treated with doxorubicin: a retrospective analysis of three trials. *Cancer*, *97*(11), 2869–2879. doi: 10.1002/cncr.11407

Szefler, B. (2018). Nanotechnology, from quantum mechanical calculations up to drug delivery. *Int. J. Nanomedicine*, *13*, 6143. doi: 10.2147/IJN.S172907

Takahashi, A., Ohtani, N., … Hara, E. (2006). Mitogenic signalling and the p16INK4a-Rb pathway cooperate to enforce irreversible cellular senescence. *Nat. Cell Biol.*, *8*(11), 1291–1297. doi: 10.1038/NCB1491

Tang, X., Li, P. H., & Chen, H. Z. (2020). Cardiomyocyte Senescence and Cellular Communications Within Myocardial Microenvironments. *Front. Endocrinol. (Lausanne).*, *11*, 280. doi: 10.3389/FENDO.2020.00280

Tebbi, C. K., London, W. B., … Schwartz, C. L. (2007). Dexrazoxane-associated risk for acute myeloid leukemia/myelodysplastic syndrome and other secondary malignancies in pediatric Hodgkin's disease. *J. Clin. Oncol.*, *25*(5), 493–500. doi: 10.1200/JCO.2005.02.3879

Thapa, R. K., Nguyen, H. T., … Kim, J. O. J. R. (2017). Progressive slowdown/prevention of cellular senescence by CD9-targeted delivery of rapamycin using lactose-wrapped calcium carbonate nanoparticles. *Sci. Rep.*, *7*(October 2016), 43299. doi: 10.1038/srep43299

Timm, K. N., Perera, C., … Tyler, D. J. (2020). Early detection of doxorubicin-induced cardiotoxicity in rats by its cardiac metabolic signature assessed with hyperpolarized MRI. *Commun. Biol.*, *3*(1), 1–10. doi: 10.1038/s42003-020-01440-z

Triana-Martínez, F., Picallos-Rabina, P., … Collado, M. (2019). Identification and

characterization of Cardiac Glycosides as senolytic compounds. *Nat Commun*, *10*(1), 4731. doi: 10.1038/s41467-019-12888-x.

Tse, C., Shoemaker, A. R., … Elmore, S. W. (2008). ABT-263: A Potent and Orally Bioavailable Bcl-2 Family Inhibitor. *Cancer Res.*, *68*(9), 3421–3428. doi: 10.1158/0008-5472.CAN-07-5836

Vallet-Regi, M., Rámila, A., … Pérez-Pariente, J. (2001). A new property of MCM-41: Drug delivery system. *Chem. Mater.*, *13*(2), 308–311. doi: 10.1021/cm0011559

van Dalen, E. C., Caron, H. N., … Kremer, L. C. M. (2011). Cardioprotective interventions for cancer patients receiving anthracyclines. *Cochrane Database Syst. Rev.*, *16*(6). doi: 10.1002/14651858.CD003917

Varela-López, A., Battino, M., … Quiles, J. L. (2019). An update on the mechanisms related to cell death and toxicity of doxorubicin and the protective role of nutrients. *Food Chem. Toxicol.*, *134*(July), 110834. doi: 10.1016/j.fct.2019.110834

Vicencio, J. M., Galluzzi, L., … Kroemer, G. (2008). Senescence, Apoptosis or Autophagy? *Gerontology*, *54*(2), 92–99. doi: 10.1159/000129697

Victorelli, S. & Passos, J. F. (2019). Reactive Oxygen Species Detection in Senescent Cells. *Methods Mol. Biol.*, *1896*, 21–29. doi: 10.1007/978-1-4939-8931-7_3

von Kobbe, C. (2019). Targeting senescent cells: approaches, opportunities, challenges. *Aging (Albany. NY).*, *11*(24), 12844–12861. doi: 10.18632/aging.102557

Von Zglinicki, T., Wan, T., & Miwa, S. (2021). Senescence in Post-Mitotic Cells: A Driver of Aging? *Antioxidants Redox Signal.*, *34*(4), 308–323. doi: 10.1089/ars.2020.8048

Walaszczyk, A., Dookun, E., … Richardson, G. D. (2019). Pharmacological clearance of senescent cells improves survival and recovery in aged mice following acute myocardial infarction. *Aging Cell*, *18*(3), e12945–e12945. doi: 10.1111/acel.12945

Wallace, K. B., Sardão, V. A., & Oliveira, P. J. (2020). Mitochondrial Determinants of Doxorubicin-Induced Cardiomyopathy. *Circ. Res.*, *126*(7), 926–941. doi: 10.1161/CIRCRESAHA.119.314681

Walsh, S., Pontén, A., … Jovinge, S. (2010). Cardiomyocyte cell cycle control and growth estimation in vivo--an analysis based on cardiomyocyte nuclei. *Cardiovasc. Res.*, *86*(3), 365–373. doi: 10.1093/CVR/CVQ005

Wang, E. (1995). Senescent Human Fibroblasts Resist Programmed Cell Death, and Failure to Suppress bcl2 Is Involved. *Cancer Res.*, *55*(11).

Wang, J., Uryga, A. K., … Bennett, M. (2015). Vascular Smooth Muscle Cell Senescence Promotes Atherosclerosis and Features of Plaque Vulnerability. *Circulation*, *132*(20), 1909–1919. doi: 10.1161/CIRCULATIONAHA.115.016457

Wang, Y., Chang, J., … Zheng, G. (2016). Discovery of piperlongumine as a potential novel lead for the development of senolytic agents. *Aging (Albany. NY).*, *8*(11), 2915–2926. doi: 10.18632/AGING.101100

Watanabe, S., Kawamoto, S., … Hara, E. (2017). Impact of senescence-associated secretory phenotype and its potential as a therapeutic target for senescence-associated diseases. *Cancer Sci.*, *108*(4), 563–569. doi: 10.1111/CAS.13184

Wen, J., Yang, K., … Sun, S. (2017). Diverse gatekeepers for mesoporous silica nanoparticle based drug delivery systems. *Chem. Soc. Rev.*, *46*(19), 6024–6045. doi: 10.1039/C7CS00219J

Wiley, C. D., Velarde, M. C., … Campisi, J. (2016). Mitochondrial Dysfunction Induces Senescence with a Distinct Secretory Phenotype. *Cell Metab.*, *23*(2), 303–314. doi: 10.1016/J.CMET.2015.11.011

Xie, J., Chen, Y., … Xu, B. (2017). Premature senescence of cardiac fibroblasts and atrial fibrosis in patients with atrial fibrillation. *Oncotarget*, *8*(35), 57981–57990. doi: 10.18632/ONCOTARGET.19853

Xu, M., Pirtskhalava, T., … Kirkland, J. L. (2018). Senolytics improve physical function and increase lifespan in old age. *Nat. Med.*, *24*(8), 1246–1256. doi: 10.1038/s41591-018-0092-9

Yanagisawa, T., Shimizu, T., … Kato, C. (1990). The preparation of alkyltrimethylammonium-kanemite complexes and their conversion to microporous materials. *Bull. Chem. Soc. Jpn.*, *63*(4), 988–992. doi: 10.1246/bcsj.63.988

Yang, N. C. & Hu, M. L. (2005). The limitations and validities of senescence associated-beta-galactosidase activity as an aging marker for human foreskin fibroblast Hs68 cells. *Exp. Gerontol.*, *40*(10), 813–819. doi: 10.1016/J.EXGER.2005.07.011

Yosef, R., Pilpel, N., … Krizhanovsky, V. (2017). p21 maintains senescent cell viability under persistent DNA damage response by restraining JNK and caspase signaling. *EMBO J.*, *36*(15), 2280–2295. doi: 10.15252/EMBJ.201695553

Yosef, R., Pilpel, N., … Krizhanovsky, V. (2016). Directed elimination of senescent

cells by inhibition of BCL-W and BCL-XL. *Nat. Commun.*, *7*, 1–11. doi: 10.1038/ncomms11190

Youn, J. C., Jung, M. K., … Shin, E. C. (2019). Increased frequency of CD4+CD57+ senescent T cells in patients with newly diagnosed acute heart failure: exploring new pathogenic mechanisms with clinical relevance. *Sci. Rep.*, *9*(1). doi: 10.1038/S41598-019-49332-5

Yousefzadeh, M. J., Zhu, Y., … Niedernhofer, L. J. (2018). Fisetin is a senotherapeutic that extends health and lifespan. *EBioMedicine*, *36*, 18–28. doi: 10.1016/J.EBIOM.2018.09.015

Yu, X., Zheng, J., … Zhu, G. (2020). Testosterone antagonizes paraquat-induced cardiomyocyte senescence via the mIGF-1/SIRT1 signaling pathway. *Brazilian J. Med. Biol. Res.*, *53*(10), 1–9. doi: 10.1590/1414-431X20209849

Yutzey, K. E. (2017). Cardiomyocyte Proliferation: Teaching an Old Dogma New Tricks. *Circ. Res.*, *120*(4), 627–629. doi: 10.1161/CIRCRESAHA.116.310058

Zamorano, J. L., Lancellotti, P., … Poland, A. T. (2016). 2016 ESC Position Paper on cancer treatments and cardiovascular toxicity developed under the auspices of the ESC Committee for Practice Guidelines: The Task Force for cancer treatments and cardiovascular toxicity of the European Society of Cardiology (ES. *Eur. Heart J.*, *37*(36), 2768–2801. doi: 10.1093/eurheartj/ehw211

Zeiss, C. J., Gatti, D. M., … Churchill, G. A. (2019). Doxorubicin-Induced Cardiotoxicity in Collaborative Cross (CC) Mice Recapitulates Individual Cardiotoxicity in Humans. *G3 Genes|Genomes|Genetics*, *9*(8), 2637–2646. doi: 10.1534/G3.119.400232

Zhang, H., Nimmer, P. M., … Tse, C. (2007). Bcl-2 family proteins are essential for platelet survival. *Cell Death Differ.*, *14*(5), 943–951. doi: 10.1038/SJ.CDD.4402081

Zhang, K., Xu, L. L., … Wu, P. (2013). Facile large-scale synthesis of monodisperse mesoporous silica nanospheres with tunable pore structure. *J. Am. Chem. Soc.*, *135*(7), 2427–2430. doi: 10.1021/ja3116873

Zhang, S., Liu, X., … Yeh, E. T. H. (2012). Identification of the molecular basis of doxorubicin-induced cardiotoxicity. *Nat. Med.*, *18*(11), 1639–1642. doi: 10.1038/nm.2919

Zhang, Y., Yu, J., … Gu, Z. (2016). Mechanical Force-Triggered Drug Delivery. *Chem. Rev.*, *116*(19), 12536–12563. doi: 10.1021/ACS.CHEMREV.6B00369

Zhao, J., Fuhrmann-Stroissnigg, H., … Robbins, P. D. (2017). Quantitative Analysis of Cellular Senescence in Culture and In Vivo. *Curr. Protoc. Cytom.*, *79*(1), 9.51.1-9.51.25. doi: 10.1002/CPCY.16

Zhao, M., Ding, X. feng, … Xu, B. (2017). Use of liposomal doxorubicin for adjuvant chemotherapy of breast cancer in clinical practice. *J. Zhejiang Univ. Sci. B*, *18*(1), 15–26. doi: 10.1631/JZUS.B1600303

Zhao, Y., Trewyn, B. G., … Lin, V. S. Y. (2009). Mesoporous silica nanoparticle-based double drug delivery system for glucose-responsive controlled release of insulin and cyclic AMP. *J. Am. Chem. Soc.*, *131*(24), 8398–8400. doi: 10.1021/ja901831u

Zhu, F., Li, Y., … Du, J. (2013). Senescent cardiac fibroblast is critical for cardiac fibrosis after myocardial infarction. *PLoS One*, *8*(9), 1–12. doi: 10.1371/journal.pone.0074535

Zhu, Y., Tchkonia, T., … Kirkland, J. L. (2016). Identification of a novel senolytic agent, navitoclax, targeting the Bcl-2 family of anti-apoptotic factors. *Aging Cell*, *15*(3), 428–435. doi: 10.1111/acel.12445

Zhu, Y., Tchkonia, T., … Kirkland, J. L. (2015). The Achilles' heel of senescent cells: from transcriptome to senolytic drugs. *Aging Cell*, *14*(4), 644–658. doi: 10.1111/acel.12344